COMPLEX COACERVATES AS LIQUID EMBOLIC AGENTS WITH A NOVEL IONIC STRENGTH DEPENDENT SETTING MECHANISM

by

Joshua Preston Jones

A dissertation submitted to the faculty of
The University of Utah
in partial fulfillment of the requirements for the degree of

Doctor of Philosophy

Department of Bioengineering

The University of Utah

December 2017

The University of Utah Graduate School

STATEMENT OF DISSERTATION APPROVAL

The dissertation of **Joshua Preston Jones**

has been approved by the following supervisory committee members:

Russell J. Stewart	, Chair	**8/9/17** Date Approved
Ryan Gene O'Hara	, Member	**8/8/17** Date Approved
Vladimir Hlady	, Member	**8/8/17** Date Approved
Jindřich Kopeček	, Member	**8/8/17** Date Approved
Patrick A. Tresco	, Member	**8/8/17** Date Approved

and by **David W. Grainger** , Chair/Dean of

the Department/College/School of **Bioengineering**

and by David B. Kieda, Dean of The Graduate School.

ABSTRACT

In a transcatheter embolization procedure, an embolic agent is delivered locally via a microcatheter to obstruct blood flow in a blood vessel or vascular bed. These interventional radiology procedures are used to treat vascular abnormalities, hemorrhage, and neoplastic growths. Current embolization agents are plagued by toxicity and handling issues. An ideal embolic agent would be water-borne and not rely on *in situ* polymerization or precipitation from organic solvents for hardening.

Complex coacervates represent a possible solution to these problems; they are an aqueous fluid morphology of associated polyelectrolytes that can be endowed with environmentally triggered solidification mechanisms. In this dissertation, the development of embolic coacervates (ECs) based upon an ionic strength driven setting mechanism is described. ECs are low-viscosity liquid coacervates in solutions of high ionic strength, but undergo a phase transition into a solid upon entering the low ionic strength environment of blood vessels. Early iterations were based upon the commercially available polycation protamine and an oligophosphate. These agents validated the ionic strength dependent setting mechanism and successfully occluded blood flow down to the capillary level in an acute transcatheter embolization of a rabbit kidney. Next, a synthetic polymer, poly(3-guanidinopropylmethacrylamide-*co*-methacrylamide), was developed to

replicate the structure of protamine while offering control over the mechanical properties of the embolic both before and after solidification. ECs made from this synthetic polymer demonstrated an increase in dynamic shear modulus of nearly 4 orders of magnitude upon injection into physiological saline. In embolization of rabbit auricular arteries, these agents incited neutrophilic inflammation which began to subside at 2-4 weeks. At the endpoint of the study (4 weeks), occlusions remained stable and early signs of fibrous tissue deposition were observed. While longer-term tissue response studies are needed, embolic coacervates (ECs) represent a promising developmental embolic agent.

In the final chapter, drug-releasing ECs were prepared with the antiangiogenic drug sunitinib malate. These ECs released 80% of their drug payload over the course of 14 days, displaying a linear zero order release profile. The results presented in this final chapter provide a framework for developing future embolics which prevent angiogenic revascularization resulting from post-embolization ischemia.

TABLE OF CONTENTS

LIST OF TABLES

LIST OF FIGURES

LIST OF SYMBOLS

^{1}H NMR	Hydrogen-1 (Proton) Nuclear Magnetic Resonance
^{13}C NMR	Carbon-13 Nuclear Magnetic Resonance
^{31}P NMR	Phosphorous-31 Nuclear Magnetic Resonance
3D	Three-Dimensional
δ	Phase Angle (Rheology)
δ	Chemical Shift (NMR)
µg	Microgram
µL	Microliter
µm	Micrometer
AA-EC	Antiangiogenic Embolic Coacervate
ACS	American Chemical Society
AIBN	Azobisisobutyronitrile
APMA	*N*-(3-aminopropyl) Methacrylamide
ATR-IR	Attenuated Total Reflectance Infrared Spectroscopy
AVM	Arteriovenous Malformation
BSS	Balanced Salt Solution
CEA	Central Auricular Artery
cm	Centimeter
CP	Coacervate-Precipitate Phase Transition
CTA	Chain Transfer Agent
Da	Dalton
DI	Deionized
DMSO	Dimethylsulfoxide
E-beam	Electron-beam
EC	Embolic Coacervate
ECM	Extracellular Matrix
ESI	Electrospray Ionization
EVOH	Ethylene-Vinyl Alcohol Copolymer
F	French (catheter diameter)
FBGC	Foreign Body Giant Cell
FDA	Food and Drug Administration
FITC	Fluorescein Isothiocyanate
g	Gram
*G**	Complex Shear Modulus
G'	Shear Storage Modulus
G"	Shear Loss Modulus
GI	Gastrointestinal

GPC	Gel Permeation Chomatography
GPMA	*N*-(3-methacrylamidopropyl) guanidinium
h	Hour
HCC	Hepatocellular Carcinoma
HIF	Hypoxia Inducible Factor
HRE	Hypoxia Responsive Element
Hz	Hertz
IACUC	Institutional Animal Care and Use Committee
ID	Inner Diameter
IgE	Immunoglobulin E
IgG	Immunoglobulin G
IP_6	Inositol Hexaphosphate (Phytic Acid)
IR	Infrared
ISO	International Standards Organization
kDa	Kilodalton
kg	Kilogram
kPa	Kilopascal
LCST	Lower Critical Solution Temperature
m	Meter
M	Molar
M_n	Number Average Molecular Weight
M_w	Weight Average Molecular Weight
MA	Methacrylamide
mg	Milligram
mL	Milliliter
mM	Millimolar
mm	Millimeter
mol	Mole
MP	Hexametaphosphate
MPa	Megapascal
MW	Molecular weight
NBCA	*N*-butyl 2-cyanoacrylate
NIPAM	*N*-isopropylacrylamide
nm	Nanometer
NMR	Nuclear Magnetic Resonance
OD	Outer Diameter
Pa	Pascal
PAA	Poly (acrylic acid)
PAH	Poly (allylamine)
PDADMA	Poly(diallyldimethylammonium)
PDGF	Platelet Derived Growth Factor
PDI	Polydispersity Index
PE	Polyelectrolyte
PEC	Polyelectrolyte Complex
PEO	Poly (ethylene oxide)
pEVOH	Ethylene-Vinyl Alcohol Copolymer

PG	Poly(GPMA-co-MA)
PG-MP	Poly(GPMA-co-MA)-Hexametaphosphate Coacervate
pH	Potential of Hydrogen
pK_a	Logarithmic Acid Dissociation Constant
ppm	Parts Per Million
PPO	Poly(propylene oxide)
PRT	Protamine
PRT-IP6	Protamine-Inositol Hexaphosphate Coacervate
PRT-MP	Protamine Hexametaphosphate Coacervate
PSS	Poly(styrene sulfonate)
PTFE	Polytetrafluorethylene
PVA	Polyvinyl Alcohol
r	Radius
RAFT	Reversible Addition Fragmentation Chain-Transfer
RI	Refractive Index
rpm	Revolutions Per Minute
RTK	Receptor Tyrosine Kinase
s	Second
SC	Solution-Coacervate Phase Transition
SD	Standard Deviation
SUN	Sunitinib Malate
Ta	Tantalum
TACE	Transarterial Chemoembolization
TAE	Transarterial Embolization
TaO	Tantalum Oxide
TEA	Triethylamine
TKI	Tyrosine Kinase Inhibitor
USP	United States Pharmacopeia
V-501	4,4′-Azobis(4-cyanovaleric acid)
VEGF	Vascular Endothelial Growth Factor
VEGFR	Vascular Endothelial Growth Factor Receptor
wt%	Weight percent

ACKNOWLEDGEMENTS

First, I would like to thank my advisor Dr. Russell Stewart for bringing me into his lab midway into my PhD. Without this generous opportunity, I would not have finished. He is an outstanding investigator whose ability to attract funding for important research has been crucial in the success of this project. Dr. Stewart demands the best from his students and everyone in his lab. This has elevated my work and made me a better scientist and critical thinker. Dr. Ryan O'Hara has been a key collaborator on this project, especially in the acute animal experiments, and I benefited greatly from his willingness to share real-world clinical knowledge.

I also appreciate the contributions of the current and former members of Dr. Stewart's lab. Monika Sima laid much of the early ground work for this project and was an invaluable resource for me throughout, always willing to go the extra mile to make sure we succeeded. Her expertise and experience was instrumental in animal experiments and polymer characterization. Dr. Mahika Weerasekare was a patient teacher in my early monomer and polymer syntheses and was always willing to help me work though chemistry issues that popped up along the way. I would also like to thank Dr. Ching-Sheuen Wang, Dr. Nicolas Ashton, Dr. Dwight Lane, Dr. In Taek Song, Jack Prather, and Jessica Karz for lending their ears and offering valuable feedback.

Additionally, I must thank other educators who inspired me long before I decided to pursue a PhD. Teachers at Suwannee Middle School and Suwannee High School: Ms. Jennifer Humbles, Mrs. Cindy Wiggins, Mrs. Paula McMillan, Mr. Randy Ethridge, and Mr. Steven Campbell. Professors at Berry College: Dr. Dominic Qualley, Dr. Ken Martin, Dr. Charles M. Earnest, Dr. Kevin Hoke, Dr. Andrew Bressette, Dr. Paul Kapitza, and Dr. Chuck Lane.

Finally, I am thankful to my family. From an early age, my parents, Mickey and Sandy Jones, taught me the importance of education, exemplified the meaning of hard work, always demanded excellence from me, and above all, encouraged me to follow my dreams. Most of all, I am grateful to my wife, Ellery. Five years ago, she agreed to accompany me on this crazy journey across the country to pursue my PhD. She has been an invaluable source of love, support, and laughter. Her encouragement has pushed me every step along the way, and most importantly, she always believed in me, even when I no longer believed in myself.

CHAPTER 1

INTRODUCTION

1.1 Scope

In this dissertation, endovascular embolic agents with a novel water-borne composition and setting mechanism are presented. This approach was inspired by the adhesive of marine sandcastle worms. The natural adhesive is packaged and stored as sets of oppositely charged polyelectrolytes (PEs) which are condensed into complex fluids [1-4]. Within seconds of secretion from the adhesive gland, the fluid adhesive hardens into a solid–liquid foam [5]. The transition in morphology is largely driven by changes in ionic composition and concentrations when the fluid adhesive is exposed to seawater [6]. The *in situ* setting embolic coacervates (ECs) were designed to mimic the polyelectrolyte composition, condensed fluid form, and environmentally triggered setting mechanism of the natural sandcastle glue. In this chapter, the clinical context for therapeutic embolization is outlined with emphasis on the need for a new liquid embolization agent. Next, the phenomenon of complex coacervation is introduced as a solution to problems seen with current liquid embolic agents. Finally, the unique setting mechanism, which is based upon ionic strength mediated transitions between morphologies of associated polyelectrolytes, is described.

1.2 Therapeutic Embolization

Transcatheter embolization is an interventional radiology procedure that results in therapeutic occlusion of one or more blood vessels. Typically, a catheter is inserted into the femoral artery using the Seldinger technique. Then, under fluoroscopic guidance, the catheter is positioned and an embolization agent is delivered to produce a controlled, localized blockage. The first reported transcatheter embolization was performed in 1972 to stop bleeding from a duodenal hemorrhage using an autologous clot [7]. With the advancement of embolic agents and interventional radiology techniques, clinical uses for embolic agents have expanded from hemorrhages to include treatment of vascular abnormalities both in the central nervous system and in peripheral circulation [8, 9]. Additionally, several types of tumors, both benign and cancerous, are treated by embolization. Generally, three factors are considered in choosing an embolization agent for a procedure: 1) the size of the vessel to be occluded; 2) the long-term viability of the target tissue; and 3) the desired duration of occlusion [8, 10]. In large vessels, coils and gelatin sponges are most often used. For small vessel occlusion, liquid embolic agents or particles are most often used. However, there is great overlap between these scenarios. In many cases, more than one embolization agent may be used to create the desired surgical outcome. The following sections describe these agents in more detail, and mention the scenarios in which they might be deployed.

1.3 Current Embolization Agents

1.3.1 Large Vessel Embolization Devices

Large vessel embolization agents are mechanical devices that rely on native thrombus from the patient to stop blood flow. The most common device used in large vessels are embolization coils, which are most often constructed of either steel or platinum [8, 11]. These coils come in a variety of shapes and three-dimensional (3D) configurations with sizes ranging from <1 millimeter up to several centimeters [8]. To increase their occlusive capability, thrombogenic polyester, nylon, or silk fibers are added to coils in a dense layer [11]. Coils are driven through the catheter and delivered by either forceful saline injection or a coil pusher wire. To prevent unwanted distal migration, coils should be oversized 20-30% compared to their target vessel. In situations requiring precision placement, detachable coils, which can be retrieved and repositioned, are used [11]. When a temporary occlusion of a large vessel is desired, gelatin sponge (Gelfoam), a material produced from porcine adipose tissue, is used. This material is sold in blocks which are formed by the surgeon into the desired geometry [10]. Gelfoam obstructs blood flow via a mixture of mechanical effects and providing a scaffold for native clot formation [12]. Typically, the sponge is cut into small 1-3 mm pieces or rolled into “torpedoes,” which can be injected into a large vessel. Placement of gelatin foam is much less precise than coils and produces a proximal occlusion [8]. Over several weeks, the Gelfoam material is resorbed and eventually the surrounding thrombus is eventually lysed, producing recanalization of the previously embolized vessel [13].

1.3.2 Particle Embolic Agents

Particle embolic agents have sizes ranging from 100 μm to 1200 μm and are typically suspended in contrast and injected under fluoroscopic guidance [10]. These agents are carried in the downstream by blood and block vessels by physical entrapment. The occlusions are stabilized by native hemostatic clots and an ensuing inflammatory reaction [13]. These particle embolics can be divided into 2 classes: nonspherical particles and microspheres. Nonspherical particles have been available since the 1970s and are generally made by mechanically processing sheets of material into small particles and diving them into size ranges using sieves [10, 13]. This process produces particles with irregular shapes and poorly defined size ranges [12]. Like Gelfoam ® sheets, gelatin sponge particles produced by this process also produce a temporary occlusion, recanalizing over several weeks. Irregularly shaped polyvinyl alcohol (PVA) particles are also produced by several manufacturers. Even though PVA is largely considered biocompatible, PVA particles adhere to the vessel wall, causing localized necrosis and a chronic, persistent foreign body reaction [12]. While PVA is considered a permanent embolic agent, instances of revascularization are seen [14]. The chief disadvantage of these irregular particles is their tendency to aggregate and cause occlusion proximal to the desired target [15]. While particles are still used in embolization procedures, embolic microspheres were developed in the 1990s to address some of their drawbacks. These systems come in well-defined size ranges from 40-1200 μm and have a well-controlled spherical shape [13]. Several iterations of PVA microspheres are approved by the FDA. Tris-acryl gelatin

microspheres (Embospheres ®) contain an acrylic polymer matrix which, in contrast to gelatin sponge particles, renders them nonresorbable. Histologically, microspheres of both types behave similarly to irregular PVA particles, causing focal angionecrosis and localized inflammation [12]. However, these microspheres are much more controllable, avoiding aggregation and off-target embolization.

1.3.3 Cyanoacrylate Glues

Alkyl cyanoacrylates are low-viscosity liquid resins that rapidly polymerize into hard adhesives on contact with anions. Historically, these were tissue adhesives that were often used off label as embolization agents [16]. In 2000, *N*-Butyl-2 Cyanoacrylate (NBCA) (TruFill ®, DePuy Synthes, Inc.) received FDA approval for the presurgical embolization of cerebral arteriovenous malformations. In addition, NBCA is often used in other small vessel embolization scenarios [12]. NBCA occludes the blood vessel by immediately polymerizing into a hard, adhesive resin upon contact with anions present in blood. Recanalization is still seen in rare instances with NBCA [17]. To achieve distal penetration, NBCA is mixed with varying amounts of ethiodized oil, which retards polymerization. Ethiodized oil also provides some fluoroscopic visualization, but more often, micronized tantalum metal particles are used for contrast. For delivery, the catheter is flushed with a solution of 5% dextrose in water to prevent occlusion. Still, the catheter often becomes occluded after 1-2 injections [12]. Even worse, the catheter can become glued into the embolization site with NBCA [17, 18]. Misjudgment of the amount of NBCA or ethiodized oil needed for a procedure can result in

embolization spreading either proximal or distal to the desired site [12, 17]. Furthermore, upon injection, NBCA causes severe necrosis to surrounding tissue. Eventually this reaction progresses to a severe inflammatory response with perivascular inflammation and finally fibrosis [17, 19-21]. It is believed that this reaction largely results from localized hyperthermia from the exothermic heat of polymerization of cyanoacrylate monomers and from the byproducts of this reaction including formaldehyde and alkyl cyanoacetate [22].

1.3.4 Precipitating Embolic Agents

Another approach used in liquid embolic agents has been to dissolve biocompatible polymers that are insoluble in water, such as ethylene vinyl alcohol (EVOH), in a water-miscible organic solvent, dimethyl sulfoxide (DMSO). This produces a low-viscosity solution that forms a polymer precipitate upon contact with aqueous media through the rapid diffusion of DMSO into the surrounding fluid [23]. In 2005, Onyx ® received the first FDA approval for this type of embolic agent. Like Trufill ®, Onyx ® is indicated for the presurgical embolization of brain arteriovenous malformations and contains micronized tantalum particles for fluoroscopic visualization [12]. Upon injection into blood, EVOH precipitates as a pliable, spongy material [23]. In comparison to NBCA, EVOH is nonadhesive and becomes less rigid, which allows for multiple injections. This also serves to reduce, but not eliminate risk of catheter entrapment compared to NBCA [12, 24]. On the other hand, DMSO is toxic and can cause vasospasm, tissue necrosis, and pain if injected too rapidly, which limits the delivery rate to 0.3 mL min^{-1}, and it creates a

foul taste that can persist for days [25-28]. The slow delivery rate and rapid setting makes it difficult to control forward flow and penetration with EVOH [29, 30]. EVOH occludes vessels via a mixture of embolic agent and thrombus [21]. Vessel wall necrosis is seen in greater than 90% of AVMs embolized with Onyx, which incites perivascular infiltration and chronic inflammation dominated by foreign body giant cells [21, 31, 32]. Other embolic agents using this general mechanism are in early clinical usage. A copolymer of poly(lactide-co-glycolide) and poly(hydroxyethyl methacrylate) dissolved in DMSO is approved for clinical use in Europe. This system (PHIL ®) incorporates a triidophenol contrast agent into the polymer, elimating the use of tantalum particles for fluoroscopic guidance [33, 34]. While early experience suggests that PHIL ® may offer preferential handling characteristics in comparison to Onyx ® [33, 35, 36], this system retains the use of DMSO as a solvent which has been implicated in many of the adverse reactions to EVOH [25, 26].

1.4 Clinical Applications

Transcatheter embolization is often applied by interventional radiologists in unique circumstances. Thus, a complete list of applications is difficult to compile. However, most clinical applications for embolic agents fall into 3 categories: (1) embolization of vascular abnormalities which have risks of complication (most often severe hemorrhage); (2) devascularization of undesirable neoplasmic growths; and (3) control of acute hemorrhage. Vascular abnormalities treated by embolization include dural arteriovenous fistulas, arteriovenous malformations

(AVMs) [37], arterial aneurysms [38], and varicoceles [39]. Tumors amenable to embolization include both benign tumors, such as uterine fibroids and hemangiomas [40], and malignant tumors like hepatocellular carcinoma [41]. Severe hemorrhage can result from a wide variety of causes, and embolization is used when bleeding cannot be managed with other techniques. Several of the most common clinical scenarios for embolization therapy are described in more detail in the following sections.

1.4.1 Arteriovenous Malformations (AVMs)

AVMs are congenital vascular abnormalities that can occur anywhere in the body; however, those within the central nervous system are the most problematic. AVMs consist of focal areas of dilated arteries and veins, referred to as a nidus. Within the nidus, no capillary bed exists, and blood flows directly from arterioles into the venous vasculature through at least one (but often several) arteriovenous fistulas, causing a lack of circulation to the surrounding parenchyma. The lack of fluid resistance from a capillary bed causes localized venous hypertension. Clinically, AVMs most often present as intracerebral hemorrhage. They carry a risk of catastrophic rupture, which can be fatal or have debilitating neurological effects [42]. AVM treatments are used to reduce the risk of hemorrhage and rupture [43]. These treatments are often guided by the Spetzler-Martin Scale, which grades AVMs based on size, location, and presence of deep venous drainage on a scale of 1-5, with 5 being the most severe [44]. With smaller AVMs, embolization may be used as a curative therapy [42]. In larger, Grade IV-V neural AVMs,

embolization is used to reduce blood flow to portions of the nidus prior to surgical resection or radiosurgery [43]. Peripheral AVMs are often left untreated, but may be treated on a case-by-case basis with embolization. Overwhelmingly, embolization of AVMs is performed using liquid embolic agents, typically either EVOH or NBCA [10, 12].

1.4.2 Aneurysms

Saccular aneurysms are thin-walled protrusions from arterial vessels, which are weakened by compromised vessel layers including tunica media and/or the internal elastic lamina [45]. Like AVMs, aneurysms can occur anywhere in the body, but intracranial saccular aneurysms are the most threatening due to their risk of catastrophic rupture and subsequent subarachnoid hemorrhages [46]. These intracranial aneurysms occur predominantly on the circle of Willis [47]. Peripheral aneurysms requiring treatment are most commonly found in the aorta [48], iliac artery [49], popliteal artery [50], and the visceral arteries [51]. While hemorrhage from catastrophic rupture can be life-threatening in large arteries, such as the aorta [48], peripheral aneurysms are a source of downstream thromboemboli which can cause stroke and other ischemic events [52]. Embolization can be used to treat diagnosed nonruptured aneurysms or hemorrhage from ruptured aneurysms. Detachable coils are the most common endovascular therapy for aneurysms [12]. However, within this indication, there has been growing usage of liquid embolics in conjunction with coils [53-55]. In addition, Onyx 500® is used in the standalone treatment of intracranial sidewall

aneurysms [56].

1.4.3 Hepatocellular Carcinoma and Malignant Hypervascular Tumors

Hepatocellular Carcinoma (HCC) is a hypervascularized tumor that most often develops in patients with chronic fibrosis and/or cirrhosis [57]. Surgical resection or orthotopic liver transplantation, depending on liver function, are considered the best option for patients with early stage HCC (<3cm) [58, 59]. Unfortunately, HCC is typically undiagnosed until it has reached an intermediate to advanced stage where resection or transplantation are no longer viable options [59]. Even in cases where resection is done, 55% of patients exhibit tumor recurrence within 2 years, most of which are inoperable [58, 60]. In these advanced cases, transcatheter embolization has emerged as the primary mode of therapy [61, 62]. HCC is especially amenable to embolization because the tumor blood supply is primarily derived from the hepatic artery, while blood supply to healthy liver tissue is supplied through the portal vein [58]. While HCC is the most common target for embolotherapy, other hypervascularized tumors such as renal cell carcinoma, head and neck tumors, and colorectal carcinoma can also be treated by embolization. Embolization for tumors can be divided into conventional transarterial embolization (TAE) and transarterial chemoembolization (TACE). In TAE, an embolic agent is delivered alone to cause ischemic tumor necrosis [63]. TACE differs in that the embolic agent is co-administered with a chemotherapeutic agent, often doxorubicin [41]. For advanced HCC, TAE and TACE are the only

therapies to have repeatedly demonstrated a survival benefit compared to supportive care [58].

1.4.4 Uterine Fibroids

Uterine fibroids are neoplasms composed of smooth muscle cells and an associated extracellular matrix of connective tissue. These tumors originate from the muscular myometrium. While benign, growth of these fibroids can cause enlargement of the uterus, menorrhagia, and localized pressure on surrounding tissues including bowel and bladder. Generally, uterine fibroids are left untreated unless associated symptoms become unacceptable to the patient [64]. In these cases, treatment with nonsteroidal anti-inflammatory agents and hormonal androgens are an option. However, many patients require further intervention [64, 65]. These interventions include surgical myomectomy, for women who wish to remain fertile, and hysterectomy. Percutaneous embolization is a less invasive option, but is not recommended for women who may want to have children [65]. Embolization of the fibroid causes ischemic infarction of the tumor, which results in gradual shrinkage and relief of associated symptoms. Treatment of a fibroid is considered permanent, although it does not prevent new fibroids from occurring [64]. Embolization is typically performed via the uterine artery with PVA particles, Gelfoam, or tris-acryl gelatin microspheres [10, 64, 66].

1.4.5 Control of Hemorrhage

Finally, percutaneous embolization can be used to control acute hemorrhage that is unmanageable with pharmacological or endoscopic interventions. Of these, traumatic and gastrointestinal (GI) hemorrhage have the highest incidence, but embolization is also used for pulmonary hemorrhage [67], severe obstetric bleeding [68], and epistaxis [69]. Trauma can destroy large vessels to extremities or to vital organs such as the liver, spleen, or kidneys causing life-threatening internal bleeding. Temporary occlusion is preferable in most trauma arterial embolization scenarios. Thus, in these cases, gelfoam blocks can be cut and crafted into cubes or torpedoes for large vessel occlusion [8]. However, in large vessels, such as the splenic artery, metallic coils are required. These coils may be used as scaffolding, in conjunction with other coils or gelfoam, particularly in patients with coagulopathy [8, 70]. Additionally, coils must be used in scenarios where a high degree of precision is required, such as near a major branch point [70]. Aside from trauma, GI hemorrhage can result from ulcers, vascular abnormalities, inflammatory diseases, and cancer [71, 72]. These lesions can include a variety of vessel sizes, and thus, the full spectrum of embolization agents including coils, particles, and liquid embolics may be used [71, 73, 74].

1.5 Developmental Liquid Embolic Agents

As previously discussed, liquid embolization agents have various problems including poor tissue responses often resulting in necrosis, risk of catheter entrapment, and limited injection rates. An embolic agent that avoids both the

reactive monomers used in cyanoacrylate-based embolics and DMSO employed in precipitating systems could offer better handling characteristics and fewer adverse tissue reactions while improving distal penetration. The key design challenge in developing liquid embolics is to provide a low-viscosity formulation for delivery through long, narrow catheters while providing a setting mechanism for occlusion at the site of delivery. Many researchers have recognized this clinical need and sought to develop water-borne liquid embolic agents. The setting mechanism for most of these approaches fall into two distinct categories: single component systems that display inverse temperature sensitivity and two component systems that solidify upon mixing. However, both setting mechanisms have significant impediments to clinical use as liquid embolic agents for embolizing small vessels.

The first approach has been to create embolic agents that solidify response to temperature changes. Most polymers have increased solubility at higher temperatures. However, certain hydrophobic polymers have a lower critical solution temperature (LCST) above which they become insoluble. At temperatures below the LCST, water forms a highly ordered structure around the hydrophobic moieties, which solvates the polymer [75]. This solvation involves the formation of enthalpically favorable hydrogen bonds. As the temperature of the solution is increased above the LCST, these hydrogen bonds are broken as solution entropy becomes dominant [75]. Stripped of their solvating water shell, the hydrophobic moieties coalesce and precipitate from solution.

Inverse temperature sensitive polymers for use as embolic agents are

liquids at room temperature and have a lower critical solution temperature near 37°C. Polymers containing *N*-isopropylacrylamide (NIPAM) are the most well-characterized inverse thermosensitive polymers in the literature. This has resulted in the use of several NIPAM copolymers as experimental embolic agents [76-78]. Poloxomers are triblock copolymers of poly(ethylene oxide) (PEO) and polypropylene oxide (PPO), p(PEO-b-PPO-b-PEO), some of which exhibit inverse thermosensitivity [79]. Raymond et. al. developed temporary liquid embolic agents by forming a slurry with poloxomer-407 and nonionic contrast media. Finally, Poursaid et. al. developed embolic agents made from silk-elastinlike protein polymers, which exhibit an irreversible temperature transition upon desolvation of elastinlike domains [80]. While many of these agents have demonstrated promising results *in vivo*, the temperature sensitive gelling mechanism represents a problem in a clinical scenario. In these settings, embolic agents must be delivered by small catheters, which are often 1 mm in diameter and up to 1.5 meters long. Because of the high surface area to volume ratio within the catheter, these agents will reach 37°C almost instantaneously while still inside the catheter, causing premature setting.

A second approach has been to create two component systems. Separately, each component is soluble in aqueous solution; when the two components are mixed, an insoluble gel is formed. The most prominent example of this type of system is a mixture comprised of calcium and alginate, which Becker et. al. first reported on in 2000 [81]. This system utilized a specialized dual lumen catheter to deliver the alginate and Ca^{2+} solutions to the embolization size

separately [81, 82]. Gore commercially acquired this system in 2006, but results from initiated phase I clinical trials have never been published [33]. In another system, Momeni et. al. used simple solutions of inorganic polyphosphate which were coacervated *in situ* with the divalent metal ions calcium, barium, and strontium. This system also requires a dual lumen delivery device that can generate mixing at the embolization site [83]. These systems present two main problems. If the diameter of the already small catheters is halved to create these dual lumen catheters, it will create a 16-fold increase in pressure (r^4 dependence) to inject the embolic at the same rate, creating injectability problems. Second, the gelation of these systems is dependent upon complete mixing of the two components. Blood is more viscous than water and flows past the catheter tip in a laminar fashion. This will make it difficult to ensure good mixing upon delivery and effective setting. Finally, other two component systems have been designed that can be mixed prior to entering the catheter, such as the carboxymethyl chitosan-oxidized carboxymethyl cellulose system developed by Weng et. al. [84]. These systems have setting mechanisms that are slow and are decoupled from the process of entering the blood stream. These agents carry the risk of occluding the catheter, if injected too slowly, and crossing into venous circulation, if delivered too rapidly.

1.6 Motivation For This Work

Complex coacervates have properties well suited to solving current problems with liquid embolic agents. This concentrated fluid morphology of

oppositely charged polyelectrolytes (PEs) has a totally water-borne composition, which can eliminate the intraarterial injection of organic solvents. Furthermore, polyelectrolyte complexes (PECs), including coacervates, have the ability to transform along a spectrum of morphologies, from liquid to solid, in response to external stimuli [85, 86]. That is, these materials can be designed with setting/hardening mechanisms based on solution conditions such as temperature, pH, presence of specific ions, or ionic strength [6, 85, 87]. In addition, coacervates have several properties which have led to their use as underwater adhesives and biomaterials: low water miscibility, low interfacial tension with water (facilitates spreading), ability to adhere to wet surfaces and dimensional stability upon injection into water [88]. In one example, these materials have been used for sealing iatrogenic fetal membrane defects [89]. Based upon these properties, embolic coacervates (ECs) were designed which transition from liquid to solid when injected into the blood vessel, in response to a decrease in ionic strength. This composition and setting mechanism are explained in more detail in the following sections.

1.7 Adhesive of the Marine Sandcastle Worm

The inspiration behind the use of coacervates as adhesive biomaterials, and, ultimately this work, came from examining the undersea adhesive of the sandcastle worm (*Phragmatopoma californica*). Living in turbulent coastal environments, colonies of these worms build massive reef-like structures by gluing together grains of sand and mineral particles one at a time. This is accomplished

with a multipart adhesive that sets upon exposure to seawater [4, 88]. The sandcastle worm adhesive is largely composed of polyelectrolytic macromolecules, which are electrostatically condensed into secretory granules. The proteins within the glue are comprised of 40-50% ionizable amino acids, including lysine, histidine, and phosphorylated serine, which are segregated into different proteins. After deployment, the adhesive transitions from a liquid precursor to a solid-liquid foam in a two-step process, responding to external stimuli. First, with exposure to seawater (pH>8), there is an increase in pH from the internal environment (pH<6). This, coupled with a change in ionic composition, drastically decreases the solubility of the highly phosphorylated proteins, and induces a phase transition which produces the initial set of the glue. Slowly, over the course of a few hours, the glue is covalently crosslinked by the catechol oxidase enzyme. The final structure adhesive is a solid-liquid closed cell foam. The pores within this foam may contribute to the overall mechanical strength and toughness of the glue [4]. While, in the classical sense, coacervation is no longer thought to play a major role in this natural adhesive, the condensed polyelectrolyte packaging, setting mechanisms, and structure can still be mimicked by coacervate based systems for biomedical applications [4, 6, 85, 88].

1.8 Coacervates as Liquid Embolization Agents

1.8.1 Coacervation

When added together in solution, oppositely charged polyelectrolytes (PEs) can form a variety of associative morphologies [86]. These range from stable

colloidal suspensions, such as polymer-nucleic acid polyplexes used in gene delivery [90], to solid precipitates used in production of layer-by-layer films [91]. In between, within a narrow range of solution ionic strength, pH, temperature, PE charge densities, and charge stoichiometry, certain PEs can condense and undergo macroscopic liquid-liquid phase separation [92]. This phenomenon was first described by Bungenberg de Jong et. al. and named complex coacervation, which distinguishes it from liquid-liquid phase separation involving a single polymer [93, 94]. With coacervation, a PE rich, amorphous dense phase is formed and exists in equilibrium with a PE-depleted supernatant phase. Complex coacervation differs from formation of solid ionic gels in that the interactions between PE chains in a coacervate are fluid, allowing for rapid dynamic exchange; whereas, in an ionic gel, these interactions are kinetically arrested [95]. This fluidity results from a high content of water and small ions within the coacervate phase [86, 96, 97]. Overbeek and Voorn introduced a theory of complex coacervation in 1957, which combined electrostatic attractions using Debye-Hückel theory and mixing entropy described by Flory-Huggins theory [92, 95]. While Voorn-Overbeek theory and subsequent extensions provide adequate descriptions of many systems, certain key observations remain unaddressed in this theory [95]. Growing evidence points to the importance of counterion release entropy as a dominating factor for association of oppositely charged PEs [92, 98]. Additionally, properties of the PEs involved and ion-specific interactions also greatly determine properties of a system [99, 100].

1.8.2 Ionic Strength Dependent Morphologies of Associated Polyelectrolytes

Perhaps the greatest determinant of phase behavior and properties of associated PE systems is ionic strength. In many PE systems, changing ionic strength causes the system to transition from a single-phase aqueous polymer solution in high salt, to a phase-separated, fluid complex coacervate in intermediate salt, and eventually transitioning into a solid at low ionic strength [86, 101]. Wang et. al. demonstrated this ionic strength dependent morphology for polyelectrolyte complexes (PECs) of poly(styrene sulfonate) (PSS) and poly(diallyldimethylammonium) (PDADMA). Within the coacervate region of this system, a continuum of rheological properties was observed, as a nonlinear increase in viscosity occurred as the salt concentration was decreased. Ultimately, the system underwent a transition from a viscously dominated coacervate (fluid-like) behavior to a precipitate, which displayed predominantly elastic character [86]. Moreover, these transitions were reversible with the addition or removal of salt, further demonstrating that salt concentration in phase separated PECs exists in an equilibrium between the dilute and concentrated phase [86, 97]. These changes were attributed to doping the PEC with monovalent ions. This salt doping process involves interrupting intrinsic ion pairs that form between oppositely charged PEs with small ions [102]. In a salt free system, no monovalent ions are present within the PEC, and 100% of the monomers on PEs are paired with a monomer of opposite charge. This results in interactions that are kinetically trapped, forming a solid [86, 95]. As salt is introduced to the system, the

monovalent ions begin to form ion pairs with a certain fraction of monomers, breaking up interactions between PEs. Since these interactions are in a state of dynamic equilibrium, the PEC gradually becomes more fluid as salt doping increases. The monovalent ions also bring in additional water molecules through increased osmotic pressure, further serving to plasticize the interactions between PEs [103]. Finally, once the system reaches a high enough ionic strength, all interactions between oppositely charged PEs are disrupted and the complex is solvated, forming a single-phase solution [86, 103].

1.8.3 Control of PEC Morphological Changes in Response to Salt

In engineering materials based upon these ionic strength dependent morphology changes in PE systems, understanding the design parameters that influence these phase transitions is key. As previously discussed, these PE systems can undergo two separate phase transitions with decreasing salt concentration, first from solution to coacervate (SC) and then from coacervate to precipitate (CP). Chollakup et. al. studied the effect of molecular weight (MW) on these transitions in a system of polyacrylic acid (PAA) and polyallylamine (PAH). In this study, it was concluded that MW of the larger PE greatly affected the salt concentration at which the CP phase transition occurred, with MW of the smaller PE component having a much smaller effect on this transition. However, as the salt concentration was increased, the MW of the smaller species ultimately determined the stability of the coacervate phase and the salt concentration at

which the SC phase transition was observed. With the size of the PAH fixed, increasing the molecular weight of the PAA from 1.8 kg/mol to 72 kg/mol increased this critical salt concentration from ~0.4 M to 3 M. In addition, these studies defined the role of charge stoichiometry in these phase transitions. At 1:1 charge ratio, the coacervate region was favored; that is, the critical salt concentration was lowered for the CP transition and increased for the SC transition in comparison to non-stoichiometric ratios [101, 104]. In other studies, increased charge density (moles of charge per gram of polymer) has also been shown increase the critical salt concentration at which the SC phase transition occurs [105].

In addition to PE properties, the chemical properties of the ions in the solution cause them to interact differently with the PE species, thus affecting these transitions. Ghostine et. al. investigated the incorporation of several anions (within the Hofmeister series) into complexes of PSS and PDADMA. The investigation revealed that weakly hydrated chaotrophic anions, such as thiocyanate and iodide, were more efficiently included in the complex than well-hydrated kosmotrophs, such as acetate and fluoride. This effect was attributed to an increased loss in entropy when a more hydrated ion entered the complex [102]. Perry et. al. examined the effects of specific cations and anions on the SC phase transition in systems of PAA and PAH [106]. Divalent salts such as calcium chloride were much more effective at suppressing coacervation (SC transition), even when considering the overall ionic strength of the solution. In addition, a less-pronounced effect was noted with the Hofmeister series. Chaotrophic ions tended to decrease the critical salt concentration while kosmotrophs were observed to increase this concentration

(favoring phase separation) [106]. This is agreement with the work done by Ghostine and suggest that weakly hydrated ions tend to better interact with the PEs and suppress the formation of coacervates [102]. The effects of ion hydration on the PC transition would likely be similar. Weakly hydrated ions are more readily taken up in a PEC [107], thus disrupting interactions between PEs and increasing the salt concentration at which the PC transition occurs.

1.8.4 Design of Embolic Coacervates with Novel Setting Mechanism

The approach presented here capitalizes on the ionic strength dependent morphologies of associated PEs and is depicted in Figure 1.1. For these condensed PE systems, cationic guanidinium-containing polymers, both natural and synthetic, are used in conjunction with anionic oligophosphates. Embolic coacervates (ECs) of these strongly associating PEs are produced in high concentrations of sodium chloride (>1 M). While still a coacervate, these systems are just below the salt concentration for the SC phase transition. Resultantly, the coacervates contain a high concentration of Na^+ and Cl^- ions. These ions shield most of the interactions between the oppositely charged guanidium and phosphate sidechains, producing a low-viscosity injectable formulation. When injected into a lower-ionic strength environment, such as a blood vessel (~150 mM), Na^+ and Cl^- ions are free to diffuse across in and out of the coacervate. As the salt concentration within the polyelectrolyte complex decreases, water becomes excluded, and the electrostatic interactions become less shielded by monovalent

ions, allowing increased intrinsic ion pairing between the PEs. This produces a phase transition of the complex from a liquid coacervate to a solid ionic gel, thereby occluding the blood vessel. To some degree, this setting mechanism mirrors that of precipitating liquid embolics but eliminates the used of organic solvents in favor of a totally water-borne composition. In precipitating systems, EVOH is dissolved in DMSO, a “good” solvent. Upon injection into the blood vessel, the DMSO diffuses away leaving copolymer in an aqueous environment (i.e., a “poor” solvent) and producing a precipitate. The high salt and water content of ECs are a “good” solvent for the PEs, while the low ionic strength environment represents a “poor” solvent and causes precipitation of the PEC.

1.8.5 Embolic Coacervates as Drug Delivery Vehicles

In the final chapter of this dissertation, ECs were loaded with an antiangiogenic drug, sunitinib malate, to prevent aggressive revascularization of embolized tissues, especially hypervascular tumors. This work is driven by another property of coacervates: the ability to encapsulate and release a wide variety of substrates. Coacervate-based encapsulation allows for the concentration and protection of proteins, nucleic acids, small molecules, and lipophilic compounds in a purely aqueous environment [108]. This loading can be facilitated by electrostatic interactions, preferential partitioning based upon differential solubility between coacervate and aqueous phases, and specific interactions between PEs and encapsulated solutes. Coacervates have been used in food science to encapsulate lipophilic compounds such as omega-3 fatty acids, polyphenolic compounds, and

various peptides [109]. More recently, the partitioning of aromatic dyes into coacervates made from adenosine triphosphate and PDADMA have revealed that these molecules are enriched 9-7200 fold in the coacervate phase [110]. This preferential partitioning into the coacervate phase is driven by differential solubility, electrostatic interactions, and aromatic π-π interactions [110, 111]. Naturally, these properties have facilitated their use as drug delivery vehicles, both for biomacromolecules and small molecules. Coacervates are often used for small molecules to overcome poor solubility of hydrophobic drugs [108]. Coacervate-based PECs for small molecule drug delivery have included chitosan/o-carboxymethyl chitosan for doxorubicin [112], gelatin coacervates for salbutamol sulfate, and alginate-chitosan for tamoxifen [113].

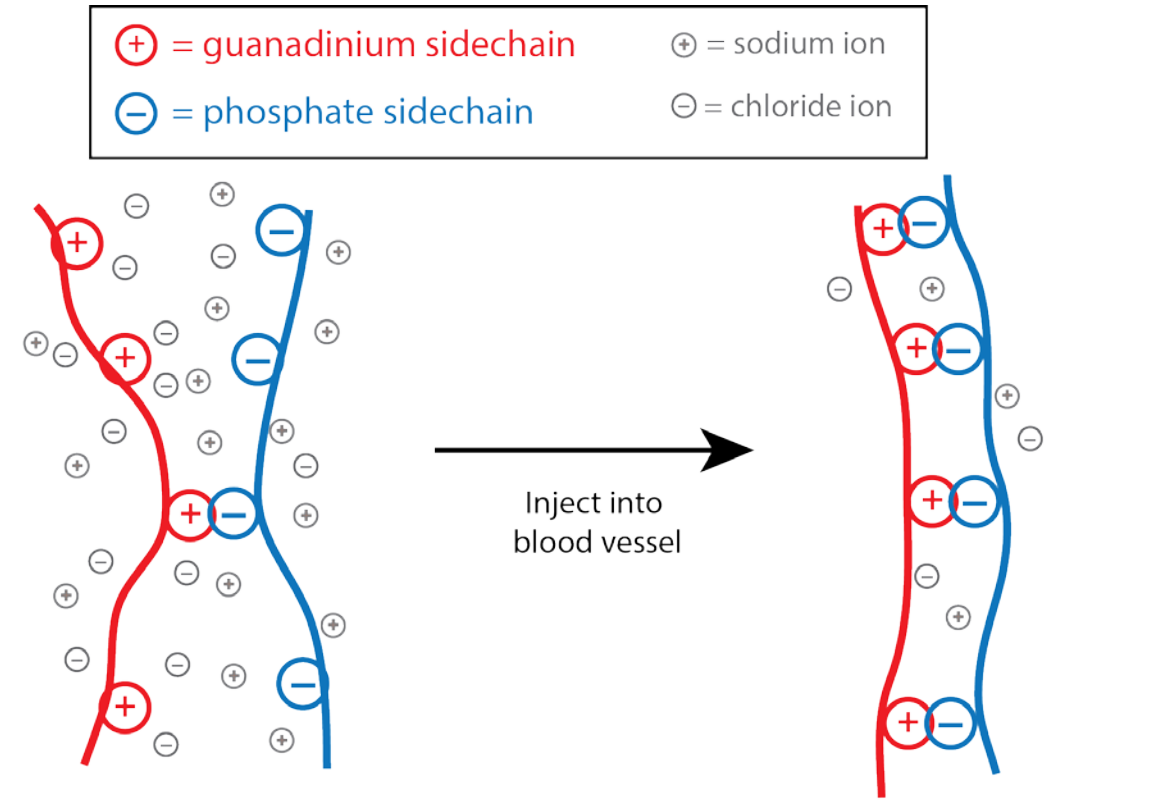

Liquid embolic coacervate:
High ionic strength (>1 M)

- PE interactions largely shielded by monovalent ions.
- Clear homogeneous fluid
- Relatively low viscosity

Ionic gel:
Low ionic strength (~150 mM)

- Monovalent ions diffuse away allowing increased ion pairing between oppositely charged PE sidechains
- Non-flowing solid

Figure 1.1. Ionic strength dependent setting mechanism. Embolic coacervates are formulated into a low-viscosity injectable form in high concentrations of sodium chloride. Upon injection, monovalent ions diffuse away causing the complex to stiffen into a solid ionic gel.

1.9 References

[1] C.S. Wang, K.K. Svendsen, R.J. Stewart, Morphology of the adhesive system in the sandcastle worm, Phragmatopoma californica, Biological Adhesive Systems, Springer 2010, pp. 169-179.

[2] C.S. Wang, R.J. Stewart, Localization of the bioadhesive precursors of the sandcastle worm, Phragmatopoma californica (Fewkes), J. Exp. Biol. 215(2) (2012) 351-361.

[3] C.S. Wang, R.J. Stewart, Multipart copolyelectrolyte adhesive of the sandcastle worm, *Phragmatopoma californica* (Fewkes): catechol oxidase catalyzed curing through peptidyl-DOPA, Biomacromolecules 14(5) (2013) 1607-1617.

[4] R.J. Stewart, C.S. Wang, I.T. Song, J.P. Jones, The role of coacervation and phase transitions in the sandcastle worm adhesive system, Adv. Colloid Interface Sci. 239 (2017) 88-96.

[5] M.J. Stevens, R.E. Steren, V. Hlady, R.J. Stewart, Multiscale structure of the underwater adhesive of Phragmatopoma californica: A nanostructured latex with a steep microporosity gradient, Langmuir 23(9) (2007) 5045-5049.

[6] H. Shao, R.J. Stewart, Biomimetic underwater adhesives with environmentally triggered setting mechanisms, Adv. Mater. 22(6) (2010) 729-733.

[7] J. Rösch, C.T. Dotter, M.J. Brown, Selective arterial embolization: A new method for control of acute gastrointestinal bleeding 1, Radiology 102(2) (1972) 303-306.

[8] M. Lubarsky, C.E. Ray, B. Funaki, Embolization agents—Which one should be used when? Part 1: Large-vessel embolization, Semin. Intervent. Radiol. 26(4) (2009) 352-357.

[9] D.M. Coldwell, K.R. Stokes, W.F. Yakes, Embolotherapy: Agents, clinical applications, and techniques, Radiographics 14(3) (1994) 623-643.

[10] M. Lubarsky, C. Ray, B. Funaki, Embolization agents—Which one should Be used when? Part 2: Small-vessel embolization, Semin. Intervent. Radiol. 27(1) (2010) 99-104.

[11] A. Medsinge, A. Zajko, P. Orons, N. Amesur, E. Santos, A case-based approach to common embolization agents used in vascular interventional radiology, Am. J. Roentgenol. 203(4) (2014) 699-708.

[12] S. Vaidya, K.R. Tozer, J. Chen, An overview of embolic agents, Semin. Intervent. Radiol. 25(3) (2008) 204-215.

[13] R. Loffroy, B. Guiu, J.-P. Cercueil, D. Krausé, Endovascular therapeutic embolisation: An overview of occluding agents and their effects on embolised tissues, Curr. Vasc. Pharmacol. 7(2) (2009) 250-263.

[14] I.M. Germano, R.L. Davis, C.B. Wilson, G.B. Hieshima, Histopathological follow-up study of 66 cerebral arteriovenous malformations after therapeutic embolization with polyvinyl alcohol, J. Neurosurg. 76(4) (1992) 607-614.

[15] A. Laurent, Microspheres and nonspherical particles for embolization, Tech. Vasc. Interv. Radiol. 10(4) (2007) 248-256.

[16] R.J. Rosen, S. Contractor, The use of cyanoacrylate adhesives in the management of congenital vascular malformations, Semin. Intervent. Radiol. 21(1) (2004) 59-66.

[17] J.S. Pollak, R.I. White, The use of cyanoacrylate adhesives in peripheral embolization, J. Vasc. Interv. Radiol. 12(8) (2001) 907-913.

[18] G.M. Debrun, V.A. Aletich, H. Shownkeen, J. Ausman, Glued catheters during embolisation of brain AVMs with acrylic glue, Interv. Neuroradiol. 3(1) (1997) 13-19.

[19] M. Brothers, J. Kaufmann, A. Fox, J. Deveikis, N-Butyl 2-cyanoacrylate--Substitute for IBCA in interventional neuroradiology: Histopathologic and polymerization time studies, Am. J. Neuroradiol. 10(4) (1989) 777-786.

[20] A. Gruber, P.R. Mazal, G. Bavinzski, M. Killer, H. Budka, B. Richling, Repermeation of partially embolized cerebral arteriovenous malformations: A clinical, radiologic, and histologic study, Am. J. Neuroradiol. 17(7) (1996) 1323-1331.

[21] S.K. Natarajan, D. Born, B. Ghodke, G.W. Britz, L.N. Sekhar, Histopathological changes in brain arteriovenous malformations after embolization using Onyx or N-butyl cyanoacrylate: Laboratory investigation, J. Neurosurg. 111(1) (2009) 105-113.

[22] H. Vinters, K. Galil, M. Lundie, J. Kaufmann, The histotoxicity of cyanoacrylates, Neuroradiology 27(4) (1985) 279-291.

[23] W. Taki, Y. Yonekawa, H. Iwata, A. Uno, K. Yamashita, H. Amemiya, A new liquid material for embolization of arteriovenous malformations, Am. J. Neuroradiol. 11(1) (1990) 163-168.

[24] A.S. Puri, R. Rahbar, J. Dearden, R.J. Graham, C. Lillehei, D.B. Orbach, Stretched and sheared microcatheter retained after Onyx embolization of infantile myofibromatosis, Interv. Neuroradiol. 17(2) (2011) 261-266.

[25] F. Mottu, A. Laurent, D.A. Rüfenacht, E. Doelker, Organic solvents for pharmaceutical parenterals and embolic liquids: a review of toxicity data, PDA J. Pharm. Sci. Technol. 54(6) (2000) 456-469.

[26] K.C. Wright, R.J. Greff, R.E. Price, Experimental evaluation of cellulose acetate NF and ethylene-vinyl alcohol copolymer for selective arterial embolization, J. Vasc. Interv. Radiol. 10(9) (1999) 1207-1218.

[27] R. Rautio, A. Haapanen, Transcatheter embolization of a renal artery aneurysm using ethylene vinyl alcohol copolymer, Cardiovasc. Intervent. Radiol. 30(2) (2007) 300-303.

[28] M. Guimaraes, M. Wooster, Onyx (ethylene-vinyl alcohol copolymer) in peripheral applications, Semin. Intervent. Radiol. 28(3) (2011) 350-356.

[29] S.L. Blackburn, Y. Kadkhodayan, W.Z. Ray, G.J. Zipfel, D.T. Cross, C.J. Moran, C.P. Derdeyn, Onyx is associated with poor venous penetration in the treatment of spinal dural arteriovenous fistulas, J. Neurointerv. Surg. 6(7) (2014) 536-540.

[30] A.M. Spiotta, R.F. James, S.R. Lowe, J. Vargas, A.S. Turk, M.I. Chaudry, T. Bhalla, R.M. Janjua, J.J. Delaney, S. Quintero-Wolfe, Balloon-augmented Onyx embolization of cerebral arteriovenous malformations using a dual-lumen balloon: A multicenter experience, J. Neurointerv. Surg. 7(10) (2015) 721-727.

[31] J.C. Chaloupka, F. Viñuela, H.V. Vinters, J. Robert, Technical feasibility and histopathologic studies of ethylene vinyl copolymer (EVAL) using a swine endovascular embolization model, Am. J. Neuroradiol. 15(6) (1994) 1107-1115.

[32] R. Jahan, Y. Murayama, Y. Pierre Gobin, G.R. Duckwiler, H.V. Vinters, F. Viñuela, Embolization of arteriovenous malformations with Onyx: Clinicopathological experience in 23 patients, Neurosurgery 48(5) (2001) 984-997.

[33] A. Poursaid, M.M. Jensen, E. Huo, H. Ghandehari, Polymeric materials for embolic and chemoembolic applications, J. Controlled Release 240 (2016) 414-433.

[34] N. Koçer, H. Hanımoğlu, Ş. Batur, S.G. Kandemirli, O. Kızılkılıç, Z. Sanus, B. Öz, C. Işlak, M.Y. Kaynar, Preliminary experience with precipitating hydrophobic injectable liquid in brain arteriovenous malformations, Diagn. Interv. Radiol. 22(2) (2016) 184-189.

[35] J.J. Leyon, S. Chavda, A. Thomas, S. Lamin, Preliminary experience with the liquid embolic material agent PHIL (Precipitating Hydrophobic Injectable Liquid) in treating cranial and spinal dural arteriovenous fistulas: Technical note, J. Neurointerv. Surg. 8(6) (2016) 596.

[36] D.F. Vollherbst, C.M. Sommer, C. Ulfert, J. Pfaff, M. Bendszus, M.A. Möhlenbruch, Liquid embolic agents for endovascular embolization: Evaluation of an established (Onyx) and a novel (PHIL) embolic agent in an *in vitro* AVM model, Am. J. Neuroradiol. (2017).

[37] I. Linfante, A.K. Wakhloo, Brain aneurysms and arteriovenous malformations advancements and emerging treatments in endovascular embolization, Stroke 38(4) (2007) 1411-1417.

[38] Y. Murayama, F. Viñuela, S. Tateshima, F. Viñuela Jr, Y. Akiba, Endovascular treatment of experimental aneurysms by use of a combination of liquid embolic agents and protective devices, Am. J. Neuroradiol. 21(9) (2000) 1726-1735.

[39] D.Y. Sze, J.S. Kao, J.K. Frisoli, S.W. McCallum, W.A. Kennedy, M.K. Razavi, Persistent and recurrent postsurgical varicoceles: Venographic anatomy and treatment with *N*-butyl cyanoacrylate embolization, J. Vasc. Interv. Radiol. 19(4) (2008) 539-545.

[40] C. Giavroglou, H. Economou, I. Ioannidis, Arterial embolization of giant hepatic hemangiomas, Cardiovasc. Intervent. Radiol. 26(1) (2003) 92-96.

[41] K.Y. Tam, K.C. Leung, Y.X. Wang, Chemoembolization agents for cancer treatment, Eur. J. Pharm. Sci. 44(1-2) (2011) 1-10.

[42] R.M. Friedlander, Arteriovenous malformations of the brain, New Engl. J. Med. 356(26) (2007) 2704-2712.

[43] J. Van Beijnum, H.B. Van Der Worp, D.R. Buis, R.A.-S. Salman, L.J. Kappelle, G.J. Rinkell, J.W.B. Van Der Sprenkel, W.P. Vandertop, A. Algra, C.J. Klijn, Treatment of brain arteriovenous malformations: A systematic review and meta-analysis, J. Am. Med. Assoc. 306(18) (2012) 2011-2019.

[44] Robert F. Spetzler, Neil A. Martin, A proposed grading system for arteriovenous malformations, J. Neurosurg. 65(4) (1986) 476-483.

[45] G. Austin, S. Fisher, D. Dickson, D. Anderson, S. Richardson, The significance of the extracellular matrix in intracranial aneurysms, Ann. Clin. Lab. Sci. 23(2) (1993) 97-105.

[46] Coil Embolization for Intracranial Aneurysms: An Evidence-Based Analysis, Ontario Health Technology Assessment Series, Medical Advisory Secretariat, 2006, pp. 1-114.

[47] W.I. Schievink, Intracranial aneurysms, New Engl. J. Med. 336(1) (1997) 28-40.

[48] R.M. Greenhalgh, J.T. Powell, Endovascular repair of abdominal aortic aneurysm, New Engl. J. Med. 358(5) (2008) 494-501.

[49] W.C. Krupski, C.H. Selzman, R. Floridia, P.K. Strecker, M.R. Nehler, T.A. Whitehill, Contemporary management of isolated iliac aneurysms, J. Vasc. Surg. 28(1) (1998) 1-13.

[50] I. Dawson, R.B. Sie, J.H. van Bockel, Atherosclerotic popliteal aneurysm, Br. J. Surg. 84(3) (1997) 293-299.

[51] M. Chadha, C. Ahuja, Visceral artery aneurysms: Diagnosis and percutaneous management, Semin. Intervent. Radiol. 26(3) (2009) 196-206.

[52] P.U. Reber, A.G. Patel, E. Stauffer, M.F. Müller, D.D. Do, H.W. Kniemeyer, Mural aortic thrombi: An important cause of peripheral embolization, J. Vasc. Surg. 30(6) (1999) 1084-1089.

[53] H. Saruhan Cekirge, Isil Saatci, Serdar Geyik, Kivilcim Yavuz, Halil Öztürk, Gülsün Pamuk, Intrasaccular combination of metallic coils and Onyx liquid embolic agent for the endovascular treatment of cerebral aneurysms, J. Neurosurg. 105(5) (2006) 706-712.

[54] M. Parildar, I. Oran, A. Memis, Embolization of visceral pseudoaneurysms with platinum coils and N-butyl cyanoacrylate, Abdom. Imaging 28(1) (2003) 36-40.

[55] R.L. Vanninen, I. Manninen, Onyx, a new liquid embolic material for peripheral interventions: Preliminary experience in aneurysm, pseudoaneurysm, and pulmonary arteriovenous malformation embolization, Cardiovasc. Intervent. Radiol. 30(2) (2007) 196-200.

[56] S.D. Simon, E. Eskioglu, A. Reig, R.A. Mericle, Endovascular treatment of side wall aneurysms using a liquid embolic agent: A US single-center prospective trial, Neurosurgery 67(3) (2010) 855-860.

[57] S.F. Altekruse, K.A. McGlynn, M.E. Reichman, Hepatocellular carcinoma incidence, mortality, and survival trends in the United States from 1975 to 2005, J. Clin. Oncol. 27(9) (2009) 1485-1491.

[58] Z.V. Fong, K.K. Tanabe, The clinical management of hepatocellular carcinoma in the United States, Europe, and Asia: A comprehensive and evidence-based comparison and review, Cancer 120(18) (2014) 2824-2838.

[59] A. Raza, G.K. Sood, Hepatocellular carcinoma review: current treatment, and evidence-based medicine, World J. Gastroenterol. 20(15) (2014) 4115-4127.

[60] C. Cha, Y. Fong, W.R. Jarnagin, L.H. Blumgart, R.P. DeMatteo, Predictors and patterns of recurrence after resection of hepatocellular carcinoma, J. Am. Coll. Surg. 197(5) (2003) 753-758.

[61] C.D. Gadaleta, G. Ranieri, Trans-arterial chemoembolization as a therapy for liver tumours: New clinical developments and suggestions for combination with angiogenesis inhibitors, Crit. Rev. Oncol./Hematol. 80(1) (2011) 40-53.

[62] L. Bester, B. Meteling, D. Boshell, T.C. Chua, D.L. Morris, Transarterial chemoembolisation and radioembolisation for the treatment of primary liver cancer and secondary liver cancer: A review of the literature, J. Med. Imaging Radiat. Oncol. 58(3) (2014) 341-352.

[63] A.D. Talenfeld, A.K. Sista, D.C. Madoff, Transarterial therapies for primary liver tumors, Surg. Oncol. Clin. N. Am. 23(2) (2014) 323-351.

[64] S.C. Goodwin, J.B. Spies, Uterine fibroid embolization, New Engl. J. Med. 361(7) (2009) 690-697.

[65] M. Aubuchon, A.B. Pinto, D.B. Williams, Treatment of uterine fibroids, Prim. Care Update Ob. Gyns. 9(6) (2002) 231-237.

[66] G.P. Siskin, M. Englander, B.F. Stainken, J. Ahn, K. Dowling, E.G. Dolen, Embolic agents used for uterine fibroid embolization, Am. J. Roentgenol. 175(3) (2000) 767-773.

[67] J. Rabkin, V. Astafjev, L. Gothman, Y. Grigorjev, Transcatheter embolization in the management of pulmonary hemorrhage, Radiology 163(2) (1987) 361-365.

[68] E. Soncini, A. Pelicelli, P. Larini, C. Marcato, D. Monaco, A. Grignaffini, Uterine artery embolization in the treatment and prevention of postpartum hemorrhage, Int. J. Gynaecol. Obstet. 96(3) (2007) 181-185.

[69] N.P. Christensen, D.S. Smith, S.L. Barnwell, M.K. Wax, Arterial embolization in the management of posterior epistaxis, Otolaryngol. Head Neck Surg. 133(5) (2005) 748-753.

[70] J.E. Lopera, Embolization in trauma: Principles and techniques, Semin. Intervent. Radiol. 27(1) (2010) 14-28.

[71] R.S. Ramaswamy, H.W. Choi, H.C. Mouser, K.H. Narsinh, K.C. McCammack, T. Treesit, T.B. Kinney, Role of interventional radiology in the management of acute gastrointestinal bleeding, World J. Radiol. 6(4) (2014) 82-92.

[72] S. Boonpongmanee, D.E. Fleischer, J.C. Pezzullo, K. Collier, W. Mayoral, F. Al-Kawas, R. Chutkan, J.H. Lewis, T.L. Tio, S.B. Benjamin, The frequency of peptic ulcer as a cause of upper-GI bleeding is exaggerated, Gastrointest. Endosc. 59(7) (2004) 788-794.

[73] R. Loffroy, L. Estivalet, V. Cherblanc, D. Sottier, B. Guiu, J.-P. Cercueil, D. Krausé, Transcatheter embolization as the new reference standard for endoscopically unmanageable upper gastrointestinal bleeding, World J. Gastrointest. Surg. 4(10) (2012) 223-227.

[74] L. Defreyne, P. Vanlangenhove, M. De Vos, P. Pattyn, G. Van Maele, J. Decruyenaere, R. Troisi, M. Kunnen, Embolization as a first approach with endoscopically unmanageable acute nonvariceal gastrointestinal hemorrhage, Radiology 218(3) (2001) 739-748.

[75] B. Jeong, S.W. Kim, Y.H. Bae, Thermosensitive sol–gel reversible hydrogels, Adv. Drug Del. Rev. 64 (2012) 154-162.

[76] Y. Matsumaru, A. Hyodo, T. Nose, S. Ito, T. Hirano, S. Ohashi, Application of thermosensitive polymers as a new embolic material for intravascular neurosurgery, J. Biomater. Sci. Polym. Ed. 7(9) (1996) 795-804.

[77] X. Li, W. Liu, G. Ye, B. Zhang, D. Zhu, K. Yao, Z. Liu, X. Sheng, Thermosensitive *N*-isopropylacrylamide–*N*–propylacrylamide-vinyl pyrrolidone terpolymers: Synthesis, characterization and preliminary application as embolic agents, Biomaterials 26(34) (2005) 7002-7011.

[78] H.H. Bearat, M.C. Preul, B.L. Vernon, Cytotoxicity, *in vitro* models and preliminary i*n vivo* study of dual physical and chemical gels for endovascular embolization of cerebral aneurysms, J. Biomed. Mater. Res. 101(9) (2013) 2515-2525.

[79] J. Raymond, A. Metcalfe, I. Salazkin, A. Schwarz, Temporary vascular occlusion with poloxamer 407, Biomaterials 25(18) (2004) 3983-3989.

[80] A. Poursaid, R. Price, A. Tiede, E. Olson, E. Huo, L. McGill, H. Ghandehari, J. Cappello, *In situ* gelling silk-elastinlike protein polymer for transarterial chemoembolization, Biomaterials 57 (2015) 142-152.

[81] T.A. Becker, D.R. Kipke, T. Brandon, Calcium alginate gel: a biocompatible and mechanically stable polymer for endovascular embolization, J. Biomed. Mater. Res. 54(1) (2001) 76-86.

[82] T.A. Becker, M.C. Preul, W.D. Bichard, D.R. Kipke, C.G. McDougall, Calcium alginate gel as a biocompatible material for endovascular arteriovenous malformation embolization: Six-month results in an animal model, Neurosurgery 56(4) (2005) 793-801.

[83] A. Momeni, E.M. Valliant, E.P. Brennan-Pierce, J.J.S. Shankar, R. Abraham, P. Colp, M.J. Filiaggi, Developing an *in situ* forming polyphosphate coacervate as a new liquid embolic agent: From experimental design to pilot animal study, Acta Biomater. 32 (2016) 286-297.

[84] L. Weng, N. Rostambeigi, N.D. Zantek, P. Rostamzadeh, M. Bravo, J. Carey, J. Golzarian, An *in situ* forming biodegradable hydrogel-based embolic agent for interventional therapies, Acta Biomater. 9(9) (2013) 8182-8191.

[85] H. Shao, K.N. Bachus, R.J. Stewart, A water-borne adhesive modeled after the sandcastle glue of P. californica, Macromol. Biosci. 9(5) (2009) 464-471.

[86] Q. Wang, J.B. Schlenoff, The polyelectrolyte complex/coacervate continuum, Macromolecules 47(9) (2014) 3108-3116.

[87] S. Kaur, G.M. Weerasekare, R.J. Stewart, Multiphase adhesive coacervates inspired by the sandcastle worm, ACS Appl. Mater. Interfaces 3(4) (2011) 941-944.

[88] R.J. Stewart, C.S. Wang, H. Shao, Complex coacervates as a foundation for synthetic underwater adhesives, Adv. Colloid Interface Sci. 167(1) (2011) 85-93.

[89] L.K. Mann, R. Papanna, K.J. Moise, R.H. Byrd, E.J. Popek, S. Kaur, S.C. Tseng, R.J. Stewart, Fetal membrane patch and biomimetic adhesive coacervates as a sealant for fetoscopic defects, Acta Biomater. 8(6) (2012) 2160-2165.

[90] J.H. Jeong, S.W. Kim, T.G. Park, Molecular design of functional polymers for gene therapy, Prog. Polym. Sci. 32(11) (2007) 1239-1274.

[91] N.A. Kotov, I. Dekany, J.H. Fendler, Layer-by-layer self-assembly of polyelectrolyte-semiconductor nanoparticle composite films, J. Phys. Chem. 99(35) (1995) 13065-13069.

[92] D. Priftis, N. Laugel, M. Tirrell, Thermodynamic characterization of polypeptide complex coacervation, Langmuir 28(45) (2012) 15947-15957.

[93] E. Kizilay, A.B. Kayitmazer, P.L. Dubin, Complexation and coacervation of polyelectrolytes with oppositely charged colloids, Adv. Colloid Interface Sci. 167(1) (2011) 24-37.

[94] H. Bungenberg de Jong, H. Kruyt, Coacervation (partial miscibility in colloid systems), Proc. Koninklijke Nederlandse Akademie Wetenschappen 32 (1929) 849-856.

[95] C.E. Sing, Development of the modern theory of polymeric complex coacervation, Adv. Colloid Interface Sci. 239 (2017) 2-16.

[96] A.B. Kayitmazer, Thermodynamics of complex coacervation, Adv. Colloid Interface Sci. 239 (2017) 169-177.

[97] C.G. De Kruif, F. Weinbreck, R. de Vries, Complex coacervation of proteins and anionic polysaccharides, Curr. Opin. Colloid Interface Sci. 9(5) (2004) 340-349.

[98] J. Fu, H.M. Fares, J.B. Schlenoff, Ion-pairing strength in polyelectrolyte complexes, Macromolecules 50(3) (2017) 1066-1074.

[99] J. Fu, J.B. Schlenoff, Driving forces for oppositely charged polyion association in aqueous solutions: Enthalpic, entropic, but not electrostatic, J. Am. Chem. Soc. 138(3) (2016) 980-990.

[100] S.L. Perry, L. Leon, K.Q. Hoffmann, M.J. Kade, D. Priftis, K.A. Black, D. Wong, R.A. Klein, C.F. Pierce III, K.O. Margossian, J.K. Whitmer, J. Qin, J.J. de Pablo, M. Tirrell, Chirality-selected phase behaviour in ionic polypeptide complexes, Nature Commun. 6 (2015) 6052.

[101] R. Chollakup, W. Smitthipong, C.D. Eisenbach, M. Tirrell, Phase behavior and coacervation of aqueous poly (acrylic acid)− poly (allylamine) solutions, Macromolecules 43(5) (2010) 2518-2528.

[102] R.A. Ghostine, R.F. Shamoun, J.B. Schlenoff, Doping and diffusion in an extruded saloplastic polyelectrolyte complex, Macromolecules 46(10) (2013) 4089-4094.

[103] H.H. Hariri, A.M. Lehaf, J.B. Schlenoff, Mechanical properties of osmotically stressed polyelectrolyte complexes and multilayers: Water as a plasticizer, Macromolecules 45(23) (2012) 9364-9372.

[104] R. Chollakup, J.B. Beck, K. Dirnberger, M. Tirrell, C.D. Eisenbach, Polyelectrolyte molecular weight and salt effects on the phase behavior and coacervation of aqueous solutions of poly(acrylic acid) sodium salt and poly(allylamine) hydrochloride, Macromolecules 46(6) (2013) 2376-2390.

[105] A. Kayitmazer, A. Koksal, E.K. Iyilik, Complex coacervation of hyaluronic acid and chitosan: Effects of pH, ionic strength, charge density, chain length and the charge ratio, Soft Matter 11(44) (2015) 8605-8612.

[106] S. Perry, Y. Li, D. Priftis, L. Leon, M. Tirrell, The effect of salt on the complex coacervation of vinyl polyelectrolytes, Polymers 6(6) (2014) 1756.

[107] J.B. Schlenoff, A.H. Rmaile, C.B. Bucur, Hydration contributions to association in polyelectrolyte multilayers and complexes: Visualizing hydrophobicity, J. Am. Chem. Soc. 130(41) (2008) 13589-13597.

[108] S.L. Perry, W.C. Blocher, Complex coacervate-based materials for biomedicine, Wiley Interdiscip. Rev. Nanomed. Nanobiotechnol. 9(4) (2016) e1442.

[109] M.A. Augustin, L. Sanguansri, Challenges and solutions to incorporation of nutraceuticals in foods, Annu. Rev. Food Sci. Technol. 6 (2015) 463-477.

[110] D.S. Williams, S. Koga, C.R.C. Hak, A. Majrekar, A.J. Patil, A.W. Perriman, S. Mann, Polymer/nucleotide droplets as bio-inspired functional micro-compartments, Soft Matter 8(22) (2012) 6004-6014.

[111] T.-Y.D. Tang, M. Antognozzi, J.A. Vicary, A.W. Perriman, S. Mann, Small-molecule uptake in membrane-free peptide/nucleotide protocells, Soft Matter 9(31) (2013) 7647-7656.

[112] C. Feng, Z. Wang, C. Jiang, M. Kong, X. Zhou, Y. Li, X. Cheng, X. Chen, Chitosan/o-carboxymethyl chitosan nanoparticles for efficient and safe oral anticancer drug delivery: *In vitro* and *in vivo* evaluation, Int. J. Pharm. 457(1) (2013) 158-167.

[113] A. Martinez, P. Arana, A. Fernández, R. Olmo, C. Teijón, M. Blanco, Synthesis and characterisation of alginate/chitosan nanoparticles as tamoxifen controlled delivery systems, J. Microencaps. 30(4) (2013) 398-408.

CHAPTER 2

WATER-BORNE ENDOVASCULAR EMBOLICS INSPIRED BY THE UNDERSEA ADHESIVE OF MARINE SANDCASTLE WORMS

Materials Views
www.MaterialsViews.com

ADVANCED HEALTHCARE MATERIALS
www.advhealthmat.de

FULL PAPER

Water-Borne Endovascular Embolics Inspired by the Undersea Adhesive of Marine Sandcastle Worms

*Joshua P. Jones, Monika Sima, Ryan G. O'Hara, and Russell J. Stewart**

Transcatheter embolization is used to treat vascular malformations and defects, to control bleeding, and to selectively block blood supply to tissues. Liquid embolics are used for small vessel embolization that require distal penetration. Current liquid embolic agents have serious drawbacks, mostly centered around poor handling characteristics and toxicity. In this work, a water-borne in situ setting liquid embolic agent is described that is based on electrostatically condensed, oppositely charged polyelectrolytes–complex coacervates. At high ionic strengths, the embolic coacervates are injectable fluids that can be delivered through long narrow microcatheters. At physiological ionic strength, the embolic coacervates transition into a non-flowing solid morphology. Transcatheter embolization of rabbit renal arteries demonstrated capillary level penetration, homogeneous occlusion, and 100% devascularization of the kidney, without the embolic crossing into venous circulation. The benign water-borne composition and setting mechanism avoids many of the problems of current liquid embolics, and provides precise temporal and spatial control during endovascular embolization.

1. Introduction

The first reported transcatheter embolization was performed in 1972 to stop bleeding from a duodenal hemorrhage using an autologous clot.[1] Since then, development of embolic agents has advanced significantly and clinical applications have expanded to include, among others, the occlusion of arteriovenous malformations (AVMs),[2,3] occlusion of arterial aneurysms,[4] control of gastrointestinal bleeding,[5,6] control of traumatic bleeding,[7] treatment of postsurgical varicoceles,[8] devascularization of head and neck tumors,[9] and chemoembolization of solid organ tumors.[10] The choice of embolic agent for a particular application is determined by the size of the vessel to be occluded, whether the occlusion is intended to be temporary or permanent, and the intended survival of the tissues supplied by the target vessel.[11] For large vessel occlusion, commonly used embolic agents include thrombosing metallic coils and plugs, plastic particles, gelatin microspheres, and gelatin foam.[11,12] Small vessels are generally occluded with liquid embolic agents that provide distal penetration into capillaries.[13]

A major design challenge of developing liquid embolics is to provide a low viscosity formulation for delivery through long, narrow catheters and a setting mechanism for permanent occlusion at the site of delivery. The simplest liquid embolics are schlerosants—alcohols and detergents that, on contact, chemically damage the endothelial lining of the vessel, leading to localized thromboembolization.[14,15] With these agents, permanent occlusion relies on natural scarring. Another approach has been to use alkyl cyanoacrylates, low viscosity liquid resins that rapidly polymerize into hard adhesives on contact with anions present in body fluids at the delivery site. Transarterial delivery of *N*-butyl-2-cyanoacrylate (NBCA, TruFill) has been approved for the treatment of cerebral AVMs since 2000. Because NBCA is adhesive and occludes blood vessels immediately and permanently, one of its drawbacks is the risk of inadvertently gluing the delivery catheter into the embolization site.[16] A third design approach has been to dissolve a water-soluble, biocompatible copolymer, ethylene vinyl alcohol (pEVOH), in a water-miscible organic solvent, dimethyl sulfoxide (DMSO), for low viscosity delivery (Onyx, PHIL). Upon contact with aqueous bodily fluids at the delivery site, the DMSO diffuses out and the copolymer precipitates into a solid mass to provide permanent, localized occlusion.[17] An advantage of precipitated pEVOH is that it is nonadhesive, which allows longer injection times and reduces the risk of catheter entrapment compared to NBCA. On the other hand, DMSO is toxic and can cause vasospasm, tissue necrosis, and pain if injected too rapidly, which limits the delivery rate to 0.3 mL min^{-1}, and it creates a foul taste that can persist for days.[18–20] The slow delivery rate and rapid setting makes it difficult to control forward flow and penetration with Onyx.[21,22] Furthermore, the DMSO-borne embolics can be used only with specialized catheters that are not weakened or degraded by exposure to the organic solvent.

In this report, we describe an alternate approach to creating in situ setting endovascular embolic agents, an approach that originated from investigations of the undersea adhesive of sandcastle worms. The natural adhesive is packaged and stored

J. P. Jones, M. Sima, Prof. R. J. Stewart
Department of Bioengineering
University of Utah
Salt Lake City, UT 84112, USA
E-mail: russell.stewart@utah.edu
MD R. G. O'Hara
Department of Radiology
University of Utah School of Medicine
Salt Lake City, UT 84112, USA

DOI: 10.1002/adhm.201500825

ADVANCED HEALTHCARE MATERIALS
www.advhealthmat.de

www.MaterialsViews.com

as sets of oppositely charged polyelectrolytes (PEs) condensed into complex fluids.[23–25] Within seconds of secretion from the adhesive gland, the fluid adhesive hardens into a solid–liquid foam.[26] The transition in morphology is triggered by changes in pH, as well as ionic composition and concentrations when the fluid adhesive is exposed to seawater.[27] The in situ setting embolic coacervates described herein were designed to mimic the polyelectrolyte composition, condensed fluid form, and environmentally triggered setting/hardening mechanism of the natural sandcastle glue.

In aqueous solution, sets of oppositely charged water-soluble PEs electrostatically associate and condense into several morphologies that range, depending on the solution conditions, from stable colloidal suspensions of polyelectrolyte complexes to solid precipitates or ionic hydrogels.[28] In between, within a narrow range of solution conditions, some pairs of oppositely charged PEs condense into a concentrated fluid morphology known as a complex coacervate.[29,30] Within the spectrum of morphologies in which identical compositions of PEs can exist, the phase separated fluid morphology has several ideal characteristics for use as underwater adhesives: density greater than water, relatively low viscosity for injection, low interfacial tension with water that presents a minute energetic barrier to creating new interfacial contact area on wet substrates, adhesion to wet surfaces, low water miscibility that prevents rapid dissolution into surrounding water, and dimensional stability when submerged—they do not swell by absorbing water, a severe limitation of crosslinked hydrogel-based materials.[31]

The morphology of a given set of PEs is determined by solution conditions that affect the positive to negative charge ratio and the strength of electrostatic interactions, conditions that include pH, temperature, dielectric constant, and ionic strength, which determines the degree of counterion shielding between PE charges. The morphology can be transformed along the spectrum, from fluid to solid, for example, by changing solution conditions, including the concentration of monovalent counterions.[27,29] The oppositely charged PEs used in this study are phase-separated adhesive fluids—complex coacervates—at ionic strengths higher than physiological ionic strength, but insoluble adhesive gels at physiological ionic strength. When the fluid, high ionic strength adhesive coacervates are introduced into a low ionic strength environment, the fluid transitions into an adhesive gel as the ionic strength decrease. Introduced into a blood vessel through a transarterial catheter, the high ionic strength coacervates do not mix with blood, adhere strongly to the blood vessel walls, and solidify as the ionic strength decreases toward physiological ionic strength, thereby occluding the blood vessel. The embolic coacervates were tested in vivo by acute embolization of rabbit renal arteries.

2. Results

2.1. Formation of Phase Separated Embolic Coacervates

Polycationic salmine sulfate and polyanionic sodium inositol hexaphosphate, also known as phytic acid, were chosen as the polyelectrolytes (PEs) because both are commercially available in pharmaceutical grade. Salmine sulfate is a protamine salt purified from salmon sperm. Protamines are densely charged, strongly basic proteins that condense chromatin into the sperm head during spermatogenesis.[32] Arginine comprises 21 of the 32 amino acids of salmine (Sal).[33] Phytic acid, also known as inositol hexaphosphate (IP_6), is a natural constituent of plants, particularly as a storage form of phosphate in seeds, and an intracellular signaling molecule in animals. To determine the optimum PE ratio to maximize the yield of the condensed PE phase, Sal and IP_6 solutions in 150×10^{-3} M NaCl, pH 7.2, were mixed at positive to negative charge ratios ranging from 6:1 to 1:6. Charge ratios were estimated assuming the guanidinyl sidechains of Sal were fully charged at pH 7.2 based on their 13.8 pK_a.[34] The charge density of IP_6, a weak polyanion, is strongly dependent on pH in the physiological range. IP_6 was estimated to have eight negative charges at pH 7.2 based on published acid-base titrations.[35] At high and low charge ratios the volume of condensed phase decreased significantly. The condensed phase volume distribution was centered around the 1:1 charge ratio as expected.[30] Therefore, a charge ratio of 1:1 was used to prepare all subsequent complex coacervates.

Shrinking or swelling of the liquid form during the transition to the solid form was investigated by adding 100 µL of the liquid 1200×10^{-3} M NaCl complex coacervate phase, prepared with a 1:1 charge ratio, into 1.0 mL of 150×10^{-3} M NaCl. After 24 h, the volume of the condensed phase shrank an average of 3.0% ($n = 3$) during solidification.

2.2. Flow Behavior versus Ionic Strength

The morphology of the Sal-IP_6 compositions was adjusted from nonflowing solids to liquids by increasing the NaCl concentration, which weakened the phosphate–guanidinium charge interaction (**Figure 1**). At 1200×10^{-3} M NaCl, Sal-IP_6 formed clear, homogeneous, fluid complex coacervates. With decreasing NaCl, the compositions transitioned to a gel-like state, and at 150×10^{-3} M NaCl were nonflowing solids. The viscosity of the compositions at 37 °C were determined as a function of ionic strength at a shear rate of 0.02 s^{-1} (**Figure 2**A). To provide X-ray contrast under a fluoroscope, 30 wt% tantalum (Ta) metal powder was added to the salmine sulfate solution before mixing with IP_6. The viscosity of the Ta-containing materials increased by more than an order of magnitude, from 1.1 to 39.7 Pa s, going from 1200×10^{-3} to 150×10^{-3} M NaCl. Addition of micronized Ta increased the viscosity approximately 50%, 56.8 versus 39.7 Pa s, in 150×10^{-3} M NaCl. Flow curves for Sal-IP_6 with and without 30 wt% Ta in 1200×10^{-3} M NaCl were generated by measuring the viscosity as the shear rate was swept from 0.01 to 500 s^{-1} (**Figure 3**B). Compositions containing Ta were 5–6 times more viscous than those without at very low shear rates, and displayed reversible shear thinning. Without Ta, the compositions were nearly Newtonian.

2.3. Injection Pressures

For transarterial delivery through long, narrow catheters, injection pressures must be below the burst pressure of the catheter system and within the physical limits of the operator to provide

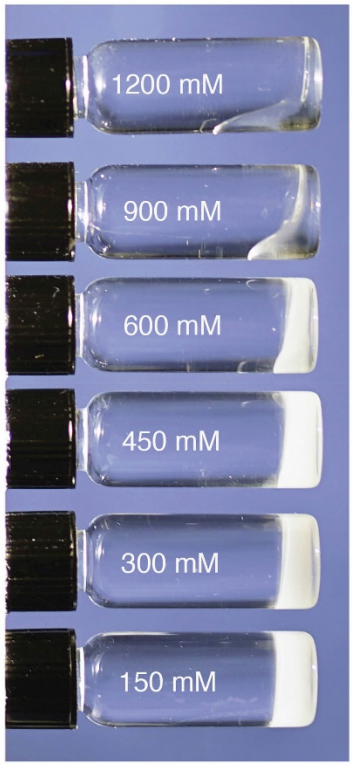

Figure 1. Morphologies of condensed Sal-IP_6 as a function of NaCl concentration. The compositions transition from liquids at high ionic strength to stiff gels at physiological ionic strength.

accurate control. The steady-state pressure at several flow rates in 3F and 5F catheters were compared to predicted pressures calculated from the measured viscosity of Sal- IP_6 with and without Ta in 1200×10^{-3} M NaCl (Figure 3). As expected, the injection pressure increased linearly with flow rate. The injection pressures with the 5F catheter were less than 20% higher than predicted by Pouseille's equation for steady laminar flow in a round tube. The injection pressures with the 3F catheter were up to 70% higher than predicted. At 0.5 mL min^{-1}, the injection force was approximately 9-fold higher in the 3F model than the 5F, while predicted from the r^{-4} dependence to be 6.8-fold higher.

2.4. Rabbit Kidney Embolization

Rabbit kidneys are a convenient model for in vivo testing of liquid embolics for small vessel embolization.[18] The procedure for preparing the injectable embolic coacervates is diagrammed in **Figure 4**. Phase separation begins immediately upon mixing sterile solutions of Sal + Ta and IP_6 in 1.2 M NaCl. The condensed Ta containing fluids were allowed to equilibrate at 22 °C for 24 h. On the day of the procedure, 0.6 mL of the dense phase was transferred aseptically into a sterile 1 mL syringe (4.8 mm bore diameter). Vascular access to the renal artery was gained through the femoral artery using a 0.014″ guide wire, over which a 135 cm 2.8 F microcatheter was introduced and positioned in the renal artery 1.5 cm from the first arterial branch. The catheter was prefilled with a sterile solution of 1.2 M NaCl before the embolic containing syringe was attached to the hub of the catheter. Approximately 0.3 mL of the Sal-IP_6 embolic agent was delivered into the kidney under fluoroscopy within ≈15 s, after which the catheter was withdrawn from the renal artery without applying negative pressure. No additional embolic agent left the catheter during withdrawal. No changes in breathing, or heart rate, or evidence of pain occurred during or after the injection.

The Sal-IP_6 embolic coacervate was observed by fluoroscopy to penetrate into the fine branching blood vessels of the entire renal arterial vasculature. No changes in the position or opaqueness of the embolic coacervate were observed during fluoroscopic observation for 90 min post injection (**Figure 5A**). Digital subtraction angiography with an iodine contrast agent (Omnipaque) showed complete occlusion of the left kidney (Figure S1, Supporting Information). Postmortem, complete and uniform embolization of the renal arteries was confirmed using in

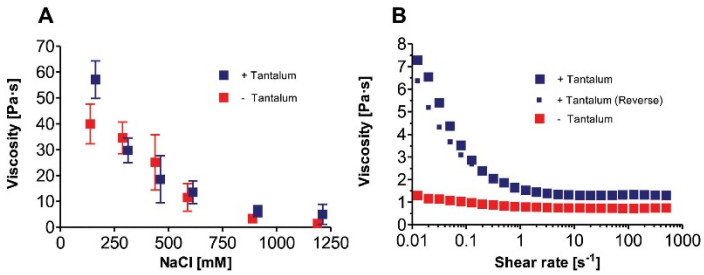

Figure 2. Viscosity and flow behavior of Sal-IP_6. A) Viscosity as a function of NaCl concentration at 37 °C at a constant shear rate of 0.02 s^{-1} (error bars represent ±1 s.d., $n = 3$). B) Flow curves in 1.2 M NaCl, at 37 °C, with and without Ta.

ADVANCED HEALTHCARE MATERIALS
www.advhealthmat.de
www.MaterialsViews.com

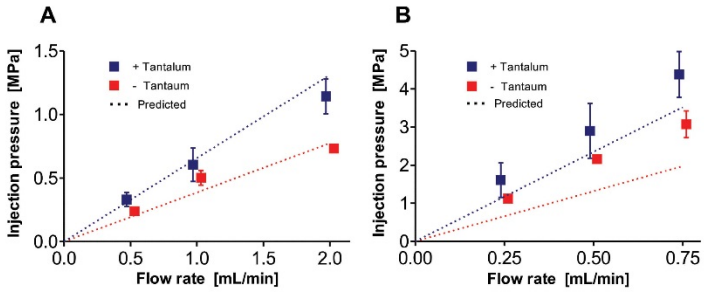

Figure 3. Injection pressure as a function of flow rate of Sal-IP_6 in 1.2 M NaCl. A) 5F catheter. B) 3F catheter. Dashed lines are injection pressures predicted from high shear rate viscosities.

3D reconstructions of fluorographic images (Figure 5B, and Figure S3, Supporting Information). Embolic agent was not observed outside of the embolization site. At the end of the experiment, the embolic coacervate was injected retrograde into the femoral artery, near the access site, before complete withdrawal of the catheter to block blood flow. The artery was fully occluded and no bleeding occurred from the access site when the catheter was withdrawn (not shown).

2.5. Histological Evaluation

The embolized kidney was excised postmortem, fixed in 10% formalin, embedded in paraffin, and sectioned for histological evaluation. Complete occlusion of arterial vessels, including arterioles, was evident throughout the renal cortex (**Figure 6**A). At higher magnification, penetration of the embolic coacervate into the capillaries of the glomeruli was apparent (Figure 6B,C). The embolic coacervate cast to the dimensions of the blood vessels with no evidence of significant in situ shrinking or swelling after delivery. Importantly, the embolic agent did not penetrate into the venous side of the renal cortex, or into the renal ducts (Figure 6C, and Figure S4, Supporting Information). Red blood cell lysis, disruption of the vascular endothelium, or adverse tissue reactions were not observed.

3. Discussion

The design of the in situ setting embolics described herein exploited both the condensed polyelectrolyte composition and environmentally triggered setting mechanism of the natural sandcastle glue. Numerous oppositely charged polyelectrolytes can be used as analogs of the natural sandcastle glue proteins to make waterborne underwater adhesives.[27,28,31] For endovascular embolic coacervates, salmine sulfate was chosen because of its long history in medical applications, including endovascular administration to reverse the anticoagulant effects of heparin.[36] Complexed with insulin (NPH insulin), salmine has been subcutaneously self-injected since 1936.[37] Likewise, IP_6 is a food additive that is generally recognized as safe (GRAS) by the FDA. Significantly, either component administered individually is quickly eliminated from blood. Salmine sulfate is eliminated from the blood stream with a half-life of approximately 5 min.[38] IP_6 is synthesized by mammalian cells as an intracellular signaling molecule, with intracellular concentrations in

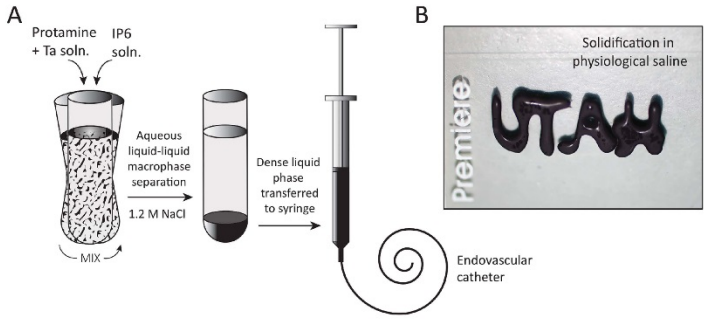

Figure 4. A) Schematic diagram of injectable in situ setting Sal-IP_6 embolic coacervate preparation. The black embolic contains 30 wt% micronized Ta powder for radiopacity. B) The radiopaque, high ionic strength, low viscosity fluid rapidly solidified into a stable gel when ejected onto a 1 × 3 in. Premiere brand microscope slide (for scale) under physiological saline.

Materials Views
www.MaterialsViews.com

ADVANCED HEALTHCARE MATERIALS
www.advhealthmat.de

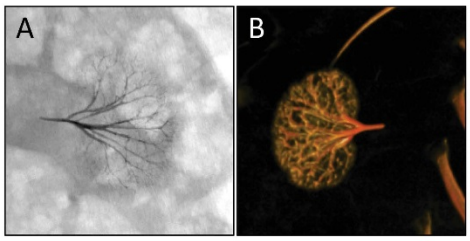

Figure 5. Embolized rabbit kidney. A) Ventral fluoroscope image 90 min after arterial embolization. B) Postmortem dorsal 3D image.

the (10–50) × 10^{-6} M range.[39] However, IP_6 is undetectable in normal human plasma, and when added to plasma is rapidly eliminated, likely by a plasma phosphatase.[40] The stabilities of the salmine complexed with IP_6 in the injected fluid and trapped solidified gel forms of the embolic agent are greater than the individual components, but longer term stability remains to be evaluated in future animal experiments. The rapid clearance of the individual components suggests that limited escape of the embolic components may be inconsequential.

The water-borne composition of the electrostatically condensed embolic coacervates will not require special syringes and catheters. More importantly, it eliminates the need for toxic solvents to control the viscosity and fluidity of the embolic agent. To decrease the viscosity and increase the setting time of Onyx, additional DMSO is added to dilute the EVOH copolymer, exasperating the potentially adverse effect of the solvent. In contrast, the viscosity of the embolic coacervates can be adjusted by changing the salinity of the composition; increasing the NaCl concentrations decreases the viscosity (Figure 2). The safety profile of endovascular injection of high concentrations of NaCl is well known. Bolus intravenous injections of hypertonic saline, some as high as 30% (5 M) but most commonly 7.5% (1.28 M) are used to treat several conditions, such as increasing blood pressure after traumatic shock, with no reported adverse long-term effects.[41,42] In this study, 1.2 M NaCl (7.2%) was sufficient to achieve delivery through a 2.8 F, 135 cm microcatheter with excellent capillary penetration. Normal plasma Na^+ concentrations are (135–145) × 10^{-3} M. Rapid injection of even several mLs of the 1.2 M NaCl embolic coacervate would have an insignificant effect of the Na^+ concentration in the ≈5 L of blood in a typical adult human. Furthermore, no adverse systemic effects were observed during injection, or in the kidney tissue during histological examination (Figure 6).

The pressure required to inject liquid embolics must not exceed the burst pressure of the catheter and must be within the physical limits of the operator. The measured pressures required for injection through the 5F catheter closely matched predictions, while the pressure in the 3F catheters were higher than predicted. At the same flow rate, the pressure in the 3F is predicted to be 6.8× higher than the 5F, whereas the measured difference was 9× higher. The discrepancy is likely due to adhesion of a thin layer of the coacervate to the catheter wall, which would have a greater effect on pressure in the narrower catheter. Nevertheless, microcatheters with rated burst pressures of 5–6 MPa are common, and the embolic coacervates were well within this pressure limit at reasonably high flow rates through both the 3F and 5F catheters. The average force that can be applied using a palmar pinch grip syringe is 23.4 lbs (104.1 N) for men and 16.3 lbs. (72.2 N) for women.[43] Using a standard 1 mL syringe, the force needed to inject the embolic coacervate through a 5F catheter at high flow rates (2 mL min^{-1}) is within the capabilities of all endovascular surgeons. The force required for the 3F catheter at high flow rates, ≈20 lbs, would be challenging for some surgeons. The viscosity can be reduced by increasing the NaCl concentration. Or, the pressure exerted on the fluid can be increased by using a smaller bore syringe; reducing the bore diameter from 4.8 to 3.2 mm would decrease the force by half.

An ideal embolic agent for capillary-level occlusion would be capable of deep penetration into the capillary bed of the target tissue while providing well-controlled distal flow to prevent nontarget embolism, or over-injection into the venous circulation. For preoperative devascularization of tumors, deep tumor penetration is more effective at controlling intraoperative bleeding than simple proximal embolization.[44] Likewise, treatment of brain AVMs is more effective if the embolic fully penetrates into the nidus.[45] Although NCBA glues provide excellent penetration for these applications, they are difficult to control because the rapid polymerization requires that the injection be performed quickly and continuously once started, which diminishes precision of delivery.[44] The catheter must be drawn back

Figure 6. Histology of embolized rabbit renal arteries. A) Low magnification cross-section through the cortex. The scattered black dots (arrows) are occluded arterioles. B) Higher magnification reveals occlusion of glomeruli capillaries (white arrow). C) The embolic coacervate was not present in venules or urine ducts (black arrows).

ADVANCED HEALTHCARE MATERIALS
www.advhealthmat.de
www.MaterialsViews.com

immediately after injection to prevent entrapment in the blood vessel. On the other hand, distal penetration of Onyx may be limited by the slow delivery rate required to minimize DMSO vasotoxicity. Reports are mixed on the effectiveness of Onyx for deep penetration of small blood vessels.[21,44,46] Poor distal flow of Onyx can cause reflux around the catheter tip leading to non-target embolization and, in rare cases, entrapment of the catheter in the blood vessel.[47] Some surgeons deliberately create a proximal plug around the catheter tip to prevent retrograde reflux, others have combined Onyx with balloon catheters to prevent reflux. [4,22,48]

In comparison, the embolic coacervates penetrated the entire arterial vasculature of a live rabbit kidney when the delivery catheter was positioned in the main renal artery ≈1.5 cm from the first primary branch (Figure 5). The embolic entered all renal artery branches equally, and uniformly penetrated into the deepest capillaries of the renal cortex, a total distance of as much as 4 cm. Because the solidification mechanism depends on the diffusion of NaCl out of the embolic, the embolic coacervate will not harden inside the catheter. The embolic therefore can be delivered discontinuously, starting and stopping flow repeatedly with no danger of catheter entrapment. Selective embolization may be possible of multiple feeder arteries of a tumor without withdrawing the catheter. The retrograde sealing of the femoral artery after the procedure suggests that it may be possible to block several arterial feeders with a single injection from a single catheter position.[44]

4. Conclusions

Water-borne embolic coacervates, designed with condensed polyelectrolytes and ionic strength dependent viscosity and form, proved effective for deep distal penetration and 100% devascularization in acute renal embolization. The novel embolic agents have many of the flow and penetration advantages of both NCBA glues and pEVOH/DMSO liquid embolics, but few of their disadvantages. The embolic coacervates are promising agents for capillary-level occlusion of blood flow to prevent hemorrhage of vascular defects and malformations, to starve tumors, to control bleeding during tissue resection or trauma, which may extend and improve quality of human life.

5. Experimental Section

Materials: Protamine sulfate (PRT) from salmon sperm (USP Grade), salmine, was obtained from MP Biomedical Inc. Sodium inositol hexaphosphate (IP6), also known as phytic acid, was obtained from Sigma. Tantalum metal powder, 1–5 μm particle size, was obtained from Atlantic Equipment Engineers, Inc. Sodium chloride (USP Grade) was obtained from MP Biomedical Inc. Solutions were made in ultrapure water.

Preparation of Complex Coacervates: Salmine sulfate and IP_6 were dissolved in the desired final NaCl concentration (1200×10^{-3} M, unless otherwise noted) at 60 and 115 mg mL^{-1}, pH 7.2. Ta metal powder was added to the Sal solution to give a final concentration of 30 wt% in the condensed phase. The IP_6 and Sal/Ta solutions were mixed at a volume ratio of 1:4, resulting in a 1:1 ratio of positive to negative charges. The solution immediately turned turbid and a dense liquid macrophase (complex coacervate) settled out within an hour at 22 °C. The condensed liquid phase was separated and used as the injectable in situ solidifying complex coacervate (Figure 4).

Rheology: The flow behavior of Sal-IP_6 coacervates was characterized on a temperature controlled rheometer (AR 2000ex, TA Instruments) using a 20 mm, 4° cone geometry. A solvent trap prevented the sample from drying out during the experiment. Shear rate was stepped from 0.01 to 500 s^{-1} at 10 points per decade. Ta containing samples were run with forward and reverse shear rate sweeps. Viscosities were compared at a shear rate of 0.02 s^{-1}.

Injection Pressure: For pressure measurements, 23 gauge (3F) and 18 gauge (5F) needles were glued into 1 m lengths of PTFE tubing (Zeus Inc.) of 23 and 18 gauge, respectively. Coacervates made in 1.2 M NaCl were loaded into 1 mL syringes, warmed to 37 °C, and attached to the tubing. The tubing was placed in a 37 °C water bath and the coacervate was injected at the specified flow rates using a syringe pump (PHD Ultra, Harvard Apparatus). To measure injection forces, a compression load cell (iLoad Mini, Loadstar Sensors) was attached to the syringe pump between the driver and the syringe plunger. Steady state injection forces were measured and converted to pressure using the bore diameter of the syringe (4.8 mm). Injection pressures were predicted using Poiseuille's equation for steady laminar fluid flow in a tube of uniform diameter.

$$\Delta P = \frac{8Q\mu L}{\pi r^4} \quad (1)$$

where P is pressure, r is the radius of the tube, L is the length of the tube, Q is the volumetric flow rate, and μ is viscosity.

Rabbit Kidney Embolization: Animal experiments were carried out under an IACUC approved protocol, following University of Utah animal research guidelines. Complex coacervates were prepared with filter-sterilized salmine sulfate and IP_6 solutions and loaded aseptically into sterile 1 mL syringes (Medallion, Merit Medical Inc.). A New Zealand white female rabbit weighing 4.5 kg was kept in an environmentally controlled animal research facility. Food was offered once a day and water was provided ad libitum. The rabbit was first anesthetized with Isoflurane in an induction chamber, then intubated with an endotracheal tube (3.5 mm, Hudson/Sheridan). Once intubated, the rabbit was connected to an anesthetic machine (Drager Narkomed 2B) equipped for noninvasive monitoring, including an anesthetic gas analyzer, respiratory monitor (Ohmeda 5250 RGM), oximeter, thermometer, and Isoflurane vaporizer. An intravenous infusion of 0.9% saline solution (Baxter) was administered during the procedure.

All surgical procedures were performed under sterile conditions. The inner side of the right leg was shaved, and the incision site and surrounding skin was cleaned with 70% isopropyl alcohol and covered with surgical drapes. The artery was exposed with a 5 cm longitudinal incision. The location of the incision was determined by palpating the artery. The artery was isolated from the femoral nerve and vein by blunt dissection. Two 4.0 silk sutures were positioned under the artery and used to gently elevate the artery for access. Topical Lidocaine (2%, Hospira) was administered to decrease the vasospasm of the femoral artery during handling.

The femoral artery was accessed using a 4F access kit (Access Point Technologies, Inc.). A 135 cm, 2.8F microcatheter (Biomerics) was maneuvered from the femoral artery into the renal artery under fluoroscopy (C-arm 9800 series OEC Medical/GE medical). Omnipaque (Iohexol 240 mg mL^{-1}) was used as the X-ray contrast agent to visualize organs and blood vessels. Once the microcatether was positioned in the renal artery, Omnipaque diluted 1:1 with normal saline was injected to visualize the blood vessels of the kidney. The catheter was flushed with saline, then prefilled with 0.2 mL of hypersaline (7.2%, 1.2 M NaCl). The coacervate containing syringe was attached to the catheter and the embolic agent was injected into the renal artery under fluoroscopic observation. The animal was euthanized with Euthanasia solution (Vet One) 90 min after the embolization procedure. 15 min postmortem, the animal was scanned on an Axiom Artis dBA biplane angiography system (Siemens Inc.) to obtain a 3D image of the embolized kidney (Figure 5B).

Histology: During necropsy, the embolized kidney was surgically removed and fixed in 10% buffered formalin. After 2 d, the renal capsule was removed and the tissue was fixed for another 4 d. The tissue was embedded in paraffin, sectioned to 5 µm, and stained with Hematoxylin & Eosin.

Supporting Information

Supporting Information is available from the Wiley Online Library or from the author.

Acknowledgements

J.P.J. and M.S. contributed equally to this work. The authors thank Dr. Lawrence McGill for help with kidney histology. Funding from the Office of Naval Research (N00014-13-1-0577), the NIH (R01 HD75863), and the University of Utah, College of Engineering is gratefully acknowledged. The authors acknowledge they have no competing financial interests.

Received: October 12, 2015
Revised: November 30, 2015
Published online: January 25, 2016

[1] J. Rösch, C. T. Dotter, M. J. Brown, *Radiology* **1972**, *102*, 303.
[2] I. Linfante, A. K. Wakhloo, *Stroke* **2007**, *38*, 1411.
[3] W. J. van Rooij, M. Sluzewski, G. N. Beute, *Am. J. Neuroradiol.* **2007**, *28*, 172.
[4] Y. Murayama, F. Viñuela, S. Tateshima, Y. Akiba, *Am. J. Neuroradiol.* **2000**, *21*, 1726.
[5] R. Loffroy, *WJGS* **2012**, *4*, 223.
[6] F. Y. Yap, B. O. Omene, M. N. Patel, T. Yohannan, J. Minocha, M. G. Knuttinen, C. A. Owens, J. T. Bui, R. C. Gaba, *Dig. Dis. Sci.* **2013**, *58*, 1976.
[7] J. Lopera, *Semin. Intervent. Radiol.* **2010**, *27*, 014.
[8] D. Y. Sze, J. S. Kao, J. K. Frisoli, S. W. McCallum, W. A. Kennedy II, M. K. Razavi, *J. Vasc. Interv. Radiol.* **2008**, *19*, 539.
[9] M. A. Lazzaro, A. Badruddin, O. O. Zaidat, Z. Darkhabani, D. J. Pandya, J. R. Lynch, *Front Neurol.* **2011**, *2*, 64.
[10] K. Y. Tam, K. C.-F. Leung, Y.-X. J. Wang, *Eur. J. Pharm. Sci.* **2011**, *44*, 1.
[11] M. Lubarsky, C. E. Ray, B. Funaki, *Semin. Intervent. Radiol.* **2009**, *26*, 352.
[12] S. Vaidya, K. Tozer, J. Chen, *Semin. Intervent. Radiol.* **2008**, *25*, 204.
[13] M. Lubarsky, C. Ray, B. Funaki, *Semin. Intervent. Radiol.* **2010**, *27*, 99.
[14] D. M. Duffy, *Dermatol. Surg.* **2010**, *36*, 1010.
[15] Y. S. Do, W. F. Yakes, S. W. Shin, B.-B. Lee, D.-I. Kim, W. C. Liu, B. S. Shin, D.-K. Kim, S. W. Choo, I.-W. Choo, *Radiology* **2005**, *235*, 674.
[16] J. S. Pollak, R. I. White, *J. Vasc. Interv. Radiol.* **2001**, *12*, 907.
[17] W. Taki, Y. Yonekawa, H. Iwata, A. Uno, K. Yamashita, H. Amemiya, *Am. J. Neuroradiol.* **1990**, *11*, 163.
[18] K. C. Wright, R. J. Greff, R. E. Price, *J. Vasc. Interv. Radiol.* **1999**, *10*, 1207.
[19] F. Mottu, A. Laurent, D. A. Rufenacht, E. Doelker, *PDA J. Pharm. Sci. Technol.* **2000**, *54*, 456.
[20] M. Guimaraes, M. Wooster, *Semin. Intervent. Radiol.* **2011**, *28*, 350.
[21] S. L. Blackburn, Y. Kadkhodayan, W. Z. Ray, G. J. Zipfel, D. T. Cross, C. J. Moran, C. P. Derdeyn, *J. NeuroIntervent. Surg.* **2014**, *6*, 536.
[22] A. M. Spiotta, R. F. James, S. R. Lowe, J. Vargas, A. S. Turk, M. I. Chaudry, T. Bhalla, R. M. Janjua, J. J. Delaney, S. Quintero-Wolfe, R. D. Turner, *J. NeuroIntervent Surg.* **2015**, *7*, 721.
[23] C. S. Wang, K. K. Svendsen, R. J. Stewart, in *Biological Adhesive Systems* (Eds: J. von Beryn, I. Grunwald), Springer, Vienna **2010**, p. 169.
[24] C. S. Wang, R. J. Stewart, *J. Exp. Biol.* **2012**, *215*, 351.
[25] C.-S. Wang, R. J. Stewart, *Biomacromolecules* **2013**, *14*, 1607.
[26] M. J. Stevens, R. E. Steren, V. Hlady, R. J. Stewart, *Langmuir* **2007**, *23*, 5045.
[27] H. Shao, R. Stewart, *Adv. Mater.* **2010**, *22*, 729.
[28] H. Shao, K. N. Bachus, R. J. Stewart, *Macromol. Biosci.* **2009**, *9*, 464.
[29] Q. Wang, J. B. Schlenoff, *Macromolecules* **2014**, *47*, 3108.
[30] C. G. de Kruif, F. Weinbreck, R. de Vries, *Curr. Opin. Colloid Interface Sci.* **2004**, *9*, 340.
[31] R. J. Stewart, C. S. Wang, H. Shao, *Adv. Colloid Interface Sci.* **2011**, *167*, 85.
[32] H. E. Kasinsky, J. M. Eirin-Lopez, J. Ausio, *Protein Pept Lett* **2011**, *18*, 755.
[33] R. D. Moir, G. H. Dixon, *J. Mol. Evol.* **1988**, *27*, 8.
[34] C. A. Fitch, G. Platzer, M. Okon, B. E. Garcia-Moreno, L. P. McIntosh, *Protein Sci.* **2015**, *24*, 752.
[35] W. J. Evans, E. J. McCourtney, R. I. Shrager, *J. Am. Oil Chem. Soc.* **1982**, *59*, 189.
[36] L. B. Jaques, *Can. Med. Assoc. J.* **1973**, *108*, 1291.
[37] H. C. Hagedorn, B. N. Jensen, N. B. Krarup, I. Wodstrup, *JAMA, J. Am. Med. Assoc.* **1936**, *106*, 177.
[38] J. Butterworth, Y. A. Lin, R. C. Prielipp, J. Bennett, J. W. Hammon, R. L. James, *Ann. Thorac. Surg.* **2002**, *74*, 1589.
[39] A. J. Letcher, M. J. Schell, R. F. Irvine, *Biochem. J.* **2008**, *416*, 263.
[40] M. S. C. Wilson, S. J. Bulley, F. Pisani, R. F. Irvine, A. Saiardi, *Open Biol.* **2015**, *5*, 150014.
[41] G. F. Strandvik, *Anaesthesia* **2009**, *64*, 990.
[42] K. Järvelä, S. E. Honkonen, T. Järvelä, T. Kööbi, S. Kaukinen, *Anesth. Analg.* **2000**, *91*, 1461.
[43] V. Mathiowetz, N. Kashman, G. Volland, K. Weber, M. Dowe, S. Rogers, *Arch. Phys. Med. Rehabil.* **1985**, *66*, 69.
[44] P. Gore, N. Theodore, L. Brasiliense, L. J. Kim, *Neurosurgery* **2008**, *62*, 1204.
[45] C. Mounayer, N. Hammami, M. Piotin, L. Spelle, G. Benndorf, I. Kessler, J. Moret, *Am. J. Neuroradiol.* **2007**, *28*, 518.
[46] M. S. Elhammady, S. Q. Wolfe, R. Ashour, H. Farhat, R. Moftakhar, B. B. Lieber, M. A. Aziz-Sultan, *J. Neurosurg.* **2010**, *112*, 1039.
[47] A. S. Puri, R. Rahbar, J. Dearden, R. J. Graham, C. Lillehei, D. B. Orbach, *Interv. Neuroradiol.* **2011**, *17*, 261.
[48] J. C. Gentric, J. Raymond, A. Batista, I. Salazkin, G. Gevry, T. E. Darsaut, *Am. J. Neuroradiol.* **2015**, *36*, 977.

ADVANCED HEALTHCARE MATERIALS

Supporting Information

for *Adv. Healthcare Mater.*, DOI: 10.1002/adhm.201500825

Water-Borne Endovascular Embolics Inspired by the Undersea Adhesive of Marine Sandcastle Worms

*Joshua P. Jones, Monika Sima, Ryan G. O'Hara, and Russell J. Stewart**

Supplemental Figures

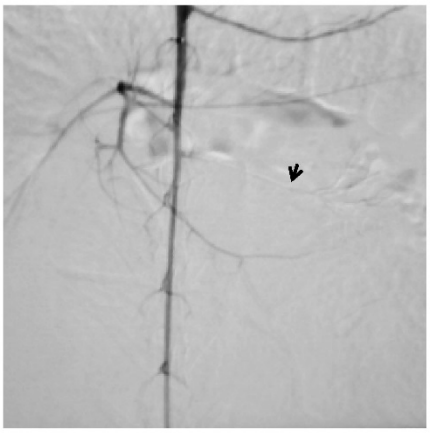

Supplemental figure 1. After renal embolization, injection of contrast agent verified complete occlusion of blood flow through the left renal artery and kidney vasculature. The black arrow indicates the beginning of the embolization.

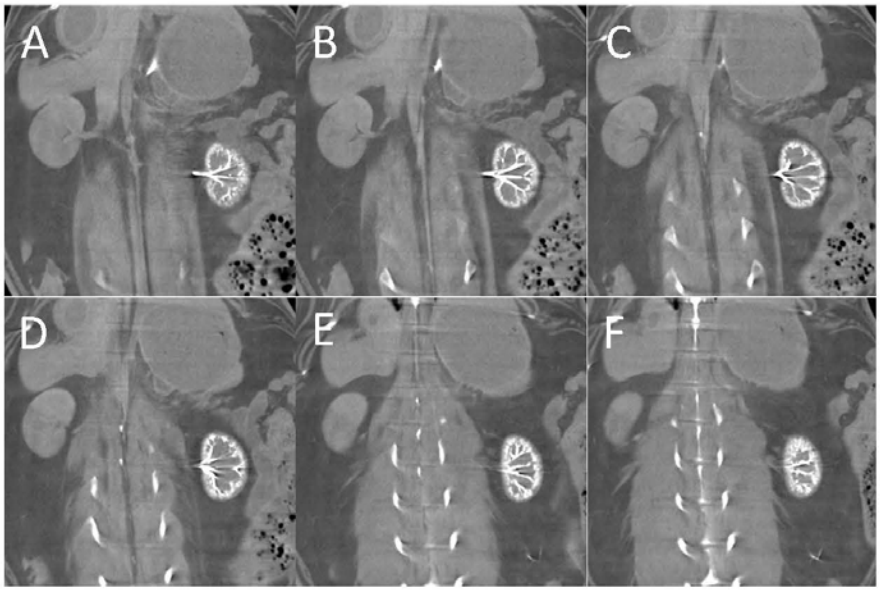

Supplemental figure 2. Post-mortem serial radiographs after left renal embolization demonstrating deep and uniform penetration of the embolic coacervate into the renal arterial vasculature.

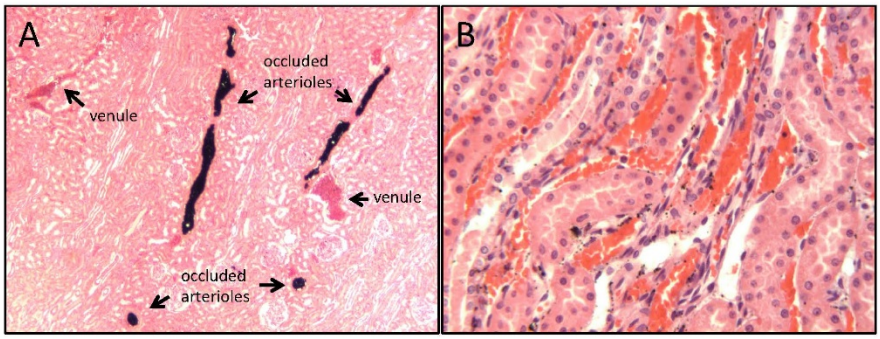

Supplemental figure 3. Histological sections from the renal cortex demonstrating penetration of embolic coacervate into A) arterioles. B) Embolic coacervate was not present in venules.

CHAPTER 3

COACERVATES OF PROTAMINE AND HEXAMETAPHOSPHATE AS TRANSCATHETER LIQUID EMBOLIC AGENTS

3.1 Abstract

Transcatheter embolization is used to treat a variety of vascular abnormalities. Small vessels are most often embolized with liquid embolic agents; however, these agents incite adverse tissue reactions. Coacervates represent a new type of liquid embolization agent that is water-borne and holds promise for eliminating some of these reactions. Here, embolic coacervates of protamine and hexametaphosphate are described. In a rabbit auricular artery embolization, these agents demonstrated a benign inflammatory response, leaving the vessel wall structure intact and causing little impact on the surrounding tissue.

3.2 Introduction

Liquid embolic agents are delivered via microcatheter to permanently stop blood flow in small vessels [1]. Most commonly, these agents are used in presurgical devascularization of arteriovenous malformations, but are also used in tumor embolization, treatment of aneurysms, renal ablations, and control of hemorrhage [1, 2]. Clinical liquid embolic agents include Onyx ®, a solution of

ethylene-vinyl alcohol copolymer dissolved in DMSO which sets *in situ* as the solvent diffuses away [3], and Trufill ®, a cyanoacrylate glue which polymerizes upon contact with anions in blood [4]. The problems with these agents are well documented. The DMSO employed in precipitating systems is toxic, limiting injection rates, and can cause vasospasm and tissue necrosis [5, 6]. Cyanoacrylate monomers polymerize rapidly and exothermically, making them difficult to control and causing localized hyperthermia. This rapid polymerization can be retarded by dispersing NBCA in ethiodized oil. However, misjudging the amount for a procedure can cause the embolus to spread proximal or distal to the desired area [4, 7]. Moreover, if the embolic agent refluxes, the catheter can become permanently glued into the embolization site [8, 9]. In addition, forward flow and distal penetration are difficult to achieve with Onyx [10].

Many researchers have identified these problems with clinically used embolic agents and sought to develop new liquid embolic agents. However, these approaches, which generally fall into two distinct categories, are clinically infeasible for transcatheter embolization of small blood vessels. The first approach has been to create embolic agents that solidify in response to temperature changes. These systems are liquids at room temperature and have a lower critical solution temperature near 37°C, which causes them to harden. Examples of this approach include poloxomers [11], *N*-isopropylacrylamide copolymers [12], and silk-elastinlike protein polymers [13]. However, because liquid embolic agents must be delivered by small catheters (<1 mm OD), up to 1.5 m in length, the embolic agents will reach 37°C before reaching the end of the catheter, causing

them to set and obstruct the catheter prior to entering the blood vessel. A second approach has been to create two component systems. Separately, each component is soluble in aqueous solution, but phase separate into insoluble gels upon mixing. Examples of this type of system include mixtures of calcium and alginate [14], inorganic polyphosphate and divalent metal ions [15], and modified chitosan [16]. Because of their rapid gelation, these systems must be delivered by dual-lumen catheters, which can create high injection pressures due to their small diameters. In addition, generating the turbulence necessary to achieve complete mixing of the components at the delivery site presents an even larger challenge.

Our lab has developed endovascular embolic agents based upon a novel ionic strength triggered setting mechanism [17]. This setting mechanism, inspired by the adhesive of the marine sandcastle worm, is made possible by interchangeable fluid morphologies of associated oppositely charged polyelectrolytes [18-23]. Under high ionic strength conditions, a liquid complex coacervate state occurs, as monovalent ions disrupt interactions between charges on the polyions. At low ionic strength, these same polyelectrolytes form a solid precipitate. When the liquid form at high ionic strength is placed into a solution of physiological ionic strength, diffusion of the monovalent ions out of the liquid coacervate phase allows the polyions to associate more strongly, leading to gelation of the coacervate. An embolic coacervate (EC) with protamine, a cationic polypeptide isolated from salmon sperm, and phytic acid, a cyclic organic polyphosphate, validated this ionic strength dependent setting mechanism. Furthermore, these ECs were injectable through clinically used 1 mm diameter, 3

F microcatheters, and in an acute transcatheter embolization of a rabbit kidney, demonstrated complete devascularization of the kidney without crossing into venous circulation [17]. Like other developmental embolics, this aqueous system eliminates use of organic solvents and rapidly polymerizing components. However, unlike the systems described above, the embolic coacervates are a single component system that can be injected through a single lumen catheter and does not begin to solidify until exiting the catheter.

Here, we present the rheological properties of ECs made from protamine (PRT) and sodium hexametaphosphate (MP), an inorganic polyphosphate. Building upon the successful acute rabbit kidney embolization, we sought to examine the subchronic vascular response to the ECs by embolizing the central auricular artery in the rabbit ear. This model is advantageous because it allows for simple access to the target blood vessel and easy visualization of the embolic agent. It has been used previously as a fast-flow vessel model to study a range of prospective embolic agents, including particle and liquid embolics [11, 15, 24-27]. Additionally, as a thermal regulation center, the ear has numerous arteriovenous anastomoses [28, 29], which allow for collateral blood flow and help contain ischemia resulting from embolization [25]. Finally, as protamine is known to reverse heparin, *in vitro* release experiments were performed to measure protamine escape as a function of arginine to phosphate ratio.

3.3 Results and Discussion

3.3.1 Production of Embolic Coacervates

Commercial MP is a mixture of inorganic phosphate oligomers, both cyclic and linear, usually containing 10-20 phosphorous atoms per chain [30-33]. In their fully ionized form, cyclic inorganic polyphosphates have the formula $(P_nO_{3n})^{n-}$, while the linear form is comprised of $(P_nO_{3n+1})^{n+2-}$. The structures of these forms are depicted in Figure 3.1. Regardless of the whether the polyphosphate is linear or cyclic, each phosphorus atom will have one strongly ionized hydrogen, which has a pK_a of around 4.5 or less [30, 34]. The weakly acidic end groups of linear polyphosphates are usually dissociated between pH 4.5 and 9.5 [30, 35]. Overall this contribution to charge density is relatively small, so 1 charge per phosphorous atom was assumed at pH 7.2, the pH used in preparation of ECs. For PRT, all 21 arginine residues were assumed to be fully protonated, based upon published pK_a values [36]. Except for the ratio experiments, coacervates of PRT and MP were prepared at a 1:1 charge ratio with PRT concentration fixed at 50 mg/mL. To maximize yield, complexes were formed in 800 mM NaCl. The supernatant was then removed, and 5 M NaCl was added to raise the [NaCl] in the coacervate to 1200 mM, forming a clear, fluid coacervate. 30 wt% micronized tantalum oxide (TaO) was added as a fluoroscopic contrast agent to produce the EC.

3.3.2 PRT-MP Rheological Characterization

The viscosity of PRT-MP coacervates as a function of NaCl concentration was measured at 0.02 s^{-1}. As with coacervates of PRT and phytic acid (IP_6) [17],

viscosity increased sharply as NaCl concentration was lowered below 600 mM (Figure 3.2). At 150 mM, the viscosity of ECs with MP was increased 2.5-fold over those made with IP_6 (100 Pa·s vs. 40 Pa·s). With the TaO contrast agent, the low shear viscosity increased to 450 Pa·s. The higher viscosities of PRT-MP coacervates, both with and without contrast, indicate a much more stable final form. While no overpenetration was observed in the acute rabbit kidney embolization [17], this further reduces the risk of the embolic agent crossing into venous circulation. The higher viscosity of PRT-MP coacervates compared with PRT-IP_6 is likely a result of the increased charge valency of MP.

From calculations using Poiseuille's Law, shear rates of up to 500 s^{-1} may be generated within the catheter during delivery of the embolic agent. To predict this flow behavior, the viscosity of PRT-MP ECs in 1200 mM NaCl was determined from 0.01-500 s^{-1} (Figure 3.3). PRT-MP displayed a small amount of shear thinning up to 1 s^{-1}, but was mostly Newtonian, having a viscosity of 2.8 Pa·s from 1 to 500 s^{-1}. With 30 wt.% TaO, the EC had a low shear viscosity of 15 Pa·s, but quickly shear thinned to a viscosity of 4.5 Pa·s by a shear rate of 10 s^{-1}. From 10 s^{-1} to 500 s^{-1}, it behaved like a Newtonian fluid. This translates to a calculated injection pressure of roughly 5-6 MPa in a 3 F, 135 cm catheter, which is higher than PRT-IP_6, but within the limitations of modern 3 F embolic catheters (up to 8 MPa).

3.3.3 Structure of Set Embolic Coacervate

The structure of the set PRT-MP EC was also examined using microscopy. Here, EC was made with 0.1% FITC labeled PRT (no TaO) and were injected into

150 mM NaCl. Upon delivery into physiological ionic strength, salt rapidly diffuses out of the EC and a phase transition occurs within seconds; the clear, flowing coacervate hardens and forms an opaque, porous gel (Figure 3.4). The lower salt concentration, in addition to increasing the strength of interactions between PEs, results in a decrease in equilibrium water content within the complex. The formation of pores likely results from the trapping of this excess water upon setting. This mechanism also explains the closed cell nature of the pores and their exclusion of FITC-PRT, as seen in the confocal image (Figure 3.4 B). The pore size varies greatly, depending on the thickness and geometry in which the EC is applied. Here, the EC was injected onto a glass slide, forming a droplet approximately 3 mm in diameter, and pores could be observed ranging in diameter from 10 to 500 μm. The formation of closed pores upon phase transition has been noted in other PEC systems [37]. Additionally, in response to changes in pH and the presence of Ca^{2+} ions, the natural adhesive of the sandcastle worm forms a closed pore network which may contribute to its adhesive and mechanical properties [38]. The contribution of the porous structure to the mechanical properties of ECs is a topic of future investigation.

3.3.4 Embolization of Rabbit Auricular Artery

Previously, ECs were successfully utilized for acute transcatheter embolization of a rabbit kidney. Here, the longer-term tissue response to ECs was evaluated using the rabbit auricular artery model. Using aseptic technique, PRT-MP EC was made with 30 wt% TaO as a fluoroscopic contrast agent. Lidocaine

was applied to numb the ear prior to the procedure. A small intravascular catheter was used to gain access to the artery, and approximately 25 µL of EC was subsequently injected. Immediate inhibition of blood flow was evident by gross observation because of the thinness of the rabbit ear. Setting of the coacervate occurred within a few seconds after distal penetration of 2-3 cm. No further migration or fragmentation was observed. The animal was monitored afterward, and no signs of distress to the animal or tissue necrosis were seen. At 28 days, the rabbit was euthanized and the ears were fixed, sectioned, and embedded for histological examination.

3.3.5 Histological Evaluation

Histological sections were stained with H&E, Masson's Trichrome, and Verhoeff-Van Gieson elastin stain. Examination showed complete occlusion of the central auricular artery and penetration into several smaller arterioles. Vessel occlusions include both mechanical obstruction of the vessel with the embolic material and associated native thrombus. The EC remained confined to the artery lumen with no extravasation into surrounding tissues. Arterial vessels are lined by a single layer of endothelial cells, also known as the tunica intima. Surrounding this layer is the internal elastic lamina, which responds to blood volume changes within the artery, and a layer of smooth muscle (tunica media). The much less prominent external elastic lamina separates the tunica media from the tunica adventitia, a layer of connective tissue that surrounds the vessel. In the embolized vessels, arterial structure remained essentially intact (Figure 3.5 A). Tunica media

and tunica adventitia were not affected by the embolization (Figure 3.5 B). Only focal disruptions are seen in the internal elastic lamina (Figure 3.5 C). While the single-layer tunica intima cannot be identified in the sections, no signs of angionecrosis or cytotoxicity were seen. By 28 days, the EC was separated into smaller globules, and tissue ingrowth can be seen (Figure 3.5 A). This tissue ingrowth includes macrophages, fibroblasts, and sporadic foreign body giant cells. Using Masson's trichrome, extensive collagen deposition by fibroblasts was seen throughout the artery (Figure 3.5 D). In sections with complete filling of the artery, no signs of revascularization were seen. In one section, only partially filled with EC, formation of endothelial tubules was seen in the associated thrombus (Figure 3.6). These tubules are signs of angiogenesis, which can occur long before clinical recanalization. In this case, none of the tubules contained RBCs, indicating a lack of patency, but over time some blood flow would be restored to the embolized area. The long-term stability of the embolus in fully filled sections will need to be investigated in future animal experiments. The process of fibrosis would likely encapsulate and sequester the EC, which may serve to stabilize the occlusion.

The tissue response seen in this pilot experiment is strikingly different from published studies with other clinical embolic agents. Polyvinyl alcohol particles cause a severe inflammatory response within the lumen of the embolized vessel. This response contains large numbers of foreign body giant cells and often leads to necrosis of the vessel wall [39]. The precipitating embolic agent Onyx ® causes angionecrosis to the vessel wall, likely due to DMSO injection. It also incites chronic perivascular inflammation and results in complete destruction of the elastic

lamina in most cases [40, 41]. Cyanoacrylate glues produce a similar reaction, with necrosis and destruction of vessel structure [42-45]. The toxicity of cyanoacrylate embolics is thought to be a result of localized hyperthermia, caused by exothermic polymerization and of the production of toxic side products, including formaldehyde [45]. In contrast, no angionecrosis was seen with the EC. As with all foreign materials, the EC incited an associated inflammatory response. In this case, infiltration of macrophages and small numbers of FBGCs were seen. However, this response was relatively mild and had little effect on the vessel wall. In a clinical scenario, this could better preserve the function of surrounding tissue, which would be significant in neural applications. This difference in response is likely a result of the water-borne nature of embolic coacervates. The ionic strength dependent setting mechanism eliminates the use of organic solvents and *in situ* polymerization, which are significant sources of the toxicity seen with other liquid embolic agents.

3.3.6 Effect of Charge Ratio on Protamine Release

The primary medical indication for PRT is reversal of the anticoagulant effects of heparin [46]. This interaction is caused by formation of a protamine-heparin complex, which prevents heparin binding and activation of antithrombin and the subsequent inactivation of several coagulation factors [47, 48]. In some transcatheter embolization procedures, heparin is given to prevent thrombus formation caused by blood-material interactions with the catheter. In a heparinized patient, if some PRT is released from the embolic complex upon injection, it could

cause an undesired systemic procoagulant state. Upon injection of ECs, this release is possible because these polymer-rich polyelectrolyte complexes exist in a state of equilibrium with the dilute phase. In systems with high salt concentration, a significant amount of polymer remains in the supernatant phase at equilibrium [20]. As the EC is injected into PE free media, this could result in release of PRT and, less significantly, MP into the blood stream. Conversely, as ionic strength decreases and the coacervate transitions to a more solid morphology, the PEs become kinetically trapped, leaving almost no polymer in the supernatant [20, 49]. Because of this shift in equilibrium, the overall release of PRT should be limited. Still, the amount of PRT released from the EC upon delivery into serum was investigated. Additionally, as a way of minimizing this PRT escape upon injection, we also evaluated ECs formed with a non-stoichiometric 1:2 ratio of guanidinium to phosphate.

To measure PRT release, known amounts of EC made with FITC-labeled PRT were injected into vials containing serum. PRT release was then determined by fluorescently quantifying the amount of PRT in the serum at given timepoints. To evaluate the effect of changing the guanidinium to phosphate ratio, release was first measured at 1 h. Increasing the charge ratio from 1:1 to 1:2 (guan:phos) resulted in a three-fold drop in the amount of PRT released, from 0.28% to 0.09% (Figure 3.7 A). To confirm that decreased PRT release in serum from the 1:2 EC was not a function of altered flow behavior, rheological properties were evaluated (Figure 3.7 B). ECs with 1:2 charge ratio displayed less shear thinning than 1:1 ECs over the first couple of decades measured, then settled to roughly the same

viscosity from 10 s^{-1} to 500 s^{-1}. Viscosity is a measure of the cohesive forces within a fluid. If this difference in release were related to the low shear viscosity, the 1:1 formulation would be expected to exhibit lower release. According to our experimental data, the opposite is true, confirming that increasing the phosphate content of the coacervate was responsible for the decrease in release. Additionally, in terms of flow behavior, this small difference at low shear rates would be indistinguishable in the high shear environment of catheter flow, making a 1:2 formulation desirable for future studies.

Despite their high concentration of PEs, coacervates retain a large amount of water. This water in the coacervate phase can harbor free, unassociated PE within the complex, resulting in non-stochiometric complexes (which are still charge neutral because of monovalent ions) [37]. Likewise, increasing the amount of oligophosphate (MP) during formation of the EC would cause some free MP to be trapped within the complex. It is hypothesized that this free NaMP accounts for the decrease in PRT release. Because PRT complexation with MP is an equilibrium process, when the ECs are injected into physiological saline, which contains no free PRT, some might become disassociated from MP and be released. By introducing free MP into the coacervate, an internal reservoir of free polyvalent guanidinium binding sites is created, increasing the chance that this disassociated PRT is bound before escaping the EC. Simultaneously, because of the decrease in ionic strength with setting, complexation between polyelectrolytes becomes more favored, further helping to kinetically trap the PRT within the embolus and limit release.

3.3.7 Protamine Release Timecourse

Based upon the decreased release of the 1:2 EC, the release profile was investigated out to 3 days (72 h) for this formulation (Figure 3.8). Very little PRT was released initially, only 0.02% after 5 min and 0.03% after 10 min. The release of PRT continued out to 3 days, where still only 0.85% had escaped. If it is assumed that release scales linearly with volume, injection of 1 mL of EC would release 0.2 mg within 5 min, 0.7 mg within 1 h, and 3.6 mg within 1 day. These values are a small fraction of the maximum endovascular PRT dosage of 50 mg. For reference, 1 mg of PRT is given to reverse the effects of 100 units of heparin. Considering that heparin is unusually infused at a rate of ~1250 units per hour, and that more heparin could be administered to counteract any PRT release, this short-term PRT escape is insignificant. Additionally, the short half-life of PRT (< 5 min) is sufficient to prevent any long-term accumulation of PRT in the blood stream. While this release data is encouraging, more studies are necessary, as *in vivo* release is likely to depend heavily upon surface area. Before clinical translation, animal studies will need to be designed to appropriately and completely answer this question.

3.4 Conclusion

Embolic coacervates produced from protamine and hexametaphosphate were more viscous than those made from protamine and phytate, resulting from the increased valency of the oligophosphate. Injection of these ECs into physiological saline produced a closed cell structure of aqueous pores. The tissue

response to the PRT-MP EC was evaluated in a rabbit auricular artery. At 28 days, the occlusion remained stable and a mild inflammatory response, resulting in tissue ingrowth and fibrosis of the embolic material was observed. While more in-depth studies of this response are needed, this preliminary experiment supports our hypothesis that water-based ECs will create a more biologically inert embolic agent. Finally, protamine release was investigated as a function of coacervate charge ratio. A 1:2 ratio of guanidinium to phosphate produced lower overall release than 1:1 without significantly changing the rheological properties. Future studies with ECs will be done using a 1:2 ratio.

3.5 Materials and Methods

3.5.1 Reagents

USP grade Protamine sulfate (PRT; cat #102752) and sodium chloride (cat#102892) were purchased from MP Biomedical. Tantalum oxide powder, particle size <20μm (TaO; cat #204536), and sodium hexametaphosphate (MP; cat#305553) were obtained from Sigma. Fluorescein isothiocyanate was purchased from Fisher Scientific (FITC; cat #119250010). Sterile sheep serum was obtained from Hemostat Laboratories, Inc. Solutions were made in ultrapure, double deionized water.

3.5.2 Production of Coacervates

PRT and MP were dissolved in 800 mM NaCl at 60 mg/mL and 105 mg/mL, respectively and adjusted to pH 7.2. When applicable, 35 mg/mL (30 wt% of the

final coacervate) of TaO powder was added to the PRT solution. The two solutions were mixed at a volume ratio of 4:1, resulting in a 1:1 charge ratio. Liquid-liquid phase separation occurred immediately, and the mixture was allowed to settle for 12 h at 22°C. The supernatant was discarded, and 5 M NaCl was added to raise the coacervate NaCl concentration to 1200 mM, assuming that the NaCl concentration in the dilute and concentrated phases was equal [50]. This material was loaded into syringes and used as the *in situ* setting embolic coacervate (EC).

In ratio experiments, the general procedure for producing the coacervate remained the same. However, coacervates were also produced with an arginine to phosphate ratio of 1:2. In this case, the overall batch concentration of PRT remained fixed at 50 mg/mL. However, MP concentration was increased from 21 mg/mL at the 1:1 charge ratio to 42 mg/mL at the 1:2 charge ratio. As a result of the increased MP, the 1:2 ratio contained 200 mM excess sodium phosphate, and therefore, 200 mM sodium chloride was subtracted to correct the overall ionic strength.

3.5.3 Production of Fluorescently Labeled Protamine

FITC-PRT was produced using procedures from Nagai et. al. [51]. In 0.1 M borate buffer (pH=9), PRT was dissolved at 25 mg/mL. FITC was added (1.2 molar equivalents) along with a few drops of ethanol. The solution was reacted for 4 h at 20°C. Afterward, the pH was adjusted to 7.5 using boric acid and kept at 4°C overnight. The product was purified by dialysis and lyophilized. Thin layer chromatography was used to confirm covalent labeling. When labeling was

required, FITC-PRT was substituted, and coacervates were produced as described previously.

3.5.4 Rheology

The flow behavior of embolic coacervates was characterized at 37°C on a strain controlled rheometer (AR 2000ex, TA Instruments). A 20 mm diameter, 4º cone geometry was used with a solvent trap to prevent evaporation. Shear rate was stepped from 0.01 s^{-1} to 500 s^{-1} at 10 points per decade. Viscosities at various salt concentrations were compared at a shear rate of 0.02 s^{-1}.

3.5.5 Confocal Microscopy

PRT-MP ECs were prepared with 0.1% FITC-PRT. 10 µL of the clear, homogenous coacervate was pipetted onto a glass slide in 150 mM NaCl and equilibrated for 24 h. Confocal images were taken with a Nikon A1R microscope using a 488 nm laser.

3.5.6 Rabbit Auricular Artery Embolization

The subchronic tissue response to the EC was evaluated in a rabbit auricular artery model. All animal studies were carried out in accordance with the University of Utah Institutional Animal Care and Use Committee (IACUC) guidelines and approved protocols. Prior to the procedure, the rabbit was weighed and the ear was shaved and cleaned with 70% isopropyl alcohol. A local anesthetic cream (EMLA) was applied topically 1 h prior to the procedure. A sterile 24 gauge

intravascular catheter (BD Medical) was advanced into the central artery of the ear. The central needle was withdrawn from the catheter, and before embolizing, the catheter was flushed with saline to confirm arterial positioning. The embolic agent was injected to fill 1-2 cm of the artery (~ 25 µL) as the catheter was slowly retracted. After 2 min, the catheter was completely removed, and pressure on the artery was maintained. Embolization was verified visually. At 28 days, euthanasia was performed by first sedating the rabbit with ketamine/xylazine (IM) followed by intravenous injection of euthanasia solution (VetOne). During necropsy, ear tissue was harvested and fixed with 10% buffered formalin. After 1 week, the ears were cut into small sections (~4 cm^2) for embedding and staining. Sections were embedded in paraffin before staining with hematoxylin and eosin, Verhoeff-Van Gieson elastin stain, and Masson's trichrome stain.

3.5.7 Protamine Escape Experiments

Coacervates for the PRT escape experiments were produced as described previously, but with 10% FITC-PRT. All samples for this experiment contained the TaO contrast agent. To measure release of PRT in serum, 25 µL of coacervate was injected into 500 µL of sheep serum in an Eppendorf tube. At designated timepoints, the serum was mixed and completely removed. Separate samples were used for each timepoint (n=4). Finally, 200 µL of serum was combined with 80 µL of borate buffer and loaded into a 96 well plate. PRT in serum was determined by measuring fluorescence intensity (Ex. 495 nm; Em. 531 nm) and comparing with known PRT standards. Percent PRT release was calculated based

upon total concentration of PRT in the coacervate phase (800 mg/mL), determined from total volume of coacervate produced and amount of FITC-PRT leftover in the supernatant (also measured by fluorescence).

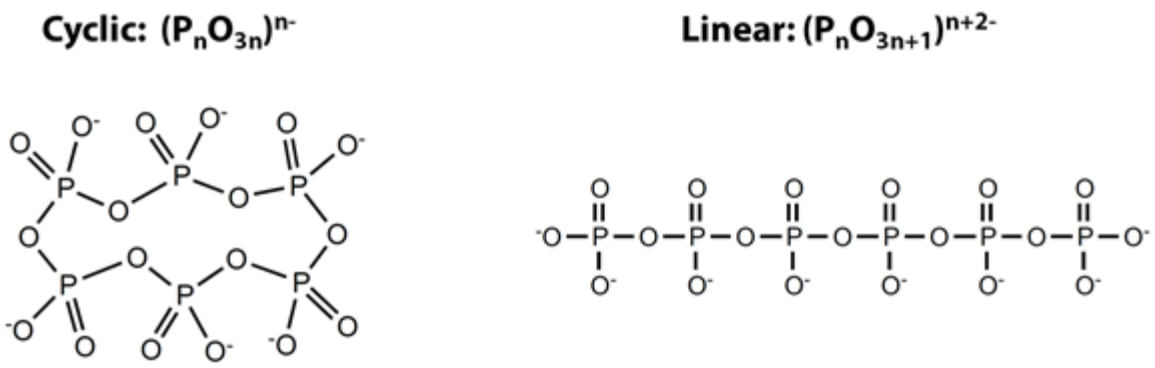

Figure 3.1. Simplified structures of hexametaphosphate (MP). The commercially available product contains mixtures of cyclic and linear inorganic polyphosphate with 10-20 P atoms per chain.

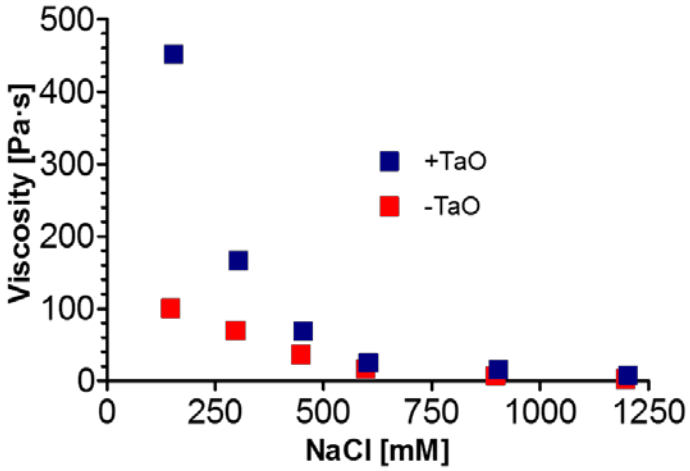

Figure 3.2. PRT-MP viscosity vs. NaCl concentration.

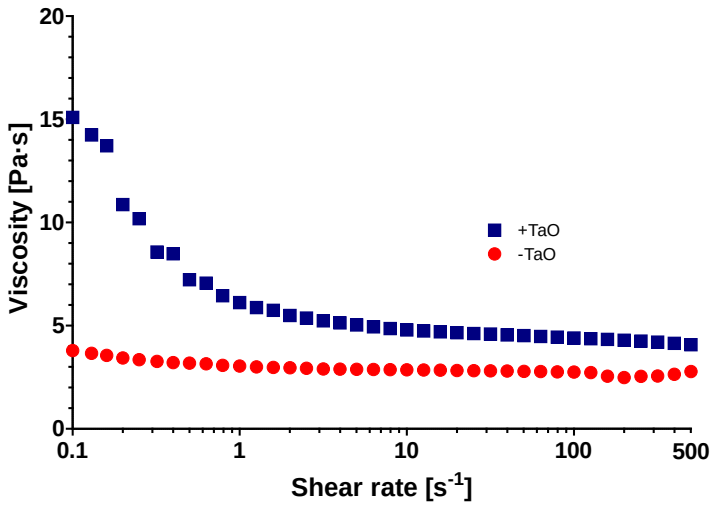

Figure 3.3. Rheological flow curves for PRT-MP ECs (*n*=3).

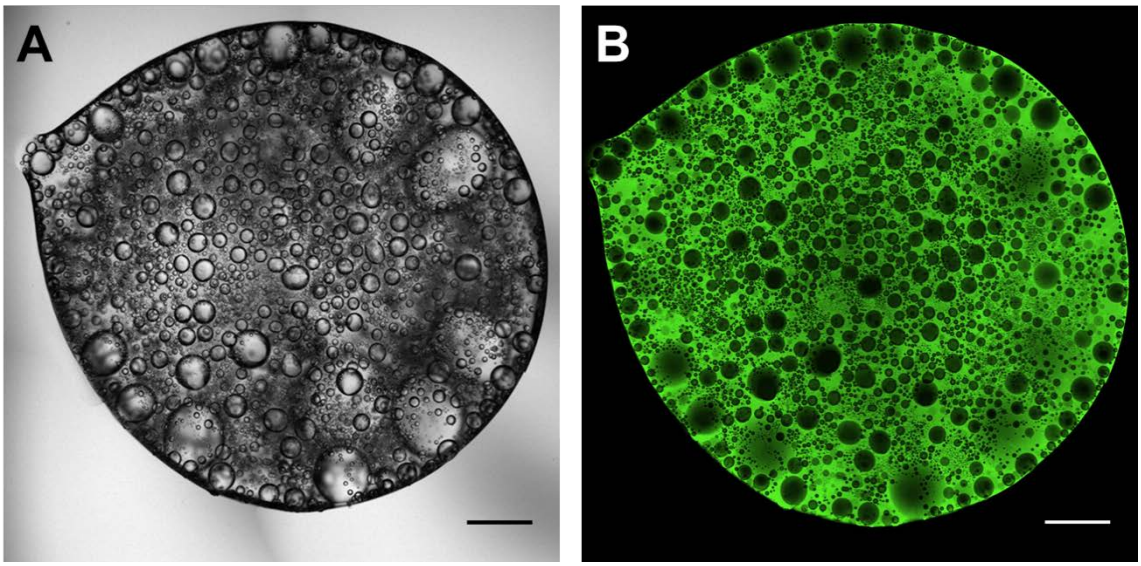

Figure 3.4. Microscopy images of FITC-labeled PRT-MP EC injected into 150 mM NaCl. (A) Brightfield (B) Confocal. Scale bars= 500 μm.

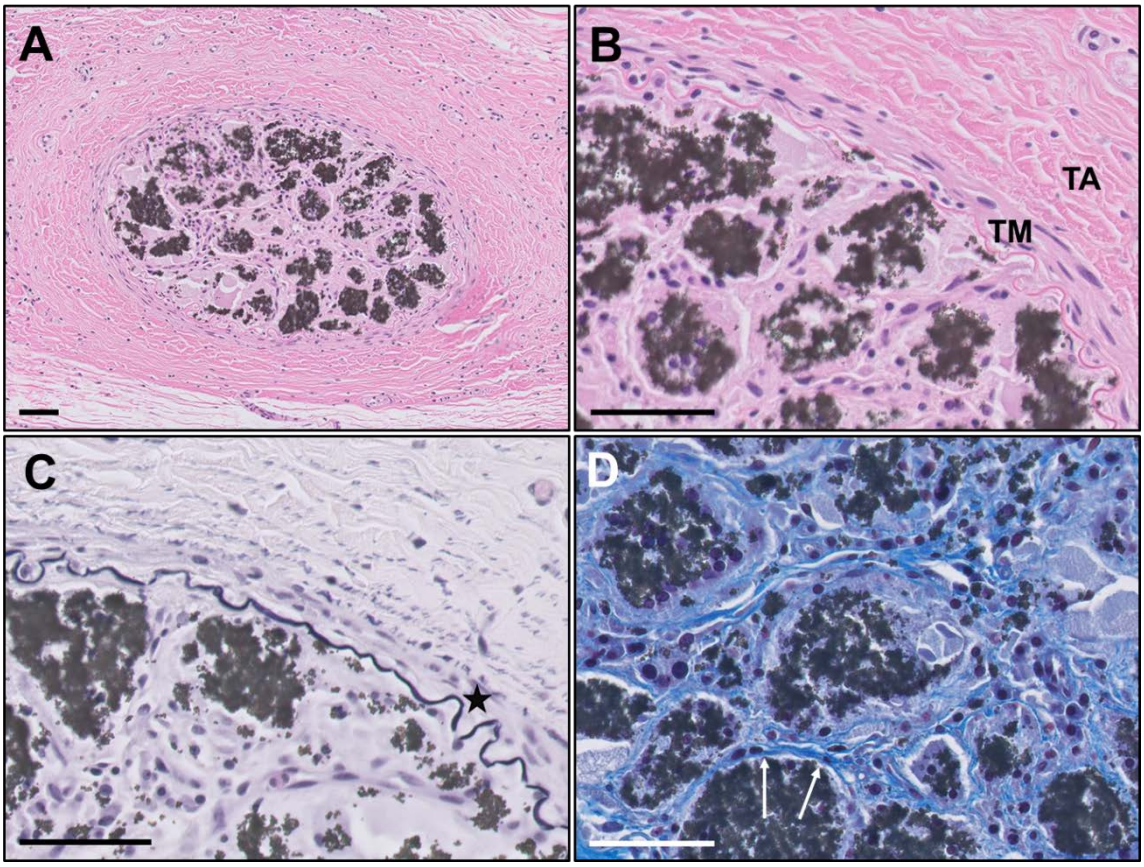

Figure 3.5. Histological response to PRT-MP (+TaO) at 28 days. (A) H&E stain showing embolized auricular artery. (B) Higher magnification of H&E stain showing tissue ingrowth. Tunica media (TM) and tunica adventitia (TA) are fully intact. (C) Elastin stain showing mostly intact inner elastic lamina (black); some focal disruption of the internal elastic lamina is seen (star). (D) Trichrome stain of embolized vessel demonstrating fibrosis throughout. One nidus of fibrosis is highlighted (arrows). Scale bars: 50 μm.

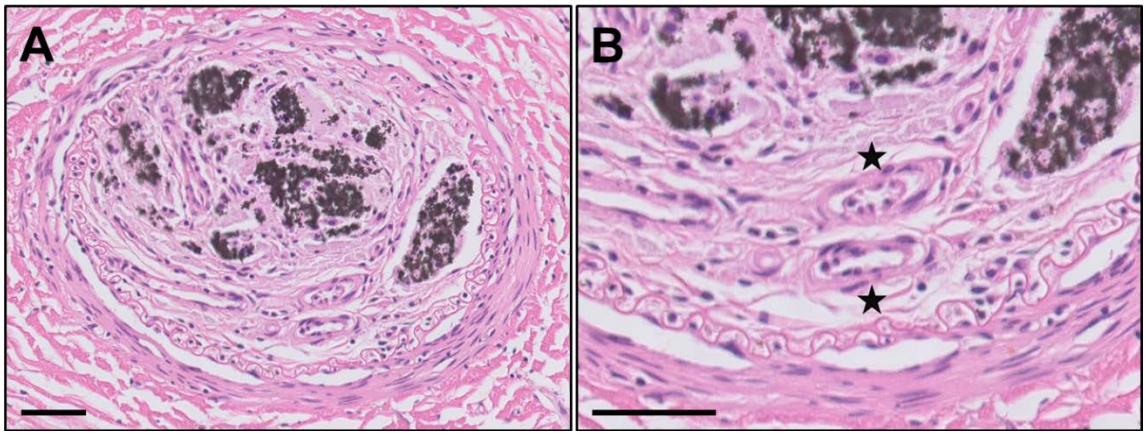

Figure 3.6. Neovascularization within embolized vessel. (A) An incompletely filled section of the auricular artery showing formation of endothelialized tubules. (B) Higher magnification of tubules (stars). No RBCs are seen, suggesting these tubules are not patent. Scale bars: 50 μm.

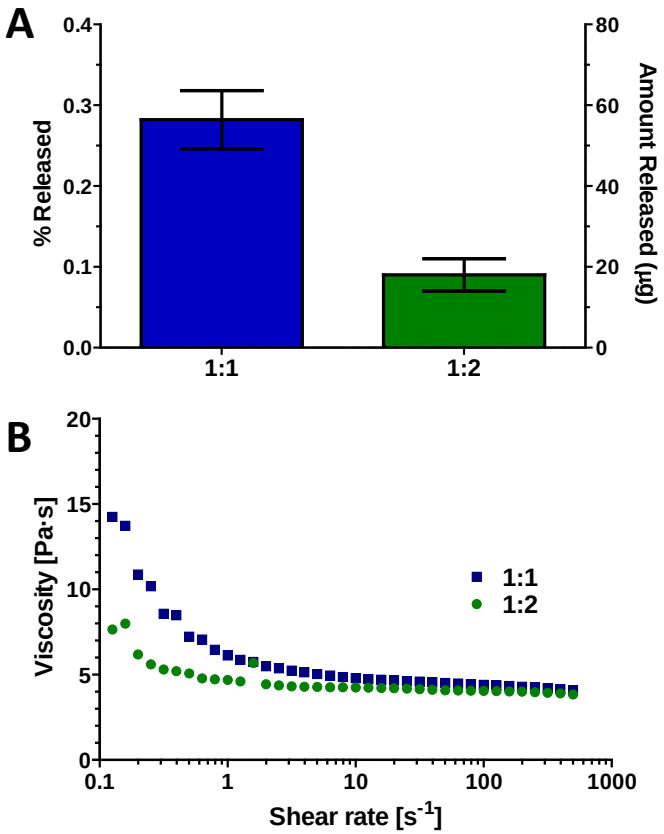

Figure 3.7. Properties of ECs (+TaO) with varying +/- charge ratios. (A) 1 h release in serum (*n*=4). (B) High salt flow curves (*n*=3).

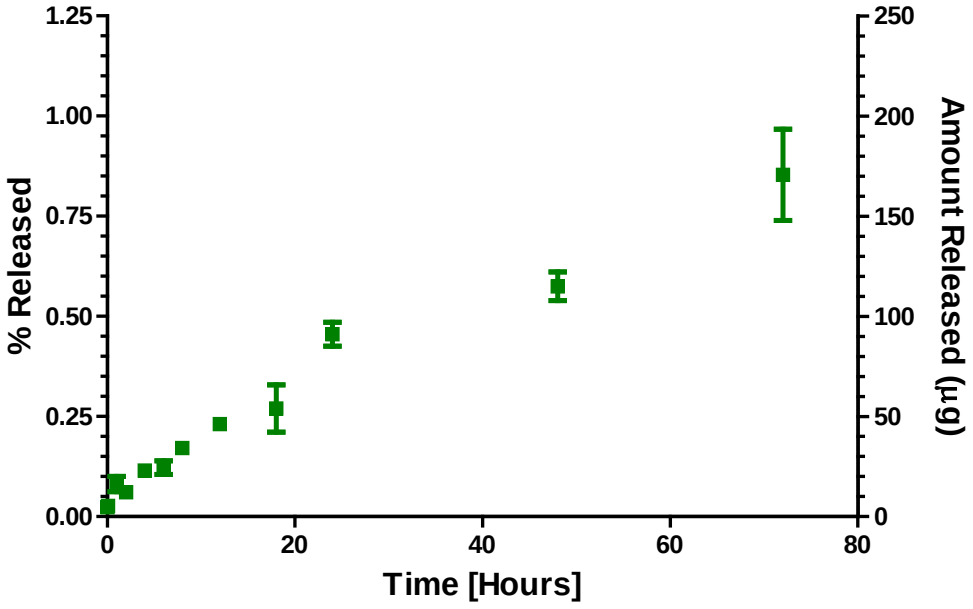

Figure 3.8. Cumulative release profile for ECs at 1:2 ratio (*n*=4).

3.6 References

[1] M. Lubarsky, C. Ray, B. Funaki, Embolization agents—Which one should be used when? Part 2: Small-vessel embolization, Semin. Intervent. Radiol. 27(1) (2010) 99-104.

[2] M. Saeed Kilani, J. Izaaryene, F. Cohen, A. Varoquaux, J.Y. Gaubert, G. Louis, A. Jacquier, J.M. Bartoli, G. Moulin, V. Vidal, Ethylene vinyl alcohol copolymer (Onyx®) in peripheral interventional radiology: Indications, advantages and limitations, Diagn. Interv. Imaging 96(4) (2015) 319-326.

[3] W. Taki, Y. Yonekawa, H. Iwata, A. Uno, K. Yamashita, H. Amemiya, A new liquid material for embolization of arteriovenous malformations, Am. J. Neuroradiol. 11(1) (1990) 163-168.

[4] J.S. Pollak, R.I. White, The use of cyanoacrylate adhesives in peripheral embolization, J. Vasc. Interv. Radiol. 12(8) (2001) 907-913.

[5] F. Mottu, A. Laurent, D.A. Rüfenacht, E. Doelker, Organic solvents for pharmaceutical parenterals and embolic liquids: A review of toxicity data, PDA J. Pharm. Sci. Technol. 54(6) (2000) 456-469.

[6] M. Guimaraes, M. Wooster, Onyx (ethylene-vinyl alcohol copolymer) in peripheral applications, Semin. Intervent. Radiol. 28(3) (2011) 350-356.

[7] S. Vaidya, K.R. Tozer, J. Chen, An overview of embolic agents, Semin. Intervent. Radiol. 25(3) (2008) 204-215.

[8] G.M. Debrun, V.A. Aletich, H. Shownkeen, J. Ausman, Glued catheters during embolisation of brain AVMs with acrylic glue, Interv. Neuroradiol. 3(1) (1997) 13-19.

[9] S. Paramasivam, D. Altschul, S. Ortega-Gutiarrez, J. Fifi, A. Berenstein, *N*-butyl cyanoacrylate embolization using a detachable tip microcatheter: initial experience, J. Neurointerv. Surg. 7(6) (2015) 458-461.

[10] S.L. Blackburn, Y. Kadkhodayan, W.Z. Ray, G.J. Zipfel, D.T. Cross, 3rd, C.J. Moran, C.P. Derdeyn, Onyx is associated with poor venous penetration in the treatment of spinal dural arteriovenous fistulas, J. Neurointerv. Surg. 6(7) (2014) 536-540.

[11] J. Raymond, A. Metcalfe, I. Salazkin, A. Schwarz, Temporary vascular occlusion with poloxamer 407, Biomaterials 25(18) (2004) 3983-3989.

[12] H.H. Bearat, M.C. Preul, B.L. Vernon, Cytotoxicity, *In vitro* models and preliminary *in vivo* study of dual physical and chemical gels for endovascular embolization of cerebral aneurysms, J. Biomed. Mater. Res. 101(9) (2013) 2515-2525.

[13] A. Poursaid, R. Price, A. Tiede, E. Olson, E. Huo, L. McGill, H. Ghandehari, J. Cappello, *In situ* gelling silk-elastinlike protein polymer for transarterial chemoembolization, Biomaterials 57 (2015) 142-152.

[14] T.A. Becker, D.R. Kipke, T. Brandon, Calcium alginate gel: A biocompatible and mechanically stable polymer for endovascular embolization, J. Biomed. Mater. Res. 54(1) (2001) 76-86.

[15] A. Momeni, E.M. Valliant, E.P. Brennan-Pierce, J.J.S. Shankar, R. Abraham, P. Colp, M.J. Filiaggi, Developing an *in situ* forming polyphosphate coacervate as a new liquid embolic agent: From experimental design to pilot animal study, Acta Biomater. 32 (2016) 286-297.

[16] L. Weng, N. Rostambeigi, N.D. Zantek, P. Rostamzadeh, M. Bravo, J. Carey, J. Golzarian, An *in situ* forming biodegradable hydrogel-based embolic agent for interventional therapies, Acta Biomater. 9(9) (2013) 8182-8191.

[17] J.P. Jones, M. Sima, R.G. O'Hara, R.J. Stewart, Water-borne endovascular embolics inspired by the undersea adhesive of marine sandcastle worms, Adv. Healthc. Mater. 5(7) (2016) 795-801.

[18] H. Shao, K.N. Bachus, R.J. Stewart, A water-borne adhesive modeled after the sandcastle glue of P. californica, Macromol. Biosci. 9(5) (2009) 464-471.

[19] R. Chollakup, W. Smitthipong, C.D. Eisenbach, M. Tirrell, Phase behavior and coacervation of aqueous poly (acrylic acid)− poly (allylamine) solutions, Macromolecules 43(5) (2010) 2518-2528.

[20] Q. Wang, J.B. Schlenoff, The polyelectrolyte complex/coacervate continuum, Macromolecules 47(9) (2014) 3108-3116.

[21] D. Priftis, X. Xia, K.O. Margossian, S.L. Perry, L. Leon, J. Qin, J.J. de Pablo, M. Tirrell, Ternary, tunable polyelectrolyte complex fluids driven by complex coacervation, Macromolecules 47(9) (2014) 3076-3085.

[22] S.L. Perry, W.C. Blocher, Complex coacervate-based materials for biomedicine, Wiley Interdiscip. Rev. Nanomed. Nanobiotechnol. 9(4) (2016) 1442.

[23] H. Shao, R.J. Stewart, Biomimetic underwater adhesives with environmentally triggered setting mechanisms, Adv. Mater. 22(6) (2010) 729-733.

[24] J.G. Ren, H.F. Wang, G. Chen, W. Zhang, H.Z. Jia, J. Feng, Y.F. Zhao, *In vivo* synergetic effect of *in situ* sclerotherapy and transient embolotherapy designed for fast-flow vascular malformation treatments with the aid of injectable hydrogel, J. Mater. Chem. 1(20) (2013) 2601-2611.

[25] N.E. Larsen, E.A. Leshchiner, E.G. Parent, J. Hendrikson-Aho, E.A. Balazs, S.K. Hilal, Hylan gel composition for percutaneous embolization, J. Biomed. Mater. Res. 25(6) (1991) 699-710.

[26] J. Raymond, A. Metcalfe, P. Leblanc, I. Salazkin, K. Papineau, D. Roy, J.P. Soucy, J.A. Krom, A. Schwarz, Production of radioactive particles for endovascular therapeutic interventions, Biomaterials 27(8) (2006) 1566-1572.

[27] A. Schwarz, H. Zhang, A. Metcalfe, I. Salazkin, J. Raymond, Transcatheter embolization using degradable crosslinked hydrogels, Biomaterials 25(21) (2004) 5209-5215.

[28] E.R. Clark, E.L. Clark, Observations on living arterio-venous anastomoses as seen in transparent chambers introduced into the rabbit's ear, Am. J. Anat. 54(2) (1934) 229-286.

[29] J.L. Morris, R.D. Bevan, Development of the vascular bed in the rabbit ear: scanning electron microscopy of vascular corrosion casts, Am. J. Anat. 171(1) (1984) 75-89.

[30] J.R. Van Wazer, C.F. Callis, Metal complexing by phosphates, Chem. Rev. 58(6) (1958) 1011-1046.

[31] J.I. Watters, S. Kalliney, R.C. Machen, A study of basicity of tri- and tetrametaphosphate and the stability of their complexes with copper(II) by means of the glass pH and the dropping amalgam electrodes—I, J. Inorg. Nucl. Chem. 31(12) (1969) 3817-3821.

[32] N. Angelova, D. Hunkeler, Effect of preparation conditions on properties and permeability of chitosan–sodium hexametaphosphate capsules, J. Biomater. Sci. Polym. Ed. 12(12) (2001) 1317-1337.

[33] M. Kawabe, O. Ohashi, I. Yamaguchi, Phosphorus nuclear magnetic resonance in polyphosphates and determination of their hydrolysis rate constants, Bull. Chem. Soc. Jpn. 43(12) (1970) 3705-3710.

[34] J.R. Van Wazer, K.A. Holst, Structure and properties of the condensed phosphates: Some general considerations about phosphoric acids, J. Am. Chem. Soc. 72(2) (1950) 639-644.

[35] F. Rashchi, J.A. Finch, Polyphosphates: A review their chemistry and application with particular reference to mineral processing, Miner. Eng. 13(10) (2000) 1019-1035.

[36] C.A. Fitch, G. Platzer, M. Okon, E. Garcia-Moreno, L.P. McIntosh, Arginine: Its pKa value revisited, Protein Sci. 24(5) (2015) 752-761.

[37] H.H. Hariri, J.B. Schlenoff, Saloplastic macroporous polyelectrolyte complexes: Cartilage mimics, Macromolecules 43(20) (2010) 8656.

[38] R.J. Stewart, C.S. Wang, I.T. Song, J.P. Jones, The role of coacervation and phase transitions in the sandcastle worm adhesive system, Adv. Colloid Interface Sci. 239 (2017) 88-96.

[39] I.M. Germano, R.L. Davis, C.B. Wilson, G.B. Hieshima, Histopathological follow-up study of 66 cerebral arteriovenous malformations after therapeutic embolization with polyvinyl alcohol, J. Neurosurg. 76(4) (1992) 607-614.

[40] J.C. Chaloupka, F. Viñuela, H.V. Vinters, J. Robert, Technical feasibility and histopathologic studies of ethylene vinyl copolymer (eval) using a swine endovascular embolization model, Am. J. Neuroradiol. 15(6) (1994) 1107-1115.

[41] S.K. Natarajan, D. Born, B. Ghodke, G.W. Britz, L.N. Sekhar, Histopathological changes in brain arteriovenous malformations after embolization using onyx or n-butyl cyanoacrylate: Laboratory investigation, J. Neurosurg. 111(1) (2009) 105-113.

[42] P.R. Mazal, M. Stichenwirth, A. Gruber, I. Sulzbacher, J.A. Hainfellner, Tissue reactions induced by different embolising agents in cerebral arteriovenous malformations: A histopathological follow-up, Pathology 38(1) (2006) 28-32.

[43] R. Loffroy, B. Guiu, J.-P. Cercueil, D. Krausé, Endovascular therapeutic embolisation: an overview of occluding agents and their effects on embolised tissues, Curr. Vasc. Pharmacol. 7(2) (2009) 250-263.

[44] M. Brothers, J. Kaufmann, A. Fox, J. Deveikis, *N*-Butyl 2-cyanoacrylate--substitute for ibca in interventional neuroradiology: Histopathologic and polymerization time studies, Am. J. Neuroradiol. 10(4) (1989) 777-786.

[45] H. Vinters, K. Galil, M. Lundie, J. Kaufmann, The histotoxicity of cyanoacrylates, Neuroradiology 27(4) (1985) 279-291.

[46] J. Carr, N. Silverman, The heparin-protamine interaction: A review, J. Cardiovasc. Surg. (Torino) 40(5) (1999) 659.

[47] D.J. Perry, Antithrombin and its inherited deficiencies, Blood Rev. 8(1) (1994) 37-55.

[48] J.A. Marcum, J.B. McKenney, R.D. Rosenberg, Acceleration of thrombin-antithrombin complex formation in rat hindquarters via heparinlike molecules bound to the endothelium, J. Clin. Invest. 74(2) (1984) 341-350.

[49] R. Chollakup, J.B. Beck, K. Dirnberger, M. Tirrell, C.D. Eisenbach, Polyelectrolyte molecular weight and salt effects on the phase behavior and coacervation of aqueous solutions of poly(acrylic acid) sodium salt and poly(allylamine) hydrochloride, Macromolecules 46(6) (2013) 2376-2390.

[50] C.G. De Kruif, F. Weinbreck, R. de Vries, Complex coacervation of proteins and anionic polysaccharides, Curr. Opin. Colloid Interface Sci. 9(5) (2004) 340-349.

[51] J. Nagai, T. Komeda, Y. Katagiri, R. Yumoto, M. Takano, Characterization of protamine uptake by opossum kidney epithelial cells, Biol. Pharm. Bull. 36(12) (2013) 1942-1949.

CHAPTER 4

ELECTRON BEAM STERILIZATION OF PROTAMINE-HEXAMETAPHOSPHATE EMBOLIC COACERVATES

4.1 Abstract

Electron beam sterilization is a commonly used radiation sterilization method. It is commonly used as an alternative to gamma radiation as it causes less damage to proteins and polymers. Here, the effects of e-beam sterilization on the material properties of embolic coacervates made from protamine sulfate and sodium hexametaphosphate are evaluated. Based upon observational, rheological, and spectroscopic data, electron beam sterilization did not change the chemical or physical properties of the embolic coacervates.

4.2 Introduction

Radiation sterilization methods are among the most commonly used for the sterilization of single-use medical devices. Their high usage stems from the simple and direct correlation of radiation dosage with killing of microbes, which makes validation relatively simple[1]. Of these methods, gamma radiation is most-widely used, followed by electron beam (e-beam). In e-beam sterilization, an electron

accelerator is used to generate a focused beam of electrons from electricity[2, 3]. The primary advantage of e-beam in comparison with gamma radiation is less oxidation of the product due to reduced processing times. Its main disadvantage is its short penetration depth, which is only a few centimeters in high density products[1, 3]. Because of this, packaging must be carefully considered to ensure adequate microbial kill.

In situ setting coacervates of sodium hexametaphosphate (MP) and protamine sulfate (PRT) (described previously in Chapter 3) are currently under preclinical investigation as liquid embolic agents. Sterilization of proteins and polymers can cause unwanted crosslinking or degradation, necessitating expensive aseptic production methods. In this study, e-beam sterilization was evaluated as a postpackaging sterilization method. PRT-MP coacervates were produced with and without tantalum oxide (TaO), an X-ray contrast agent for endovascular embolization. These embolic coacervates were sterilized using a 15 kGy dose of e-beam radiation. Material properties of the sterilized samples were compared to unsterilized material from the same batch.

4.3 Results and Discussion

4.3.1 Observation of Setting Behavior

Solidification of the salt-setting coacervates was observed by dispensing them into physiological saline. PRT-MP coacervates, in both e-beam sterilized and control groups, became cloudy and hardened immediately after immersion into saline, forming a foamy structure. Vigorous shaking did not disturb the set

coacervates. The sterilized and control TaO-containing material also solidified and formed identical structures upon addition into saline (Figure 4.1). No color change or separation was observed in any of the samples. These observations, while only quantitative, established that there are no gross differences in sample behavior within the two groups. The following sections describe further investigations into the strength of the electrostatic interactions between PRT and MP, in addition to evaluation of chemical changes as a result of the sterilization process.

4.3.2 Flow Behavior

Trans-catheter delivery is essential for a liquid embolic agent. The pressure required to deliver the embolic at any flow rate can be reliably predicted from flow curves (viscosity vs. shear rate) and the physical dimensions of the catheter[4]. Flow curves of the embolic coacervates were evaluated at 37°C. PRT-MP exhibited a viscosity of 3.7 Pa·s at 0.1 s^{-1} and shear-thinned to 2.7 Pa·s at 500 s^{-1} (Figure 4.2A). TaO containing embolic coacervates exhibited much more shear-thinning, going from 15 Pa·s to 3.4 Pa·s over the same range (Figure 4.2B). More importantly, no significant differences were observed between e-beam sterilized and control samples, indicating that the e-beam sterilized samples will be deliverable under the same conditions as control samples. Additionally, these results suggest that no significant degradation or crosslinking occurred within the sterilized samples, as these changes would have likely modified the molecular weights of PRT and/or MP and been reflected by increased or decreased viscosity.

4.3.3 ^{31}P Nuclear Magnetic Resonance (NMR) Spectroscopy

MP is a mixture of cyclic and linear inorganic polyphosphates of varying lengths, which contain hydrolysable pyrophosphate bonds. ^{31}P NMR can be used to resolve internal and terminal phosphate groups of inorganic polyphosphates in addition to their degradation product, ortho-phosphate[5]. An example spectra depicting these phosphate groups and their associated NMR peaks is shown in Figure 4.3A. This technique was used to evaluate MP degradation resulting from the sterilization process in coacervates with and without TaO. PRT-MP embolic coacervates did not degrade significantly in either group, with an orthophosphate peak present but too small to integrate (Figure 4.3B). TaO containing embolic coacervates (Figure 4.3C) had slightly more degraded phosphate in the unsterilized form (4.8%) than in the sterilized form (3.2%). This difference is likely insignificant, especially given that it is unlikely that radiation would recondense degraded inorganic phosphate. Notably, the amount of degraded phosphate within these NMR spectra is greater than coacervates without TaO. However, it is clear from these results (and the proceeding flow curves) that e-beam sterilization does not accelerate the degradation of MP in the coacervate form.

4.3.4 Attenuated Total Reflectance Infrared (ATR-IR) Spectroscopy

While NMR was used to monitor the degradation of MP in response to e-beam radiation, PRT contains many infrared (IR) active chemical bonds.

Therefore, any destruction or formation of chemical bonds within PRT as a result of the sterilization process would likely alter the IR spectrum. The IR of freeze dried PRT-MP coacervate (Figure 4.4A) contained several overlapping peaks from 3500 cm^{-1} to 2500 cm^{-1}. Within this region, the amide A band (PRT backbone), a carboxylic acid band (C-terminus of PRT), several aliphatic bands, and N-H stretching bands (PRT arginine side chains) are contained. Other strong absorption peaks, corresponding to the amide I and amide II bands are found at 1622 cm^{-1} and 1524 cm^{-1}, respectively. The normalized spectra of control and sterilized samples are indistinguishable at all of these major peaks, in addition to other smaller peaks in the fingerprint region. Spectra of coacervates containing TaO (Figure 4.4B) were nearly identical to those without it, and no significant differences were observed between control and sterilized samples. This IR data, while only qualitative, demonstrates that a wide variety of IR active chemical bonds remained undisturbed during the e-beam sterilization process.

4.4 Conclusions

In-situ setting PRT-MP coacervates (+/- TaO) were sterilized using 15 kGy of e-beam radiation. Follow-up evaluations showed no differences in flow-behavior, chemical composition, degradation, and gelation between sterilized and control groups. This suggests that e-beam radiation will be a viable method for in package sterilization. While the e-beam sterilization process did not affect the integrity of PRT-MP coacervates, future studies must be done to validate effective sterilization of the material. These tests include dosimetry and microbiological

evaluations using test organisms. Packaging will be especially important in TaO containing coacervate products, as their high density will limit e-beam penetration considerably. If penetration problems make e-beam sterilization impractical, gamma radiation could be evaluated as an alternative.

4.5 Materials and Methods

4.5.1 Sample Preparation

PRT (MP Biomedical) and MP (Sigma) were dissolved in 800 mM NaCl at 60 mg/mL and 105 mg/mL, respectively and adjusted to pH 7.2-7.4. When applicable, 35 mg/mL (30% w/w of the final coacervate) of TaO powder (Sigma) was added to the PRT solution. The two solutions were mixed at a volume ratio of 4:1, resulting in a 1:1 charge ratio. Liquid-liquid phase separation occurred immediately, and the mixture was allowed to settle for 12 h at 22°C. The supernatant was discarded, and 5 M NaCl was added to raise the coacervate NaCl concentration to 1200 mM.

4.5.2 E-Beam Sterilization

Complex coacervates were loaded using a positive displacement pipette into 3 mL clear polycarbonate syringes (Medallion, Merit Medical). Dry powders of MP, PRT, and TaO were placed in eppendorf tubes. Samples were placed inside a small cardboard box (75mm thick) and shipped to Sterigenics (San Diego, CA). The box was placed in an electron accelerator and exposed to 15 kGy of ionizing radiation. Nonsterilized control samples were from the same batches and tested

at the same time. Samples were homogenized via trituration prior to testing.

4.5.3 Setting of Embolic Coacervates

Samples were dispensed from the syringe into a glass dish filled with physiological saline (1xBSS, no buffers). As solidification occurred, the sample was observed for integrity, foam structure, spreading, and any other differences between control and sterilized samples.

4.5.4 Flow Behavior

The flow behavior of PRT-MP coacervates was characterized on a temperature controlled rheometer (AR 2000ex, TA Instruments) using a 20 mm, 4^{o} cone geometry. A solvent trap prevented the sample from drying out during the experiment. Shear rate was stepped from 0.01 s^{-1} to 500 s^{-1} at 10 points per decade.

4.5.5 ^{31}P NMR

^{31}P NMR was done with a Mercury 400 NMR (Varian). 50 µL coacervate samples were freeze dried, then redissolved in 1 mL of 6 M guanidine hydrochloride, containing 50 µL of D_2O. If applicable, TaO was removed from the redissolved samples by centrifugation at 500 *xg* before loading 700 µL into NMR tubes. Dry MP samples were dissolved directly in 6 M guanidine hydrochloride. Chemical shifts (δ) of internal phosphates are -20 to – 25 ppm; external phosphates are between -5 and -9 ppm, while the degraded orthophosphates appear between

1-3 ppm (Figure 4.3A).

4.5.6 ATR-FTIR

ATR-FTIR was done using a Nicolet 6700 Spectrometer (Thermo Scientific). Coacervates were freeze dried and ground into fine powders before being clamped onto the diamond ATR crystal. Spectra were collected from 4000 cm^{-1} to 600 cm^{-1}, using a resolution of 4 cm^{-1} and an average of 512 scans. A linear baseline subtraction was applied before normalizing each of the spectra to its maximum absorbance.

Figure 4.1. PRT-MP (+TaO) equilibrated in physiological saline after 8 weeks.

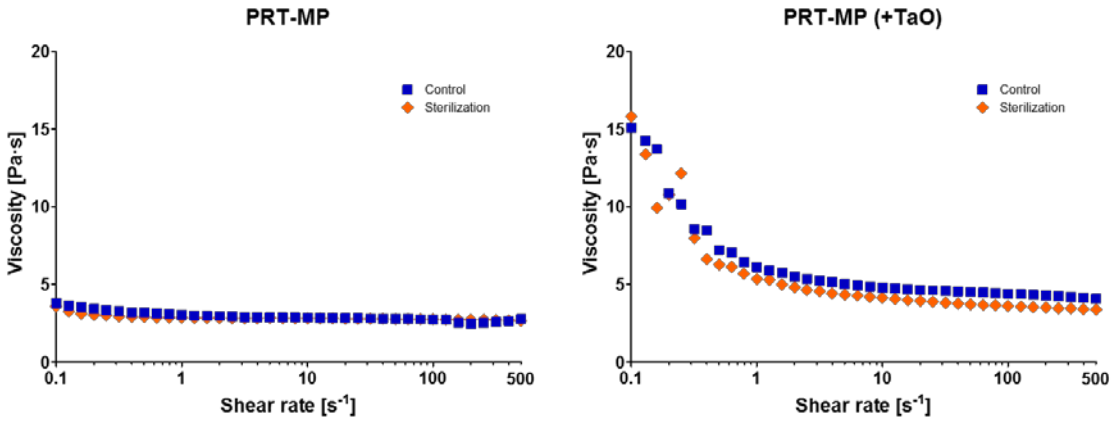

Figure 4.2. Flow curves of e-beam and unsterilized embolic coacervates.

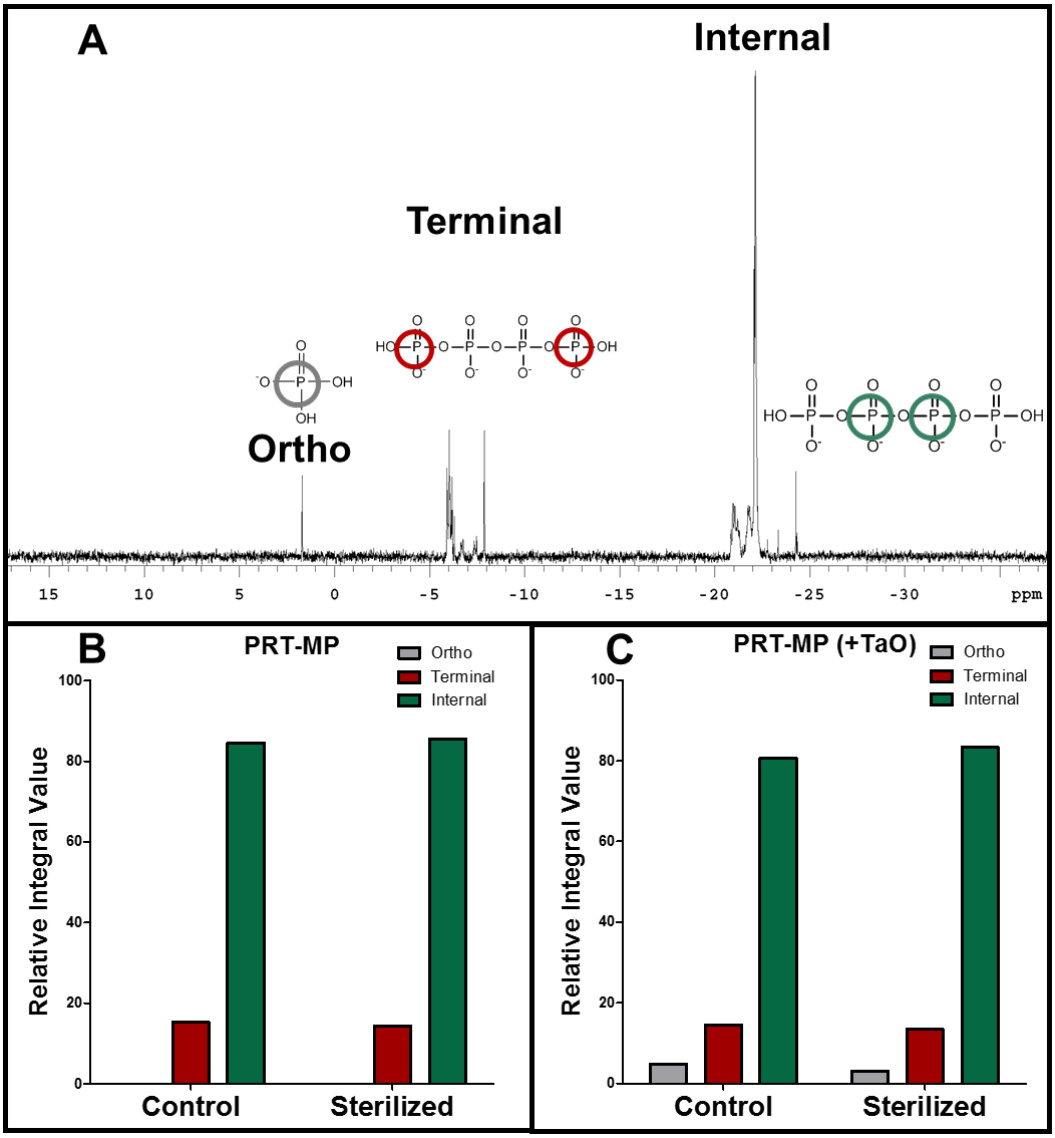

Figure 4.3. ^{31}P NMR. (A) Example NMR with peaks labeled. (B, C) Relative integration values of sterilized and unsterilized embolic coacervates +/- TaO.

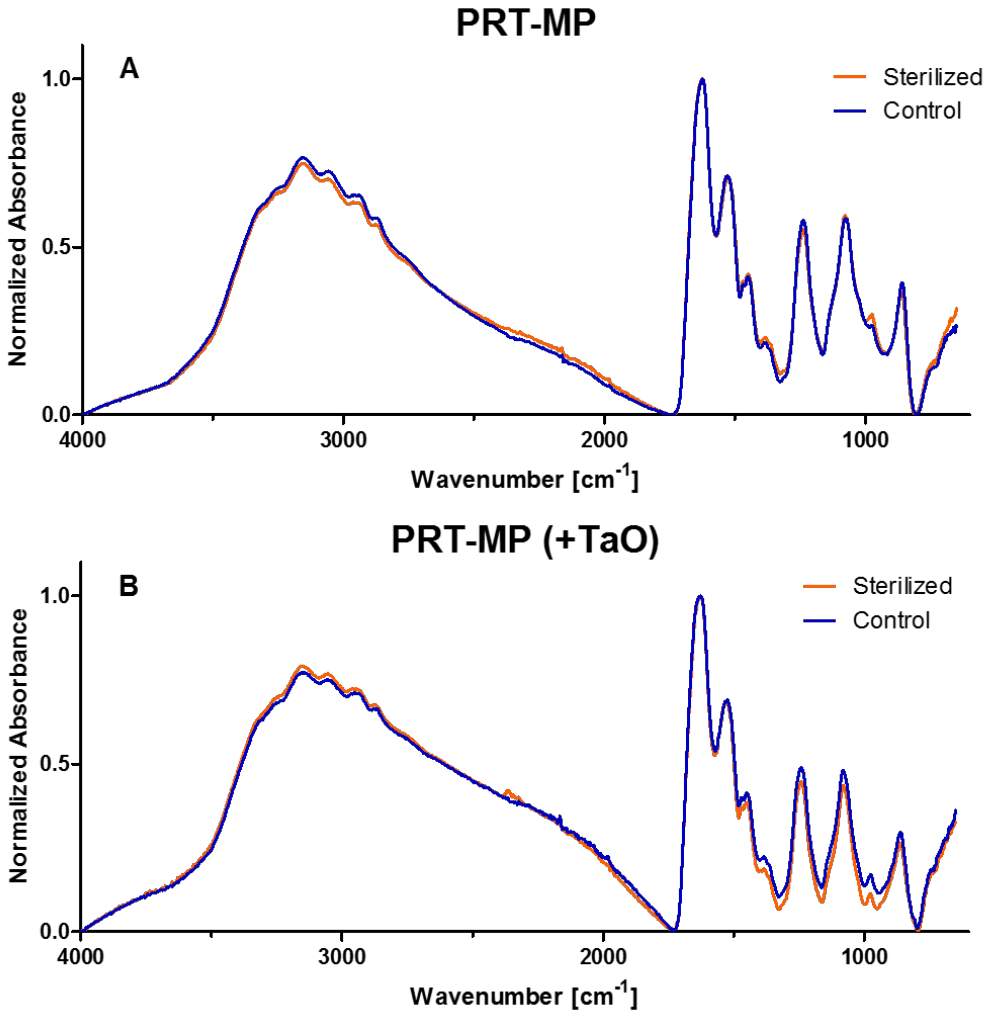

Figure 4.4: FTIR of e-beam sterilized and unsterilized coacervates.

4.6 References

[1] B. Lambert, J. Martin, Implants, Devices, and Biomaterials: Special Considerations, in: B.D. Ratner (Ed.), Biomaterials Science: An Introduction to Materials in Medicine, Elsevier, Boston, MA, 2013.

[2] Sterigenics, Sterilization Alternatives: Electron Beam Radiation, in: Sterigenics (Ed.) Oak Brook, IL, 2016.

[3] J.A. Sugranes, Basic operating principles and validation of electron beam irradiation systems, J. Valid. Technol. 12(1) (2005) 42-48.

[4] J.P. Jones, M. Sima, R.G. O'Hara, R.J. Stewart, Water-borne endovascular embolics inspired by the undersea adhesive of marine sandcastle worms, Adv. Healthc. Mater. 5(7) (2016) 795-801.

[5] M. Kawabe, O. Ohashi, I. Yamaguchi, Phosphorus nuclear magnetic resonance in polyphosphates and determination of their hydrolysis rate constants, Bull. Chem. Soc. Jpn. 43(12) (1970) 3705-3710.

CHAPTER 5

SECOND GENERATION EMBOLIC COACERVATES PRODUCED WITH A SYNTHETIC GUANIDINIUM-CONTAINING COPOLYMER

5.1 Abstract

Previously, endovascular embolic agents have been developed based upon solution dependent properties of condensed polyelectrolytes [1]. These materials were produced from the commercially available polyelectrolytes protamine and hexametaphosphate. Here, we report on the creation of a second generation embolic coacervate (EC). This version replaces protamine with a guanidinium-containing synthetic copolymer, which offers tunable properties and avoids some of the potential adverse reactions to protamine. As before, a low-viscosity injectable formulation can be produced in high concentrations of NaCl. However, in physiological saline, the synthetic version demonstrates superior mechanical properties, including a 2-order of magnitude increase in dynamic shear modulus. The tissue response to the synthetic EC was evaluated using embolization of the rabbit auricular artery. Occlusion of the artery was complete and remained stable out to the longest timepoint, 32 days. The EC produced a neutrophilic inflammatory

reaction. Around 4 weeks, inflammation began to subside and fibrous tissue deposition was observed. Embolic coacervates represent a promising developmental liquid embolic agent. However, larger scale animal studies are needed to examine chronic tissue response and stability of occlusion.

5.2 Introduction

Embolization therapy is used for treating a wide array of conditions including arteriovenous malformations, aneurysms, internal hemorrhage, hypervascular tumors, and varicose veins [2, 3]. In a transcatheter embolization procedure, an embolic agent is delivered locally via a microcatheter to obstruct blood flow in a blood vessel or vascular bed. Liquid embolic agents are used in situations where distal penetration into capillaries is desired [3]. These agents have a low-viscosity injectable form, allowing their delivery through long microcatheters, but harden upon entering blood vessels. Clinical liquid embolic agents include Onyx ®, a solution of ethylene-vinyl alcohol copolymer dissolved in DMSO which precipitates *in situ* as the solvent diffuses away [4], and Trufill ® (NBCA), a cyanoacrylate glue which polymerizes upon contact with anions in blood [5]. The problems with these agents are well documented. The DMSO employed in precipitating systems is toxic, limiting injection rates, and can cause vasospasm and tissue necrosis [6, 7]. In addition, forward flow and distal penetration are difficult to achieve with Onyx [8]. Cyanoacrylate monomers polymerize rapidly and exothermically, making them difficult to control and causing localized hyperthermia. This rapid polymerization can be retarded by dispersing NBCA in ethiodized oil. However, misjudging the

amount for a procedure can cause the embolus to spread proximal or distal to the desired area [5, 9]. Moreover, if the embolic agent refluxes, the catheter can become permanently glued into the embolization site [10, 11].

The problems with liquid embolic agents have been identified, and a clincal need for new liquid embolic agents persists. However, the approaches to solve this problem, which generally fall into two distinct categories, are clinically infeasible for transcatheter embolization. The first approach has been to create embolic agents that solidify in response to temperature changes. These systems are liquids at room temperature and have a lower critical solution temperature near 37°C, which causes them to solidify in response to increasing temperature. Examples of this approach include poloxomers [12], *N*-isopropylacrylamide copolymers [13], and silk-elastinlike protein polymers [14]. However, because liquid embolic agents must be delivered by small catheters (<1 mm OD), up to 1.5 m in length, the embolic agents will reach 37°C before reaching the end of the catheter, causing them to set and obstruct the catheter prior to entering the blood vessel. A second approach has been to create two component systems. Separately, each component is soluble in aqueous solution, but phase separate into insoluble gels upon mixing. Examples of this type of system include mixtures of calcium and alginate [15], inorganic polyphosphate and divalent metal ions [16], and modified chitosan [17]. Because of their rapid gelation, these systems must be delivered by dual-lumen catheters, which can create high injection pressures due to their small diameters. More importantly, generating the turbulence necessary to achieve adequate mixing of the components at the delivery site presents an even larger

challenge, which could result in incomplete gelation and overpenetration of the embolic agent.

Previously, we have developed water-borne embolic agents based on a unique setting mechanism: ionic strength triggered *in situ* phase inversion of liquid complex coacervates. This system eliminates the injection of organic solvents and exothermically polymerizing monomers associated with clinically available liquid embolic agents [1]. In the process of coacervation, solvated oppositely charged polyelectrolytes (PEs) condense through both ion-specific interactions and entropic release of counterions [18-21]. This process forms a macro liquid-liquid phase separation, with a polymer depleted supernatant, and a polymer-rich, fluid coacervate phase [22]. Here, liquid embolic coacervates (ECs) are formed in a high ionic strength sodium chloride solution. This salt concentration, while low enough to allow phase separation, dopes the coacervate with a large number of monovalent Na^+ and Cl^- ions and high water content, vastly decreasing interactions between oppositely charged PEs [19, 23]. When injected into solutions of physiological ionic strength, the concentration of freely diffusing monovalent ions inside the EC decreases. This, along with a decrease in equilibrium water content, allows for more numerous and longer-lived interactions between the oppositely charged PEs, resulting in solidification of the polyelectrolyte complex.

While initial results with protamine based ECs have been promising, replacing protamine with a synthetic polymer reduce the risk of rare, but life-threatening protamine specific allergic reactions [24-26]. Additionally, changing polymer properties, such as mol% guanidinium and molecular weight could allow

for tuning the properties of the coacervate in both high salt and final form. Finally, a synthetic polymer would eliminate environmentally-caused supply disruptions [27] and provide better process control. The distinguishing feature of protamine is its high charge density, with arginine comprising 21 of its 32 amino acids [28]. The guanidinium sidechain on arginine has a pK_a of ~13.8 [29], making it charged across nearly the entire pH spectrum. Thus, synthetic polyguanidinium represents a logical choice for replacing protamine in ECs. Previously, guanidinium containing polymers have been synthesized by the McCormick and Shea groups [30-32]. These approaches required synthesis of a guanidinium monomer (GPMA) by guanidylating commercially available *N*-(3-aminopropyl) methacrylamide.

Here, we built on this approach and designed a copolymer of GPMA and methacrylamide as a synthetic protamine analog. Following synthesis and characterization of the polymer, ECs were made by combining the synthetic polymer with hexametaphosphate, an inorganic oligophosphate. The ECs were formulated for injectability through microcatheters by adjusting sodium chloride concentration. Rheological properties of both the initial (high salt) and set forms (injected into saline) were characterized. Finally, we sought to examine the vascular response to the ECs out to 4 weeks by embolizing the central auricular artery in the rabbit ear.

5.3 Results

5.3.1 Production of Synthetic Guanidinium Polymer

First, 3-guanidinopropyl methacrylamide (GPMA), was synthesized by guanylation of 3-aminopropyl methacrylamide (APMA) using *1H*-pyrazole-1-carboxamidine hydrochloride (Figure 5.1) [33]. After purification, the product was analyzed using NMR and mass spectroscopy. In ^{1}H NMR, the conversion of APMA to GPMA most notably caused a downfield shift of the (-CH_2-amine/guan) peak from 2.88 to 3.10 ppm, along with a slight deshielding of the vinyl peaks (~0.03 ppm). No residual APMA peak remained at 2.88 ppm (Figure 5.2). In ^{13}C NMR, the guanidinium carbon in GPMA became apparent at 156.6 ppm, and a slight deshielding of the (-CH_2-amine/guan) peak was also observed, from 37.0 to 38.7 ppm (Figure 5.3). Finally, ESI mass spectrometry (Figure 5.4) showed formation of the GPMA product at 185.40 Da, nearly identical to the predicted value of 185.2 Da. Importantly, there was no remaining APMA (143.2 Da), or emergence of the diguanidine monomer side product (228.2 Da). However, HPLC analysis on a C18 column did show a small amount of the APMA starting material. Together, these results confirmed the production of GPMA monomer, which was used to make the synthetic protamine analog.

5.3.2 Production of p(GPMA-co-MA)

Reversible addition fragmentation chain-transfer (RAFT) polymerization was used to prepare copolymers of GPMA and methacrylamide (MA) with a controlled molecular weight and low polydispersity index (PDI) (Figure 5.5). A

molecular weight of 20 kDa was targeted, and a monomer feed ratio of 80% GPMA and 20% MA was selected. The reaction was done in an aqueous acetate buffer, pH 5.3. To set polymerization parameters, the kinetics of this reaction were studied (Figure 5.6). The rate of polymerization was directly proportional to monomer concentration out to 16 h, as indicated by the pseudo-first order plot in Figure 5.6 B. In addition, this reaction had a minimal induction period and reached 90% monomer conversion (Figure 5.6 C). Correspondingly, refractive index traces from GPC (Figure 5.6 A) show a decrease in elution volume and increase in peak intensity, consistent with a growing polymer out to 16 h From 16 to 20 h, no increase in conversion or elution volume was seen; thus, the polymerization time was set at 16 h for future reactions. Additionally, the slight shielding of the vinyl peaks in GPMA relative to MA (0.1 ppm) allowed us to compare reactivity of the two monomers: the ratio of unreacted GPMA:MA stayed constant throughout the 20 h time course, indicating equal reactivity.

Next, large scale polymer synthesis (batch size 6-20 g) was performed eight times, which typically yielded around 50% after conversion to the hydrochloride salt and ultrafiltration. SEC analysis with light scattering was used to determine molecular weights and size distributions with an experimentally determined *dn/dc* value of 0.1782. A representative SEC profile (RI) from a purified polymer is shown in Figure 5.7. In large scale polymerizations, average molecular weight (M_n) was 18.6 kg/mol (+/- 2.3 kg/mol), and PDI was 1.08 (+/- 0.05). GPMA content was 78 mol% (+/- 2.6%), as determined via ^{1}H NMR.

5.3.3 Formation of Embolic Coacervates

ECs were formed using the synthetic p(GPMA-*co*-MA) (PG) and sodium hexametaphosphate (MP). For comparison of synthetic PG to the naturally occurring polyelectrolyte protamine (PRT), coacervates were also made with PRT and MP. Commercial MP is a mixture of inorganic phosphate oligomers, both cyclic and linear, usually containing 10-20 phosphorous atoms per chain [34-37]. In their fully ionized form, cyclic inorganic polyphosphates have the formula $(P_nO_{3n})^{n-}$, while the linear form is comprised of $(P_nO_{3n+1})^{n+2-}$. Regardless of the whether the polyphosphate is linear or cyclic, each phosphorus atom has one strongly ionized hydrogen, with a pK_a of ~4.5 or less [34, 38]. The weakly acidic end groups of linear polyphosphates are usually dissociated between pH 4.5 and 9.5 [34, 39]. Overall, this contribution to charge density is relatively small, so 1 charge per phosphorous atom was assumed at pH 7.2. The strongly basic GPMA sidechains on the polymer were considered fully protonated. Polyelectrolyte complexes of PG and MP were made in a series of salt concentrations (Table 5.1). From 150 mM to 800 mM NaCl, cloudy gels were formed with yields of 12%-8% of total batch volume, respectively. Between 800 mM and 1200 mM NaCl, the cloudy complexes became fluid, clear coacervates, and yield dropped precipitously to only 2.5% of total batch volume. Therefore, to generate clear, flowing ECs while maintaining high yield, coacervates were first formed in 800 mM NaCl. After removal of the supernatant, salt content of the coacervate was raised by mixing 5 M NaCl into the condensed phase. Unless otherwise noted, 30 wt.% tantalum metal powder was added to the complex as a radiocontrast agent, necessary for the delivery of the

embolic agent under fluoroscopic guidance.

5.3.4 Formulation of Injectable EC and Flow Behavior

For delivery, liquid embolic agents must have a viscosity that allows for injection through microcatheters without exceeding their rated burst pressure. Clinically used embolic microcatheters have rated pressures of 5-8 MPa; thus, an injection pressure less than 4 MPa at 0.3 $mL \cdot min^{-1}$, the maximum injection rate of current liquid embolics, was set as a design specification. To formulate an EC that met this limit, viscosity of the EC was lowered by increasing the amount of NaCl in the coacervate. Corresponding changes in injection pressures were determined in model catheters. The model catheters have the same inner surface (PTFE) and internal diameter (0.026”) as commonly used 3 F embolic catheters. ECs were loaded into 1 mL syringes and a syringe pump, equipped with a force transducer, was used to measure the steady state injection force through the model catheter at 0.3 mL min^{-1} (Figure 5.8). Using the bore diameter of the syringe, the measured forces were converted to pressure and extrapolated to a catheter length of 135 cm, the most common length used in the clinic. At 1200 mM, injection pressure was 10.1 MPa, exceeding the limits of clinically used catheters. Increasing NaCl concentration drastically reduced injection pressures, with 1400 mM NaCl being sufficient to lower injection pressures below 4 MPa (3.25 MPa). A further increase in NaCl concentration resulted in lower injection pressure. However, to minimize the amount of salt injected, an NaCl concentration of 1400 mM was chosen for further development.

After fixing the NaCl concentration at 1400 mM, the viscosity of both PG-MP and PRT-MP ECs was investigated over a range of shear rates (0.1-500 s^{-1}) to simulate transcatheter delivery (Figure 5.9). PG-MP without Ta demonstrated slight shear thinning within the first decade of shear rates, but was nearly Newtonian, from 1 to 500 s^{-1}, with a viscosity of 1.1 Pa·s. Adding Ta more than doubled the viscosity at low shear rates (~5 Pa·s). However, by 10 s^{-1}, the material shear thins to a viscosity approaching PG-MP (-Ta) (1.2 Pa·s). The flow behavior of polymer-based ECs in this high NaCl concentration was nearly indistinguishable from PRT-MP with Ta. Using these viscosity measurements and Poiseuille's Law, injection pressures can be predicted. Here, the predicted injection pressures for PG-MP are roughly 60% of the experimentally determined values (2 MPa).

5.3.5 Viscoelasticity of PG-MP ECs

Next, the viscoelastic properties of ECs were compared before and after solidification in balanced salt solution (BSS). This was done using rheological frequency sweeps, where a fixed oscillatory strain (1%) was applied at a series of stepped frequencies (0.1 to 10 Hz). These frequency sweeps are shown in Figure 5.10, and dynamic rheological properties at 1 Hz. are compared with statistical analysis in Figure 5.11. In high salt, the fluid PG-MP EC is a viscously dominated fluid with a complex modulus (G^*) of 0.025 kPa at 1 Hz. Upon solidification in BSS, G^* increased by almost 4 orders of magnitude at the same frequency (195 kPa). Additionally, the ECs transitioned from a liquid to a viscoelastic material, which demonstrated a crossover to solid-dominated (elastic) behavior ($G' > G''$) at 5.2 Hz.

Without Ta, the material was less elastic, with crossover frequency at 17 Hz. Furthermore, the presence of Ta had a statistically significant effect (p<0.05) on the complex modulus, increasing G^* by approximately 75%. Similarly, PRT-MP ECs also set in BSS, but G^* only increases ~2 orders of magnitude. In contrast to PG-MP, the final form of PRT-MP remained viscously dominated, with G'' significantly higher than G' over the entire frequency range. Furthermore, PG-MP had complex moduli (G^*) 2 orders of magnitude higher than that of PRT-MP.

5.3.6 Evaluation of Catheter Entrapment

With both cyanoacrylate glues and precipitating liquid embolics, the catheter can become glued into the injection site by the embolic agent [10, 40]. Thus, gauging the risk of catheter entrapment is important for developmental liquid embolic agents. Here, the force required to remove the catheter from solidified ECs was measured both 2 min and 24 h after injection of the EC into saline. Sections of 3 F catheters were embedded into 1 cm of EC. After allowing the EC to solidify in saline, the force required to remove the catheter from the embolic plug was measured at 2 min and 24 h. At 2 min, the force required to remove the catheter at 1 $cm \cdot s^{-1}$ was 16.7 mN (+/- 5.8 mN). Even in the worst-case scenario (24 h), the force required to remove the embolic was only 384 mN (+/- 107 mN). Additionally, no embolic agent remained adhered to the catheter upon removal. These results suggest that adhesion to the catheter is not a problem with embolic coacervates and that catheter entrapment does not present a major risk with this system.

5.3.7 Rabbit Auricular Artery Embolization

To examine the perivascular tissue response to the synthetic ECs, auricular artery embolization was performed in rabbit ears. This model is advantageous because it allows for simple access to the target blood vessel and easy visualization of the embolic agent. It has been used previously as a fast-flow vessel model to study a range of prospective embolic agents, including particle and liquid embolics [12, 16, 41-44]. Additionally, the rabbit ear contains multiple arteriovenous anastomoses, which allow collateral blood flow and help to localize any ischemic effects resulting from embolization [45, 46]. Eight rabbit ear embolizations were performed, and animals were sacrificed at timepoints ranging from 1-32 days. Before the procedure, a topical anesthetic cream was applied to the ear. Embolization was performed by gaining retrograde access to the central auricular artery with an intravascular catheter. The catheter was flushed with saline to confirm positioning, before continuously injecting approximately 25 µL of EC to fill ~2 cm of the artery. With backlighting of the ear, ECs were observed to completely fill the targeted section of the central auricular artery (CAA). In one case, the central auricular vein (CAV) was injected. Setting of the ECs occurred within seconds, after which, the embolus did not migrate. No hematomas or bleeding from the access site was observed, indicating achievement of hemostasis.

After embolization, the gross tissue response at the embolization site was monitored daily. No signs of discomfort or irritation were seen in any of the animals. The embolic plugs demonstrated positional stability, and no migration or

fragmentation was observed over the 4 week course of the experiment. The progression of the gross response is shown for the longest timepoint (Figure 5.12). Gross inflammation appeared to reach a peak 4-7 days after embolization, as visualized by redness surrounding the embolization site. Over the next week, this response appeared to subside. At this point, the embolus remained clearly visible and moderately swollen. After 2 weeks, the macroscopic appearance changed little throughout the rest of the study. Ears remained healthy, and no visible signs of tissue necrosis were seen in any of the animals.

5.3.8 Histological Evaluation

Postmortem, the embolized ears were removed, fixed in 10% formalin, and cut into sections. Sections containing the embolus and adjacent proximal and distal sections were embedded in paraffin and stained for histological evaluation. The ECs were observed to completely occlude the CAA, and no sign of revascularization was present out to 32 days. There was also evidence of reduced blood flow distal to the EC, as the arteries appeared collapsed and contained native thrombus. Proximally, vessels became more patent farther away from the embolus. In arterially embolized ears, no embolic agent was seen in venous circulation. Within the embolized arteries, a progressive inflammatory response, dominated by neutrophils, was seen. The progression of this response is shown with histological sections of the embolized CAA in Figure 5.13. One day after embolization, there was little damage to the vessel wall, but perivascular inflammation was present. This early-stage inflammation was indicated by the

presence of neutrophils surrounding the embolized vessel. Neutrophils are highly-mobile phagocytic granulocytes which arrive at the site of inflammation by migrating through the bloodstream and extravasate into the tissue through chemotaxis. This process is evident in Figure 5.13 B (high magnification; 1 day), as neutrophils can be seen extravasating from the longitudinally sliced blood vessel on the left and migrating toward the EC-filled CAA. By day 4 (Figure 5.13 C), the structure of the vessel wall is compromised, likely through enzymes secreted by neutrophils which degrade collagen and elastin. From days 4-14, progressive vessel wall obliteration continued, perivascular neutrophilic inflammation became more severe, and the nodule of inflammation grew. At 14 days (Figure 5.13 E), significant neutrophil ingrowth can be seen within the EC, as the inflammatory response begins to degrade the material. By the longest timepoint at 32 days (Figure 5.14), most of the tantalum was removed from the embolus due to phagocytosis. At this point, neutrophils remained the predominate cell type within the lesion, but globules of EC and Ta left behind were being actively phagocytosed by macrophages (Figure 5.14 B). The vessel structure was also destroyed; however, inflammation had greatly diminished. Additionally, there was deposition of fibrous connective tissue surrounding the nodule of inflammation (Figure 5.14 C).

In one ear, the central auricular vein, which lies close to the CAA was unintentionally accessed and injected with EC. Grossly, the ear appeared normal with little inflammation observed, and the animal was kept until 29 days. Upon histological sectioning, no material was found within the CAA. However, the vein

was occluded with the EC (Figure 5.15). In this specimen, neutrophilic inflammation appeared milder than in the arterially embolized ears. This inflammatory response had destroyed the vessel endothelium and tunica media. However, in this case, the inflammatory response was confined inside the layered collagen of the tunica adventitia, which remained intact. As seen in the artery, phagocytosis had removed a majority of the Ta powder from the embolization site, and collagen deposition by fibroblasts was seen (Figure 5.15 C).

5.4 Discussion

First-generation embolic coacervates were composed of protamine and an oligophosphate [1]. Here, a methacrylamide-based synthetic guanidinium copolymer is reported as a substitute for protamine in producing ECs. The synthetic polymer can be produced via RAFT polymerization, which allows for a well-controlled molecular weight and polydispersity, preventing production problems resulting from endogenous heterogeneity and supply disruptions with the natural product [27]. Furthermore, the randomly-ordered, nonimmunogenic nature of synthetic polymers makes them far less likely to incite severe IgG-mediated immune responses, a risk associated with endovascular administration of PRT.

As seen with PRT, polyelectrolyte complexes (PECs) of this synthetic polymer and hexametaphosphate have morphologies and rheological properties strongly dependent on salt concentration. To formulate a low-viscosity embolic coacervate deliverable via embolic microcatheters, the NaCl concentration of the coacervate was increased to 1400 mM. At this high salt concentration, the

interactions between the oppositely charged PEs, which exist in a state of dynamic equilibrium, are relatively few and short-lived, resulting in a low-viscosity fluid coacervate. This behavior is driven by the presence of high concentrations of monovalent ions and water in the coacervate, which plasticize interactions between the PEs [23, 47]. In this high salt concentration, the pressure required to inject the synthetic EC at 0.3 $mL \cdot min^{-1}$ through a 3 F model catheter (135 cm) was 3.25 MPa, which is well below the burst pressure of most embolic microcatheters (5-8 MPa). This injection pressure was approximately 60% higher than those predicted by rheological flow curves, a more drastic difference than was seen previously with protamine and phytic acid [1]. While some of this increased pressure results from non-Newtonian behavior at low shear rates, most of it is likely due to interactions between the material and catheter wall. Injection pressure has an r^4 inverse proportionality (*r*=radius of the catheter), meaning that any adhesion of the material to the catheter wall and subsequent lowering of the effective diameter drastically affects injection pressure.

When the EC is injected into a lower-ionic strength environment, such as a blood vessel (~150 mM), Na^+ and Cl^- ions are free to diffuse in and out of the complex. As the salt concentration within the polyelectrolyte complex decreases, water becomes excluded, and polyion pairing becomes less shielded by monovalent ions. This allows higher numbers of interactions between the oppositely charged PEs and increases their kinetic stability, producing a phase transition of the complex from a liquid coacervate to a viscoelastic material. This transition can be seen in the rheological data for synthetic ECs (Figures 5.10,

5.11). In 1400 mM NaCl, PG-MP was a weak, purely viscous liquid with loss modulus (*G"*) considerably higher than the storage modulus (*G'*) over the entire range of frequencies. After injection into physiological saline, the PG-MP complex became a strong viscoelastic material, with complex modulus (*G**) increasing nearly 4 orders of magnitude (0.025 to 195 kPa). In physiological saline, differences in mechanical properties between ECs made with PRT and with PG are dramatic. While PRT-MP does harden significantly, PRT-based ECs remain viscous fluids after injection into BSS, which contrasts with the viscoelasticity seen with PG-MP. Furthermore, the complex moduli of PG-MP are more than two orders of magnitude higher than PRT-MP. This drastic difference in mechanical properties was only evident in low salt concentrations, as the two systems behave almost identically in 1400 mM NaCl (Figure 5.9). Molecular weight (18 kDa vs. 5 kDa) likely accounts for part of this difference, as increased molecular weight has been shown to favor a solid morphology [48]. The fraction of guanidinium sidechains (78 mol% vs. 65 mol%) was also increased in the synthetic polymer, but the charge density per unit mass remained the same (4.1 mol/g). Furthermore, lowering the water content within a PEC strengthens mechanical properties through decreased polymer mobility and increased PE interactions [19, 47]. Because the aliphatic backbone of the synthetic polymer is more hydrophobic than the peptide backbone in PRT, additional water may be excluded from PG-MP complex in low salt resulting in stronger mechanical properties in the PEC [49]. The contribution and magnitude of each of these effects on mechanical properties of the complexes are an avenue of future study with the synthetic polymers.

The ability of synthetic polymer-based ECs to transition from low-viscosity injectable liquids, to strong viscoelastic materials gives them clinical utility as embolic agents. For comparison, rheological characterizations of clinically available embolic agents, such as Onyx ®, are difficult to find in the literature. However, the elastic and complex moduli of PG-MP (>100 kPa) are more than 2 orders of magnitude higher than PRT ECs as well as several other systems that have demonstrated efficacy in animal models [50-52]. These values also compare favorably to reported values for native whole blood and fibrin clots (2-600 Pa) [53-55], allowing them to structurally support stable occlusion of blood vessels. Despite their strong rheological properties, a minimal amount of force (<0.4 N or 1.4 oz) was required to remove catheters solidified ECs, demonstrating that catheter entrapment is unlikely to present a clinically significant problem with this embolization agent.

After embolization of rabbit ears, ECs incited a neutrophilic inflammatory response. Neutrophils are phagocytes responsible for removal of foreign materials and damaged tissue, which are typically the predominate cell type in an inflammatory nidus within the first few days. Presence of neutrophils beyond this point can indicate chronic non-healing [56]. Here, neutrophils decreased significantly from 2 weeks to 4 weeks and were replaced by increasing numbers of macrophages and some fibroblasts. This decrease in inflammation and associated presence of fibroblasts indicates the beginning of a proliferative phase of healing [56]. Continuation of the processes seen here would likely result in full resorption of the material and formation of fibrous scar tissue in place of the blood

vessel. The eventual fate of this fibrotic tissue is unclear. Even with ‘permanent’ embolic agents, high rates of revascularization are seen [57-61]. Accordingly, Onyx® and Trufill ®, the two liquid embolics in widespread clinical use, are only approved by the FDA for embolization of AVMs destined for later surgical resection. Considering the obliteration of vessel structure, it seems unlikely that revascularization will proceed by recanalization of the previous vessel lumen. Arterial blood flow to the surrounding tissue would probably be restored via a combination of enhancement of extant collateral blood flow and neovascularization. While no revascularization was seen in this preliminary 1 month study, examining the spatial and temporal stability of the occlusion is an important objective of future larger scale *in vivo* experiments.

Another important histological finding from this study was that the small tantalum particles were easily phagocytosed and removed from the embolization site by neutrophils and macrophages. The Ta used in this study (1-5 μm) are within the optimal range for macrophage phagocytosis [62, 63]. The phagocytosed Ta would likely be transported to the regional lymph nodes. Avoidance of phagocytosis is dependent upon particle shape, but generally particles larger than the macrophage cell volume are not readily phagocytosed [64]. Larger Ta particles would likely avoid phagocytotic clearance, but might incite a more persistent inflammatory response and formation of significant numbers of foreign body giant cells.

A complication in examining tissue responses to embolic agents is separating material specific effects from natural biological responses to ischemia.

Neutrophils are largely responsible for clearing out cellular debris from a wound site [56]. Especially within the arterial system, occlusion causes tissue degeneration and necrosis due to ischemia, creating an overwhelming amount of cellular debris. This loss of nutrition also compromises arterial wall integrity resulting in upregulation of various proinflammatory transcription factors and cytokines [65]. These factors could be responsible for the extended presence of neutrophils seen here. At 4 weeks after venous embolization with the EC, the collagen layer surrounding the vessel, tunica adventitia, was still intact. Neutrophils secrete a variety of enzymes that degrade collagen and elastin, and thus, this intact layer suggests that neutrophilic inflammation was less severe in the days after embolization than in the arterial embolizations. Localized ischemia is much less severe with venous occlusion and could be the reason for the reduced neutrophil-mediated response and increased proliferation in this specimen.

While its severity varies with choice of embolic agent and site of embolization (or animal model), all embolic agents incite inflammation. Onyx ® has been shown to incite perivascular inflammation and cause angionecrosis in both animal models and resected human AVMs [57, 66]. Cyanoacrylate glues incite heavy neutrophilic inflammation and total destruction of vessel wall architecture [61]. Intraluminal and mural infiltration of neutrophils and monocytes, focal angionecrosis, and formation of foreign body giant cells are seen after embolization with polyvinyl alcohol particles [58, 60, 67]. Here, the severe inflammation seen here at early timepoints did subside by day 28, but the vessel wall was largely destroyed even in the venous injection. The eventual resolution of

this inflammatory response and its impact on surrounding tissues warrants further investigation. Utilizing more sophisticated animal models with interventional radiology techniques, such as embolization of the swine rete mirabile will provide a more complete picture of the tissue response and better comparison with current embolization agents. In addition, subcutaneous injection of the EC could be used to examine the tissue response in the absence of ischemia.

5.5 Conclusion

First generation embolic coacervates were comprised of protamine, a natural polycation with 65 mol% positively charged guanidinyl sidechains, and an oligophosphate. To provide better design control and preclude hypersensitivities associated with endovascular administration of protamine, a synthetic polycation was produced which mimics the high charge density and guanidinium content of protamine. Coacervates of this polymer, poly(3-guanidinopropylmethacrylamide-*co*-methacrylamide), and hexametaphosphate display a greater change in properties with decreasing ionic strength: they have a similar viscosity in their injectable form and possess vastly stronger mechanical properties in their set form. Embolization of 8 rabbit auricular arteries was performed, and at the longest timepoint (1 month), occlusions remained stable. No signs of direct cytotoxicity were observed. Histological evaluation showed inflammation comparable to current embolization agents. While embolic coacervates represent a promising new liquid embolic, a thorough investigation of the long-term fate of the embolus and surrounding tissue is still needed.

5.6 Materials and Methods

5.6.1 Reagents

N-(3-aminopropyl) methacrylamide hydrochloride (APMA) was obtained from Polysciences, Inc. (cat# 21200). 1H-Pyrazole-1-Carboxamidine hydrochloride was purchased from Chem-Ipex International (cat# 21678). Methacrylamide (MA; L15013) and glacial acetic acid (cat# 36289) were obtained from Alfa Aesar. 4-methoxyphenol was purchased from TCI chemicals (cat #M0123). 4,4′-Azobis(4-cyanovaleric acid) (V501; cat# 11590) and azobisisobutyronitrile (AIBN; cat# 441090) were obtained from Sigma-Aldrich. 4-Cyano-4-(thiobenzoylthio)pentanoic acid was purchased from Strem Chemicals (cat# 16-0422). Sodium acetate was obtained from VWR (cat# 0602). USP grade sodium chloride (NaCl; cat# 102892) and protamine sulfate (PRT; cat #102752) were purchased from MP Biosciences. Triethylamine (TEA) was obtained from Fischer Scientific (cat# # BP616-500). Tantalum metal powder (1-5 micron particle size) was purchased from Atlantic Equipment Engineers, Inc. (cat# TA-101). All solvents were ACS grade or better. Solutions were made in ultrapure double deionized water.

5.6.2 Synthesis of GPMA Monomer

N-(3-methacrylamidopropyl) guanidinium chloride (GPMA) was synthesized (Figure 5.1) using procedures adapted from the literature [32, 33]. Briefly, a flask was charged with *N*-(3-aminopropyl) methacrylamide hydrochloride (APMA) (20 g; 112 mmol) and the inhibitor 4-methoxyphenol (0.2 g; 1.6 mmol). DMF (112 mL)

was added to dissolve APMA at a concentration of 1 M. TEA (18.7 mL; 134 mmol) was added to the flask and the mixture was stirred for 5 min under N_2. Next, *1H*-pyrazole-1-carboxamidine hydrochloride (16.4 g; 112 mmol) was added. The mixture was reacted at 20°C under N_2. After 16 h, TEA·HCl salts were separated from the reaction mixture by vacuum filtration using a Büchner funnel. The monomer was extracted with diethyl ether 3 times, forming a dense oil. Finally, the monomer was collected dried under vacuum. The product was confirmed by proton and carbon NMR. ^{1}H NMR (400 MHz, D2O): δ (ppm) 1.68 (q, CH_2-C$\underline{H_2}$- CH_2), 1.77 (s, CH_3), 3.08 (m, CH_2-N), 3.18 (m, CH_2-N), 5.30 (s, =CH_2), 5.55 (s, =CH_2). ^{13}C NMR: (400 MHz, D2O) δ (ppm) 17.74 (CH_3), 27.62 (CH_2), 36.62 (CH_2-N), 38.71 (CH_2-N), 121.13 (C=CH_2), 138.83 (CH_2=C), 156.6 2(C), 171.55 (C=O). Formation of GPMA was also verified by ESI mass spectroscopy (185.1 Da).

5.6.3 RAFT Polymerization of GPMA and MA

Synthesis of p(GPMA-*co*-MA) was adapted from that of similar polymers by Treat et. al. [30]. RAFT polymerization was employed using 4-cyano-4-(thiobenzoylthio)pentanoic acid as the chain transfer agent (CTA) and V-501 as the initiator at a 5:1 molar ratio. A fixed molar ratio of 80:20 (GPMA:MA) and molecular weight of 20 kD were utilized. GPMA (9.12 g, 41 mmol), MA (0.88 g, 10 mmol), 4-cyano-4-(thiobenzoylthio)pentanoic acid (112 mg, 0.400 mmol), and V-501 (22.4 mg; 0.080 mmol) were dissolved in 1 M (pH 5.3) acetate buffer (52 mL). The resulting solution was degassed by bubbling for 2 h with N_2 before being septum sealed. The reaction was kept under N_2 while it proceeded at 70°C for 16

h (Figure 5.2 A). The resulting polymer was cooled, exposed to air, and precipitated in acetone. For end group modification, the polymer was redissolved in methanol (~ 100 mL), and AIBN (1.3 g, 8 mmol) was added (Figure 5.2 B). The solution was degassed and reacted under N_2 for 4 h at 60°C. The product was precipitated in acetone, collected by filtration, and dried under vacuum. A Millipore ultrafiltration system equipped with a Pellicon 2 Minicassette (Biomax ® 5 kDa) was used to purify the final product. To convert the polymer to the hydrochloride salt, PG was dissolved in DI water and washed with a 20x volume of 150 mM NaCl at pH 3 (adjusted with HCl). Next, an additional 20x volume exchange was performed with DI water. Finally, the purified retentate was freeze dried.

For polymerization kinetics, aliquots the reaction mixture (1 mL each) were dispensed into glass ampules. The aliquots were bubbled with nitrogen for 1 h, sealed, and placed in a 70°C oil bath. At each designated timepoint (0, 1, 2, 4, 5, 6, 10, 12, 16, and 20 h), samples were quenched by bubbling with air and freezing at -20°C. GPC was run directly on the quenched reaction mixture (as described below). For ^{1}H NMR, the quenched reaction mixtures were lyophilized and reconstituted in D_2O using 2 mg/mL DMSO as an external standard. The integration values of the vinyl peaks were compared to that of the constant DMSO external standard to follow remaining monomer concentration and conversion.

5.6.4 Polymer Characterization

The polymer was characterized by aqueous size exclusion chromatography (SEC) on an Aglient HPLC 1260 Infinity equipped with refractive index detector

and a Wyatt miniDAWN TREOS light scattering detector. An elutent of 1 wt% acetic acid in 0.1 M LiBr (pH=3.3) was run at 1 mL/min on an Eprogen CATSEC 300 column. Kinetics runs were analyzed on a CATSEC 100 column. For molecular weight analysis using light scattering, the *dn/dc* value for p(GPMA-*co*-MA) was determined (0.1782) by injecting known stock solutions of PG ranging from 0.25-2 mg/mL at 1 mL/min using a syringe pump (PHD Ultra, Harvard Apparatus). Final monomer composition was calculated using ^{1}H NMR.

5.6.5 Production of Embolic Coacervates

Coacervates of PG and MP were prepared with 1-5 μm Ta powder added as a radiocontrast agent (30 wt% of final coacervate), unless otherwise noted. Aqueous stock solutions of PG and MP were made at 100 mg/mL and 200 mg/mL, respectively. The pH of both solutions was adjusted to 7.2. Coacervation was achieved by sequential addition of DI water, 5M NaCl, MP solution, Ta powder, and PG solution, while mixing with an overhead mixer. In this final mixture, PG concentration was fixed at 50 mg/mL; MP concentration was 42 mg/mL based upon calculated charge densities and a 1:2 charge ratio. Amounts of DI water and 5 M salt were adjusted to form an NaCl concentration of 800 mM. Phase separation occurred immediately upon addition of PG, and the coacervate was allowed to settle for 12 h. Afterwards, the supernatant was removed and 5 M NaCl was mixed into the condensed phase using trituration to bring the overall [NaCl] in the coacervate to its final concentration (1400 mM, unless otherwise noted). PRT-MP coacervates were prepared using the same method, substituting PRT for PG.

5.6.6 Injection Pressures

For pressure measurements, 22 gauge dispensing tips (Jensen Global Inc.) were glued into 50 cm lengths of 23 gauge PTFE tubing (Zeus Inc.), which have an internal diameter (0.026 in.) closely matching that of clinically used 3 F catheters. ECs in 1 mL syringes (Medallion, Merit Medical Inc.) were warmed to 37°C, and attached to the tubing. The tubing was placed in a 37°C water bath and the coacervate was injected at the 0.3 $mL \cdot min^{-1}$ using a syringe pump (PHD Ultra, Harvard Apparatus). To measure injection forces, a compression load cell (iLoad Mini, Loadstar Sensors) was attached to the syringe pump between the driver and the syringe plunger. Steady state injection forces were measured and converted to pressure using the bore diameter of the syringe (4.8 mm). Injection pressures were measured in 50 cm model catheters, but converted to those that would be generated in 135 cm catheters using a linear conversion, as predicted by Poiseuille's equation for steady laminar fluid flow in a tube of uniform diameter:

$$\Delta P = \frac{8\mathrm{Q}\mu L}{\pi r^4}$$

where P is pressure, r is the radius of the tube, L is the length of the tube, Q is the volumetric flow rate, and μ is viscosity. This linear conversion was also verified experimentally in our model. Poiseuille's law was also used to compare measured injection pressures with rheological flow curves.

5.6.7 Rheology

The complex fluid behavior of ECs was characterized on a temperature controlled rheometer (AR 2000ex, TA Instruments) at 37°C. High salt (1400 mM) samples were analyzed using a 4° cone and plate geometry equipped with a solvent trap to prevent evaporation during the experiment. First, an oscillatory frequency sweep from 0.1 to 10 Hz with a fixed strain of 1% was used to examine viscoelastic properties. Next, viscosity was evaluated as shear rate was stepped from 0.1 s^{-1} to 500 s^{-1} at 10 points per decade. A 20 mm flat plate geometry was used for rheological evaluation of the ECs in physiological saline. Adhesive sandpaper was cut to size with a laser cutter and attached to the geometry to prevent slippage (1 mm gap). The ECs were injected into BSS atop the geometry in a circular mold and allowed to equilibrate for 12 h before loading onto the rheometer. An oscillatory frequency sweep was done using the same method as the high salt ECs.

5.6.8 Catheter Pull-Out Force

ECs were injected into filtration tubes (Supelco, Inc.; cat #57240-U) to a height of 1 cm (~300 µL of EC). A cut section (~10 cm in length) of 3 F catheter (Renegade HI-FLO, Boston Scientific Inc.) were placed in the center of each EC-filled tube. The filtration tubes were completely submerged in a dish containing BSS and allowed to incubate. At predetermined intervals of 2 min and 24 h, the force required to remove the catheter from the solidified EC was measured on an Instron 3342 materials tester (Instron, Inc.) equipped with a 10 N load cell and

controlled with Bluehill 3 software. The catheter was removed in extension mode with a strain rate of 600 mm·min^{-1}.

5.6.9 Rabbit Auricular Artery Embolization

The subchronic tissue response to ECs was evaluated in a rabbit auricular artery model. All animal studies were carried out in accordance with the University of Utah IACUC guidelines and approved protocols. One hour prior to the procedure, the rabbit was weighed, the ear was shaved and cleaned with 70% isopropyl alcohol, and a local anesthetic cream (EMLA) was applied topically. Buprenorphine (Buprenex) was also given to prevent pain or irritation. Immediately before the procedure, EMLA was reapplied to the ear to dilate the blood vessels. A sterile 24 gauge intravascular catheter (BD Medical) was advanced into the central artery of the ear within the distal third. The central needle was withdrawn from the catheter, and before embolizing, the catheter was flushed with saline to confirm arterial positioning. The embolic agent was injected to fill ~2 cm of the artery (~ 25 µL) as the catheter was slowly retracted. After 2 min, the catheter was completely removed, and pressure on the artery was maintained. Embolization was verified visually. The embolic plug was monitored for signs of movement for 10 min. At the designated timepoints, the animals were euthanized by first sedating the animals with ketamine/xylazine (IM) followed by intravenous injection of euthanasia solution (VetOne). During necropsy, ear tissue was harvested and fixed with 10% buffered formalin. After 1 week, the ears were cut into small sections (~4 cm^2). Tissue sections within the embolization site were collected, in

addition to proximal and distal sections. Sections were embedded in paraffin and sectioned prior to staining with hematoxylin and eosin and Masson's trichrome.

5.6.10 Statistical Analysis

Unless otherwise noted, values reported here represent an average of three runs +/- standard deviation. Using IBM SPSS Statistics 24 software, one-way ANOVAs with post-hoc Tukey tests were performed to analyze means for statistical significance.

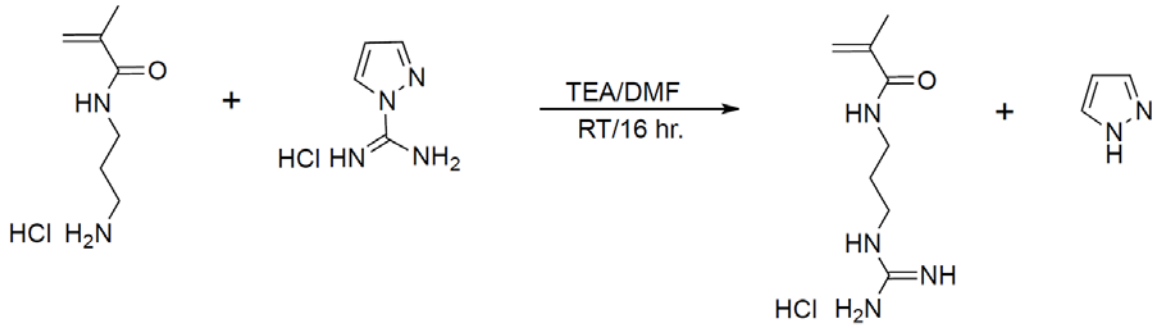

Figure 5.1. GPMA monomer synthesis. 3-Guanidinopropyl methacrylamide (GPMA) was produced by guanylation of 3-Aminopropyl methacrylamide (APMA).

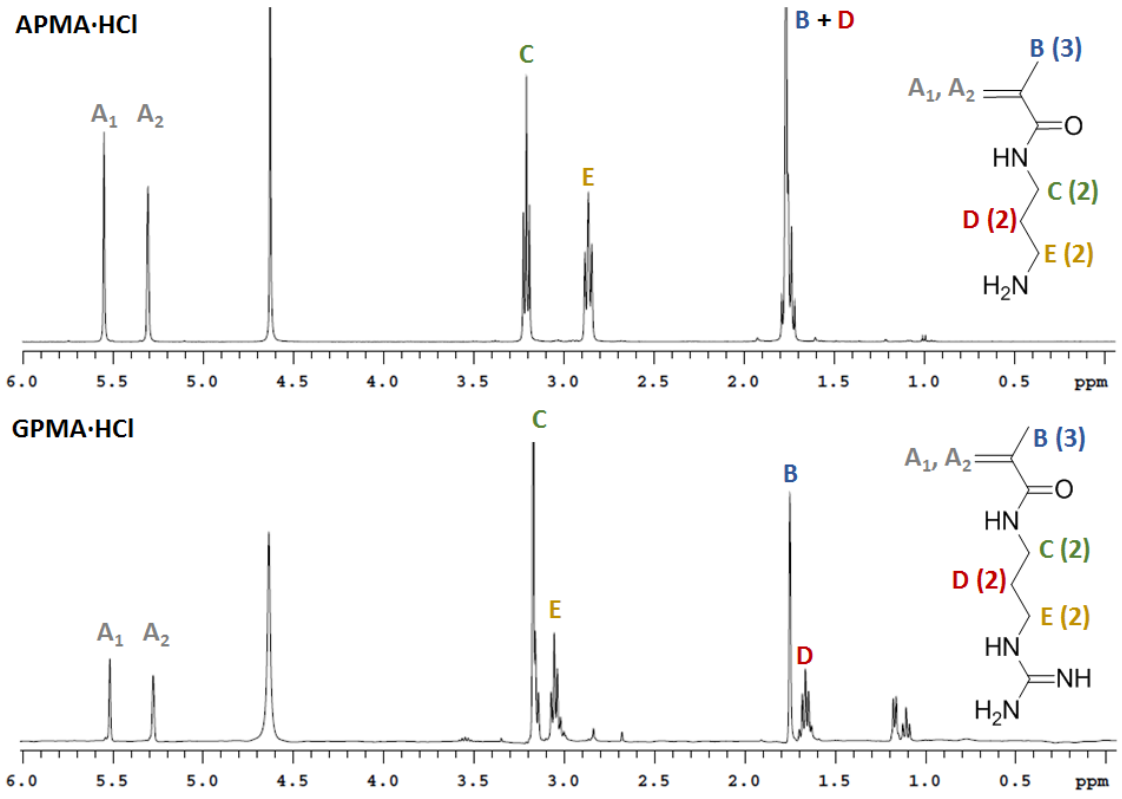

Figure 5.2. ^{1}H NMR of APMA and GPMA. Production of GPMA product is indicated by the deshielding of (E) created by converting the amine to guanidinine.

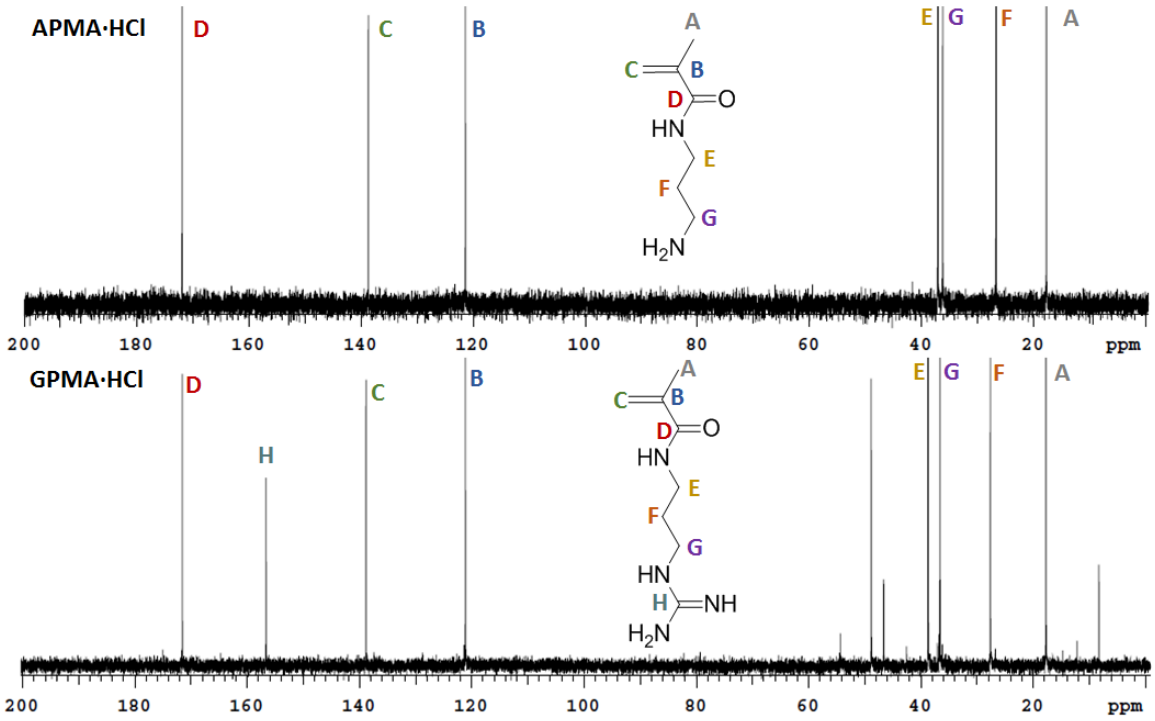

Figure 5.3. ^{13}C NMR of APMA and GPMA. Formation of the GPMA product is indicated by appearance of the guanidinium carbon (H) and slight deshielding of G.

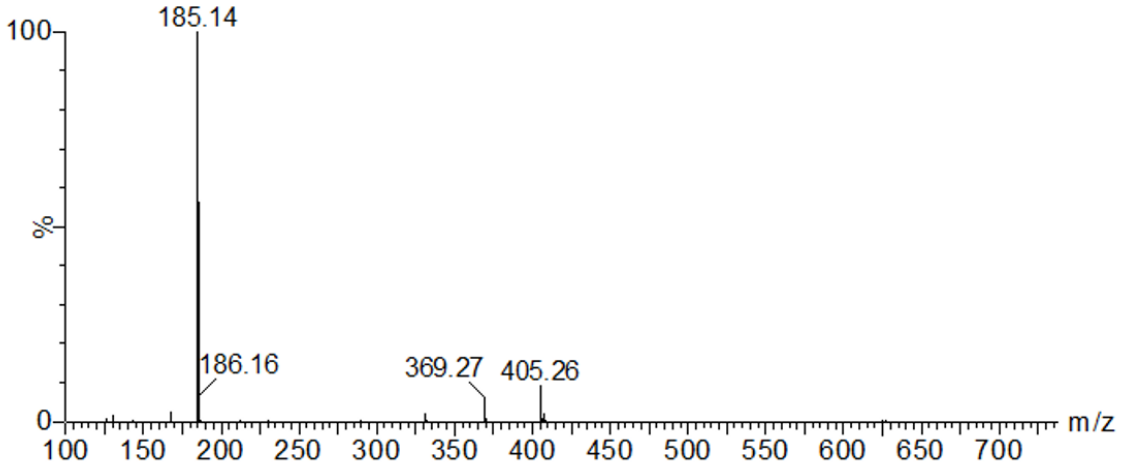

Figure 5.4. ESI mass spectrum of GPMA. The GPMA product is found at 185.1 Da. APMA starting material is not present in final product (143.1 Da).

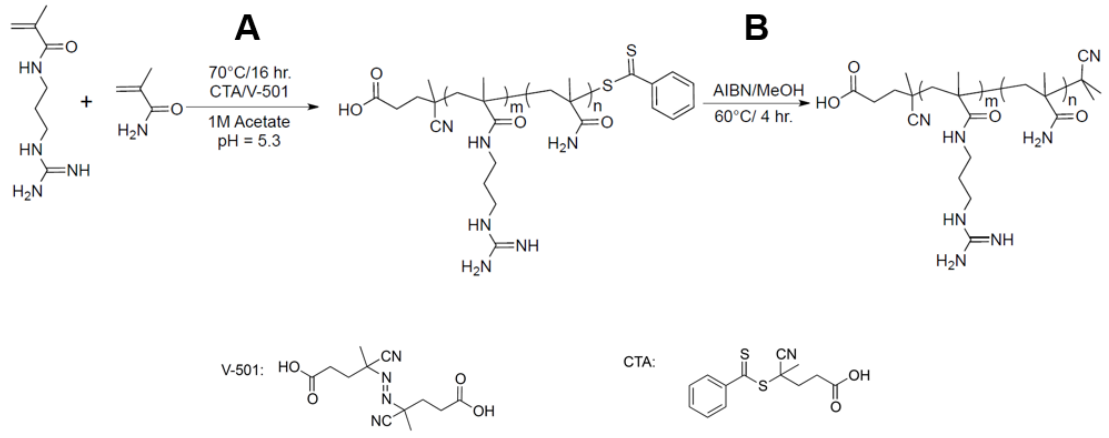

Figure 5.5. Production of p(GPMA-*co*-MA). (A) Aqueous RAFT polymerization of GPMA and MA followed by (B) End-group modification to remove CTA. Structures of CTA and initiator (V-501) shown at bottom.

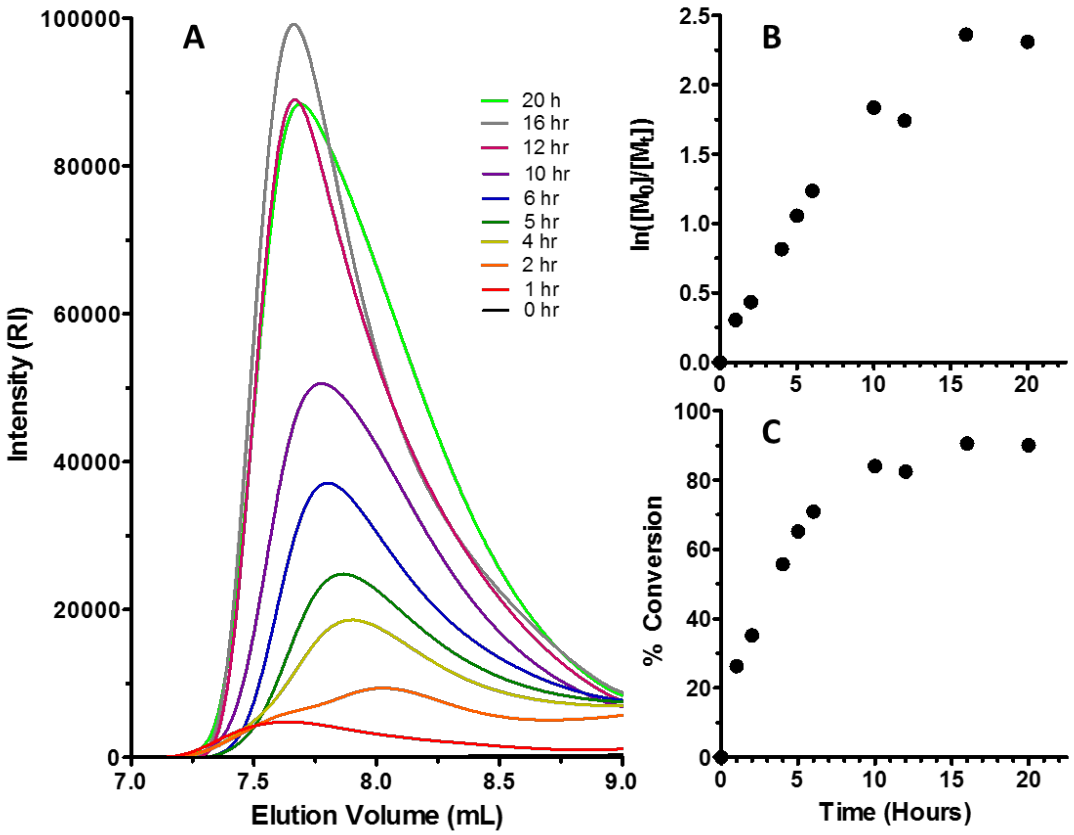

Figure 5.6. RAFT polymerization kinetics. (A) RI traces from GPC. (B) Pseudo-first order kinetics plot. (C) Monomer conversion as a function of time.

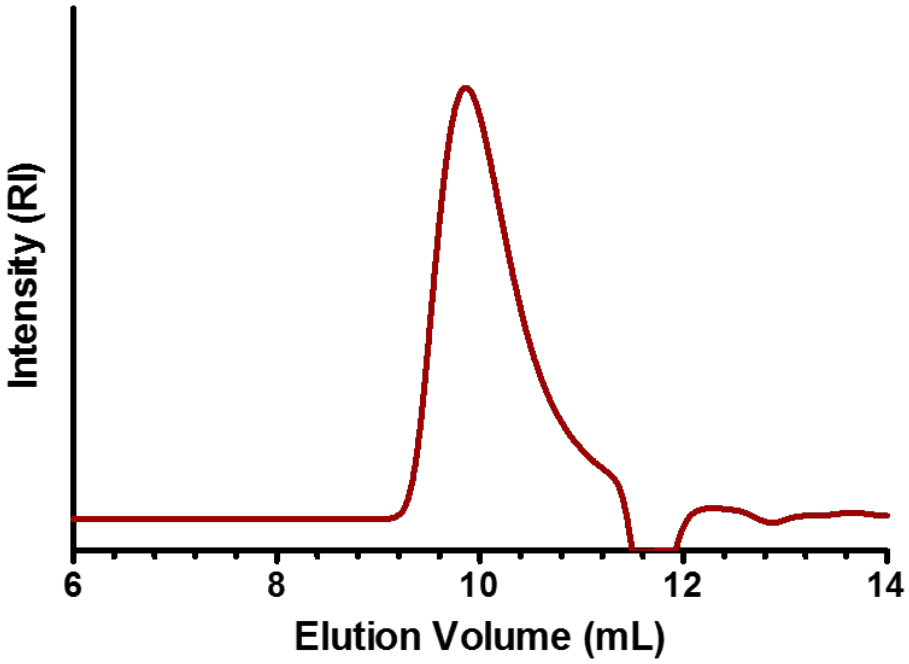

Figure 5.7. SEC profile (RI) of p(GPMA-co-MA) on CATSEC300 column after purification.

Table 5.1. Properties of PG-MP PE complexes at various NaCl concentrations. Volume yield is a percent of overall batch size (i.e. with a 10% yield, a 1 mL batch produced 100 µL of coacervate). A dramatic drop in yield from 800 mM to 1200 mM is accompanied by transition to a clear, flowing coacervate (No Ta).

NaCl Concentration	Appearance	Volume Yield
150 mM	Opaque	12%
400 mM	Opaque	9.0%
800 mM	Opaque	8.0%
1200 mM	Clear	2.5%
1400 mM	Clear	2.0%

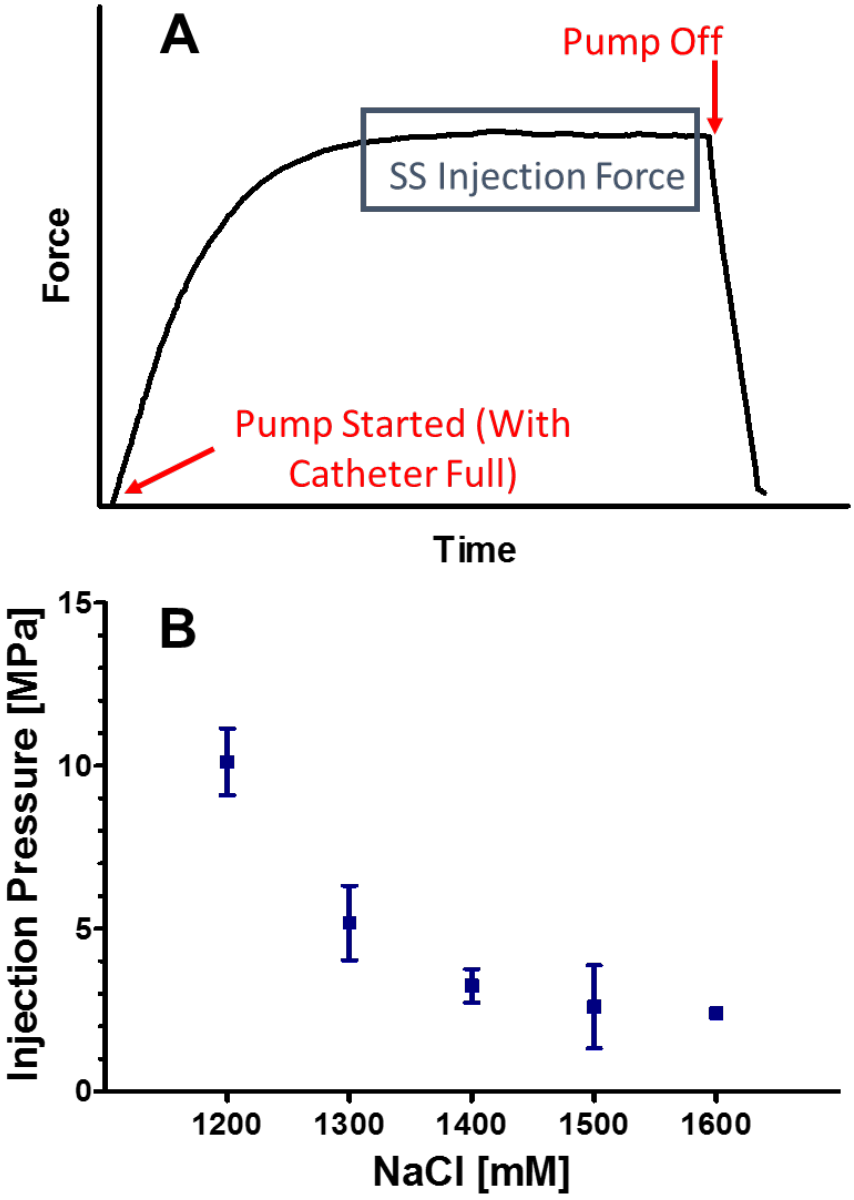

Figure 5.8. Injection pressures. (A) Illustrative raw force profile for single run. (B) SS injection pressures for PG-MP (+Ta) in 135 cm catheters, 0.026" ID vs. [NaCl]. For all points, *n*=3, and error bars are +/- SD.

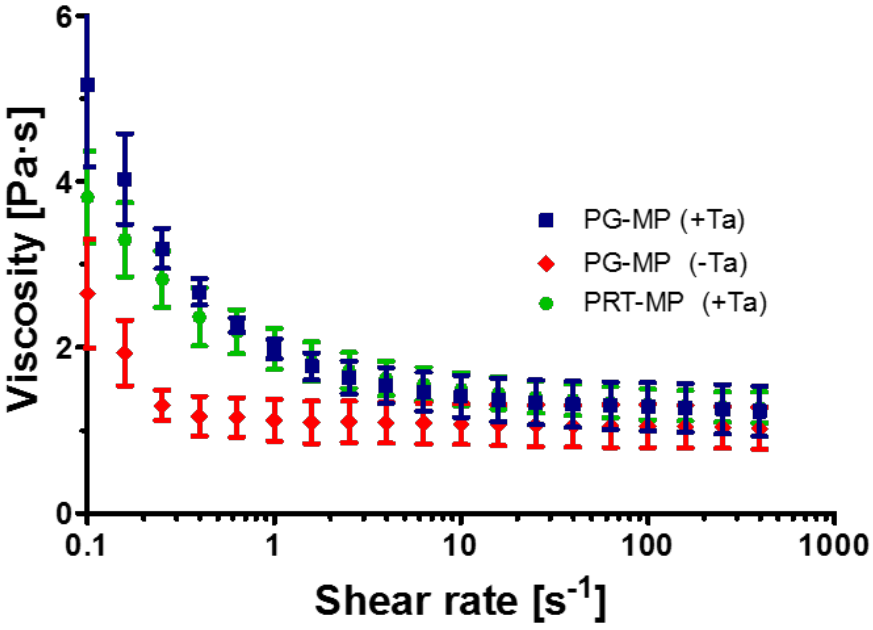

Figure 5.9. Rheological flow curves for ECs in high salt. For all points, *n*=3, and error bars are +/- SD.

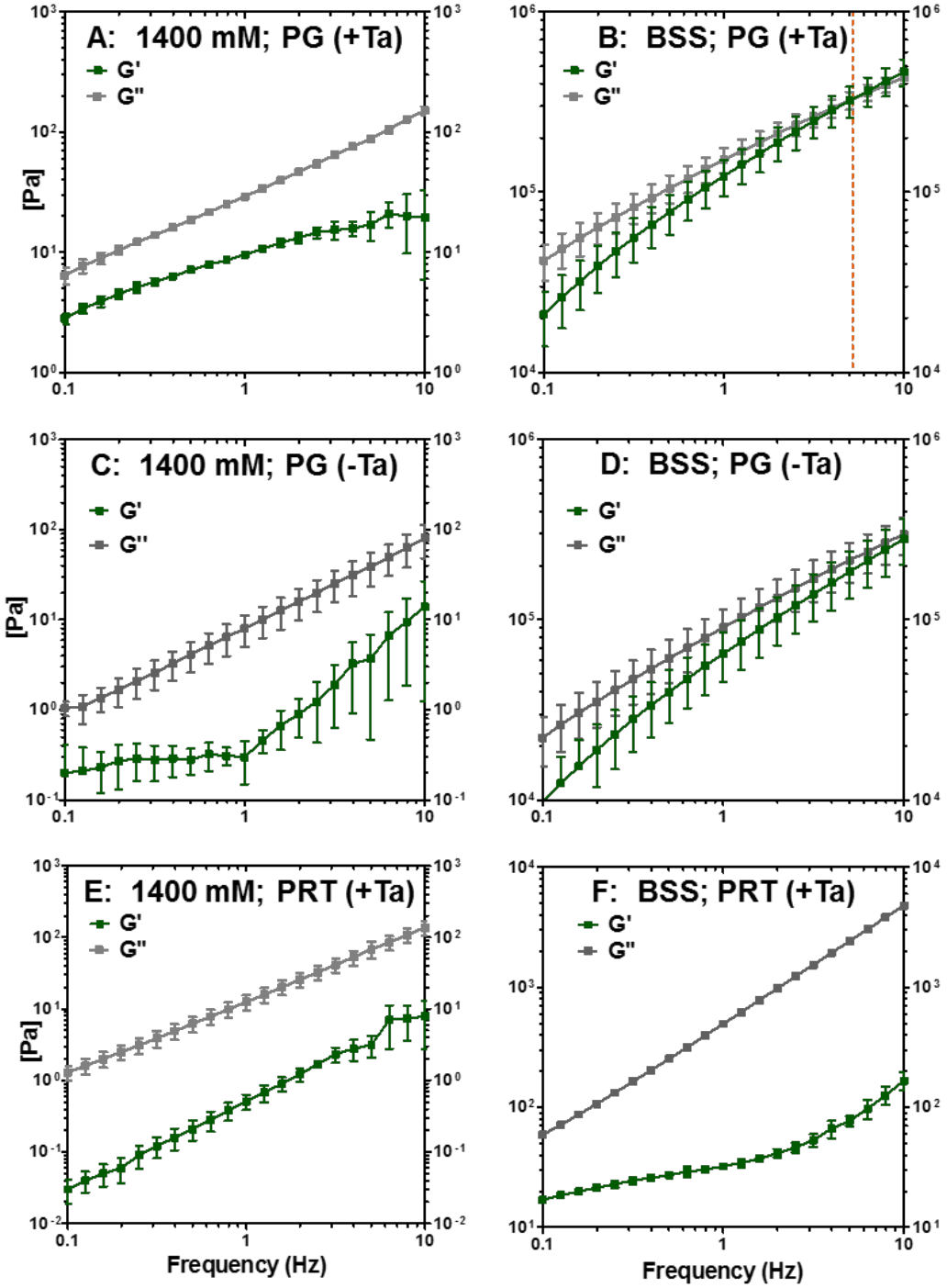

Figure 5.10. Frequency sweep for ECs before and after injection into BSS. (A,B) PG-MP (+Ta). (C,D) PG-MP (-Ta). (D,E) PRT-MP (+Ta). Crossover frequency (G'=G") indicated by orange dashed line. MP. For all points, *n*=3, and error bars are +/- SD.

A

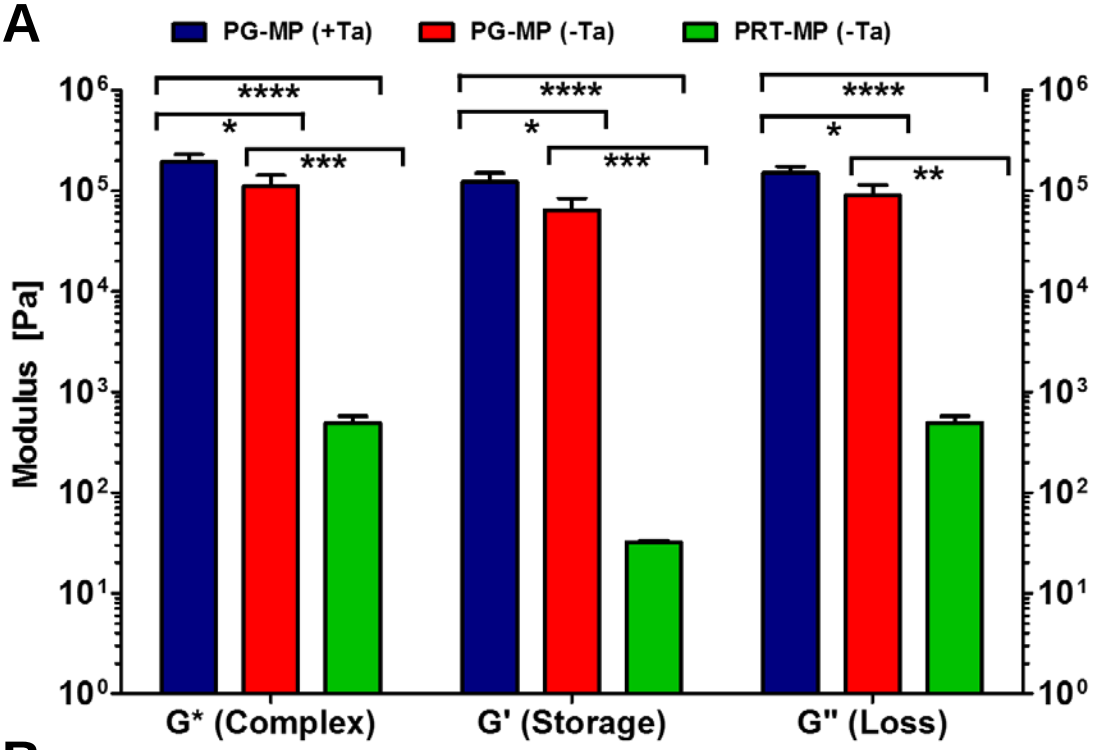

B

Coacervate	Complex Modulus (G*)/kPa	Storage Modulus (G')/kPa	Loss Modulus (G")/kPa	Crossover Freq. (G'=G") Hz
PG-MP +Ta into BSS	195 (+/- 36.2)	123 (+/- 27.9)	150 (+/- 24.2)	5.2
PG-MP into BSS	111 (+/- 31.2)	64.8 (+/- 19.9)	90.5 (+/- 24.2)	17
PRT-MP +Ta into BSS	0.497 (+/- 0.076)	0.032 (+/- 0.001)	0.496 (+/- 0.077)	N/A
PG-MP +Ta 1400 mM	0.025 (+/- 0.009)	0.006 (+/- 0.005)	0.031 (+/- 0.001)	N/A
PG-MP 1400 mM	0.008 (+/- 0.003)	0.0003 (+/- 0.0002)	0.008 (+/- 0.003)	N/A
PRT-MP +Ta 1400 mM	0.013 (+/- 0.003)	0.0005 (+/- 0.0001)	0.013 (+/- 0.003)	N/A

Figure 5.11. Summary of oscillatory rheology properties at 1 Hz and 1% strain. (A) Moduli of ECs injected into BSS. *p<0.05; ** p<0.02; ***p<0.01; ****p<0.001. (B) Table of oscillatory rheology properties in high salt (1400 mM) and after injection into BSS. For all points, n=3, and error bars are +/- SD.

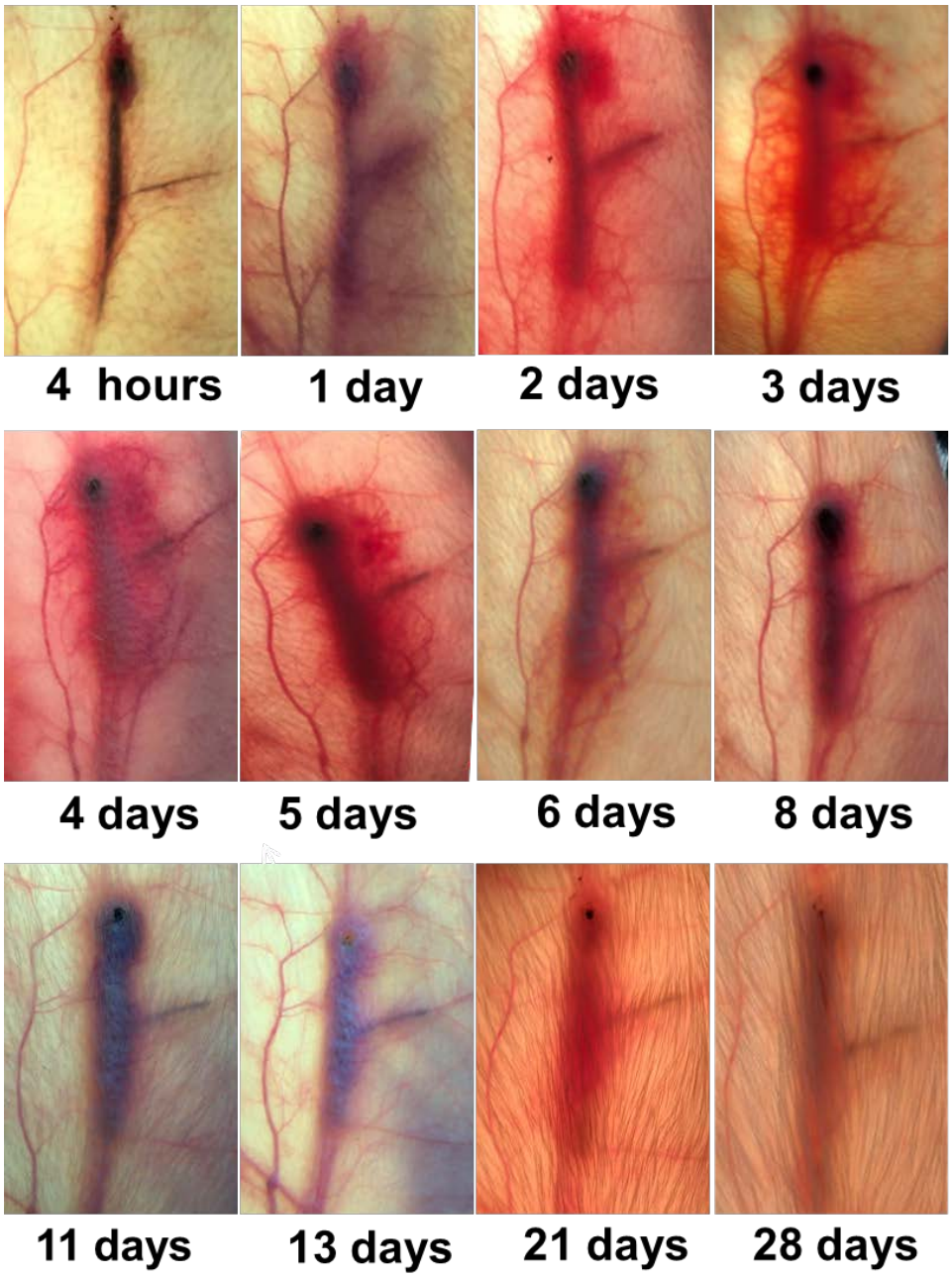

Figure 5.12. Gross tissue response to embolization. Central auricular artery and associated branching artery are shown embolized with PG-MP (+Ta). Access site is at top; all photos are from the same ear.

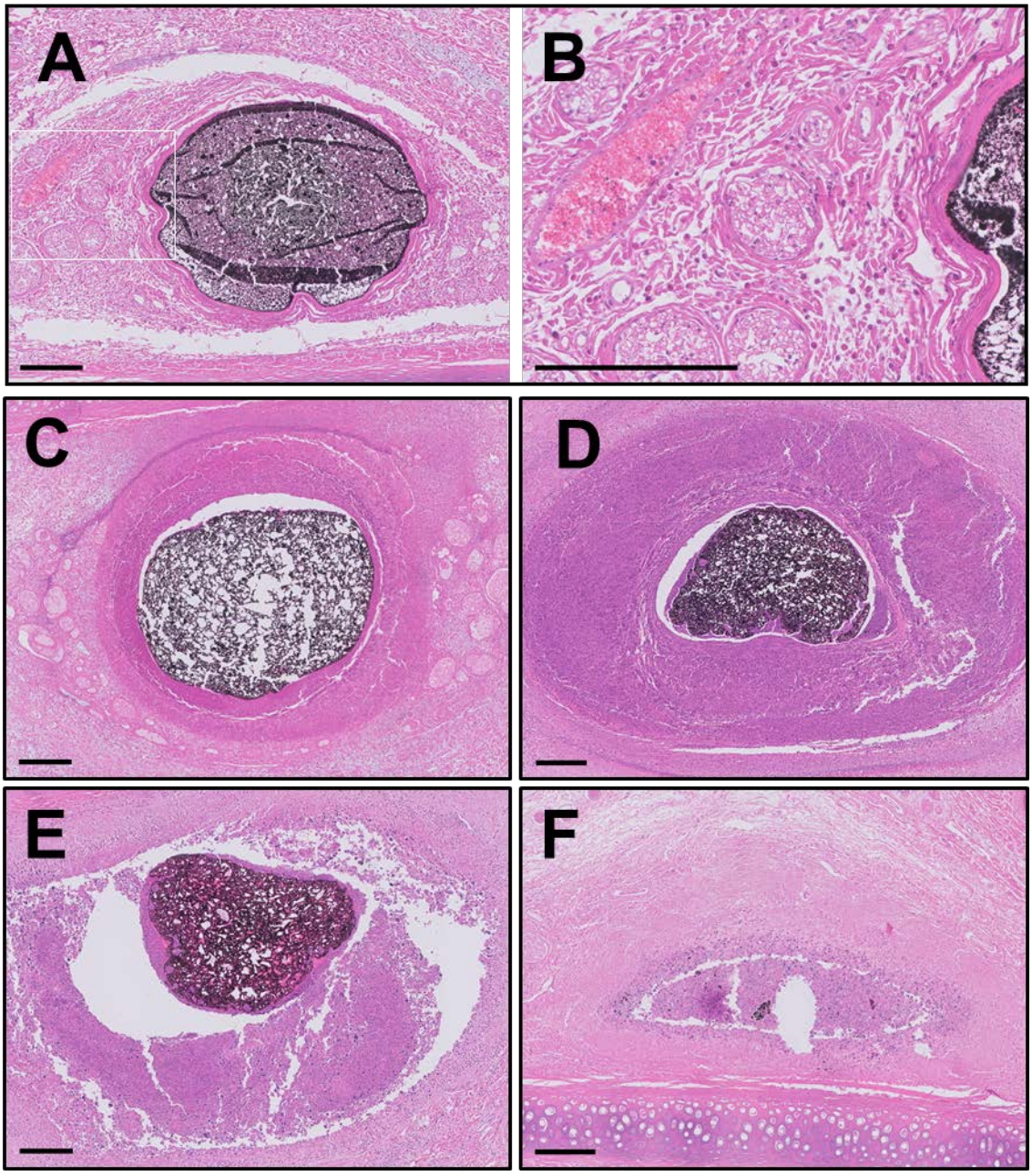

Figure 5.13. Histological response to PG-MP +Ta. (A) 1 day with inset (B) showing neutrophil migration from patent vessel at left; Neutrophilic inflammation grows progressively thicker at 4 days (C), 7 days (D), and 14 days (E). By 32 days (F), vessel is completely obliterated and tantalum has been carried away by phagocytes. No signs of recanalization are observed. Scale bars =200 μm.

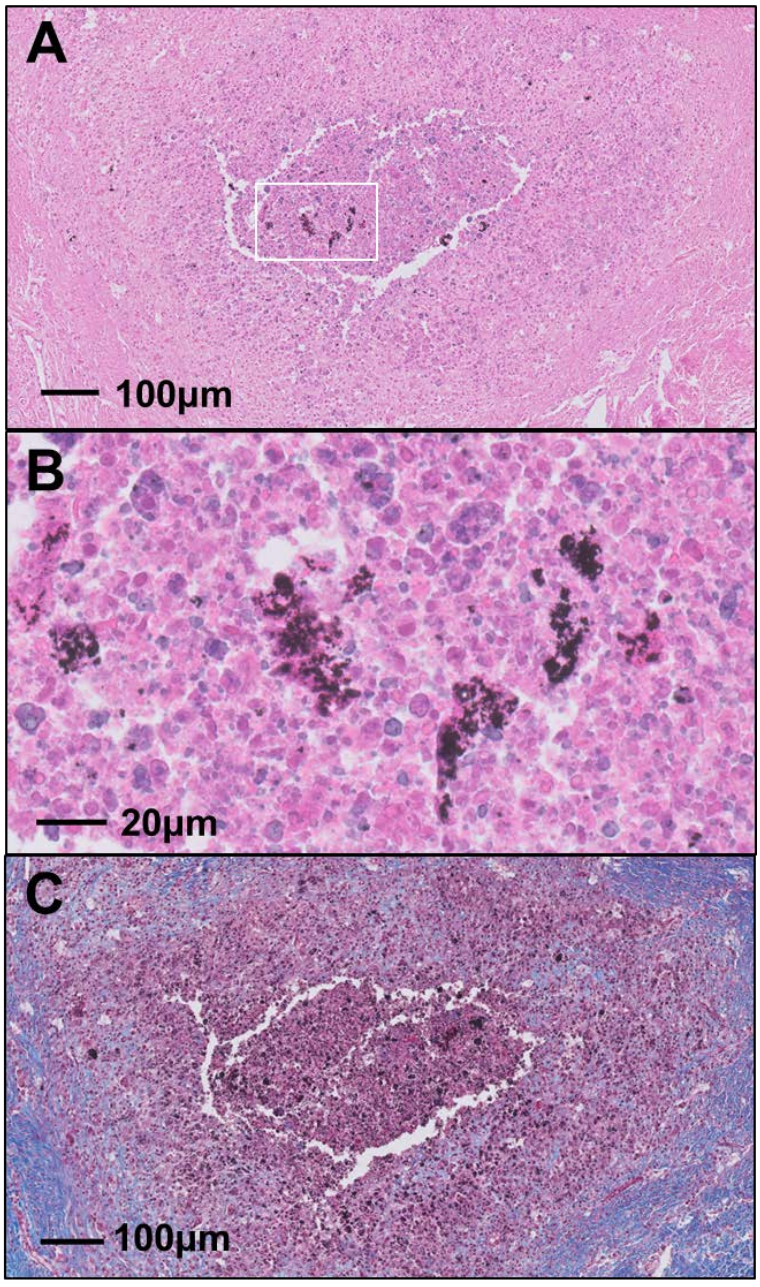

Figure 5.14. Artery embolized with EC at 32 days. (A) H&E stain showing complete obliteration of vessel wall with subsiding neutrophilic inflammation. (B) Trichrome of same section showing early stage fibrosis within nodule of inflammation (C) High magnification inset from H&E showing globules of material and Ta phagocytosis.

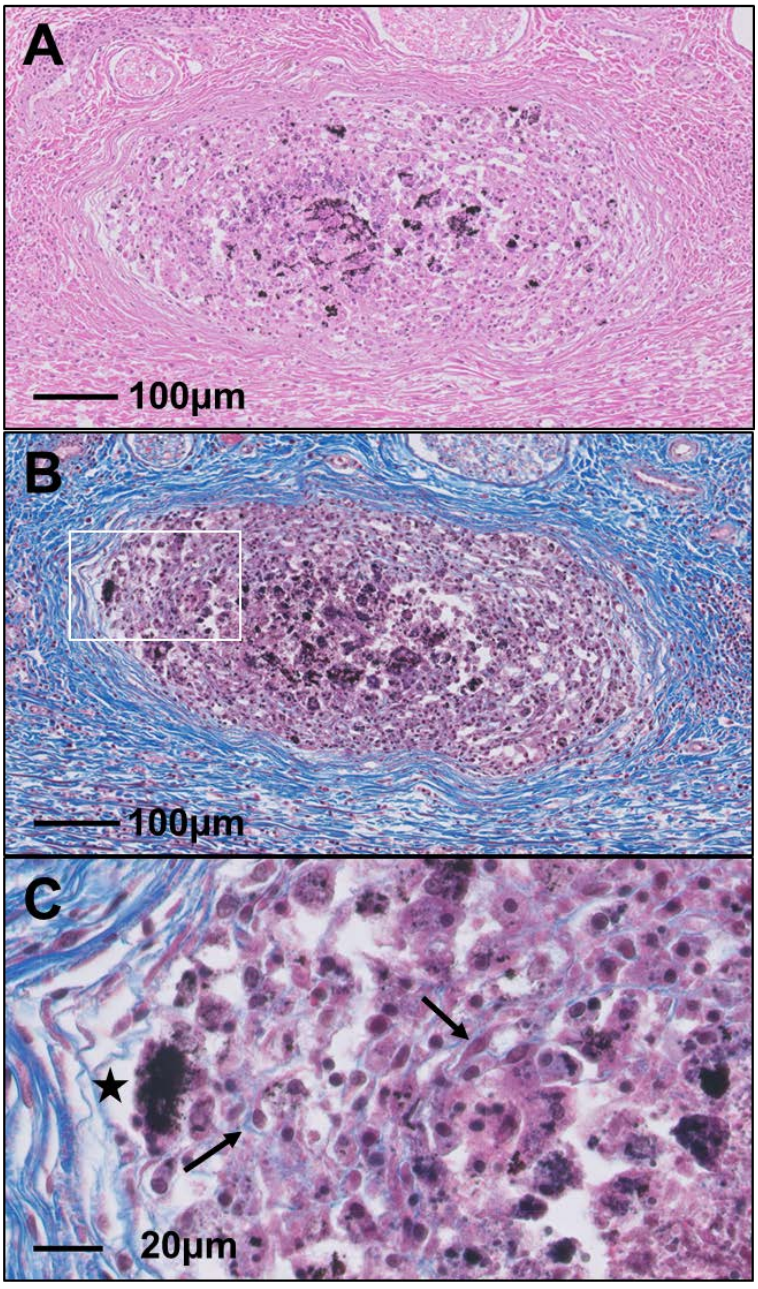

Figure 5.15. Histology of PG-P6 +Ta injected into vein at 29 days. (A) H&E stain (B) Trichrome, with intact layers of tunica adventitia surrounding embolus (C) High-magnification inset from B, showing Ta phagocytosis (star) and deposition of collagen within the embolus (arrows).

5.7 References

[1] J.P. Jones, M. Sima, R.G. O'Hara, R.J. Stewart, Water-borne endovascular embolics inspired by the undersea adhesive of marine sandcastle worms, Adv. Healthc. Mater. 5(7) (2016) 795-801.

[2] M. Lubarsky, C.E. Ray, B. Funaki, Embolization agents—Which one should be used when? Part 1: Large-vessel embolization, Semin. Intervent. Radiol. 26(4) (2009) 352-357.

[3] M. Lubarsky, C. Ray, B. Funaki, Embolization agents—Which one should be used when? Part 2: Small-vessel embolization, Semin. Intervent. Radiol. 27(1) (2010) 99-104.

[4] W. Taki, Y. Yonekawa, H. Iwata, A. Uno, K. Yamashita, H. Amemiya, A new liquid material for embolization of arteriovenous malformations, Am. J. Neuroradiol. 11(1) (1990) 163-168.

[5] J.S. Pollak, R.I. White, The use of cyanoacrylate adhesives in peripheral embolization, J. Vasc. Interv. Radiol. 12(8) (2001) 907-913.

[6] F. Mottu, A. Laurent, D.A. Rüfenacht, E. Doelker, Organic solvents for pharmaceutical parenterals and embolic liquids: a review of toxicity data, PDA J. Pharm. Sci. Technol. 54(6) (2000) 456-469.

[7] M. Guimaraes, M. Wooster, Onyx (ethylene-vinyl alcohol copolymer) in peripheral applications, Semin. Intervent. Radiol. 28(3) (2011) 350-356.

[8] S.L. Blackburn, Y. Kadkhodayan, W.Z. Ray, G.J. Zipfel, D.T. Cross, C.J. Moran, C.P. Derdeyn, Onyx is associated with poor venous penetration in the treatment of spinal dural arteriovenous fistulas, J. Neurointerv. Surg. 6(7) (2014) 536-540.

[9] S. Vaidya, K.R. Tozer, J. Chen, An overview of embolic agents, Semin. Intervent. Radiol. 25(3) (2008) 204-215.

[10] G.M. Debrun, V.A. Aletich, H. Shownkeen, J. Ausman, Glued catheters during embolisation of brain AVMs with acrylic glue, Interv. Neuroradiol. 3(1) (1997) 13-19.

[11] S. Paramasivam, D. Altschul, S. Ortega-Gutiarrez, J. Fifi, A. Berenstein, *N*-butyl cyanoacrylate embolization using a detachable tip microcatheter: initial experience, J. Neurointerv. Surg. 7(6) (2015) 458-461.

[12] J. Raymond, A. Metcalfe, I. Salazkin, A. Schwarz, Temporary vascular occlusion with poloxamer 407, Biomaterials 25(18) (2004) 3983-3989.

[13] H.H. Bearat, M.C. Preul, B.L. Vernon, Cytotoxicity, *in vitro* models and preliminary *in vivo* study of dual physical and chemical gels for endovascular embolization of cerebral aneurysms, J. Biomed. Mater. Res. 101(9) (2013) 2515-2525.

[14] A. Poursaid, R. Price, A. Tiede, E. Olson, E. Huo, L. McGill, H. Ghandehari, J. Cappello, *In situ* gelling silk-elastinlike protein polymer for transarterial chemoembolization, Biomaterials 57 (2015) 142-152.

[15] T.A. Becker, D.R. Kipke, T. Brandon, Calcium alginate gel: A biocompatible and mechanically stable polymer for endovascular embolization, J. Biomed. Mater. Res. 54(1) (2001) 76-86.

[16] A. Momeni, E.M. Valliant, E.P. Brennan-Pierce, J.J.S. Shankar, R. Abraham, P. Colp, M.J. Filiaggi, Developing an *in situ* forming polyphosphate coacervate as a new liquid embolic agent: From experimental design to pilot animal study, Acta Biomater. 32 (2016) 286-297.

[17] L. Weng, N. Rostambeigi, N.D. Zantek, P. Rostamzadeh, M. Bravo, J. Carey, J. Golzarian, An *in situ* forming biodegradable hydrogel-based embolic agent for interventional therapies, Acta Biomater. 9(9) (2013) 8182-8191.

[18] J. Fu, J.B. Schlenoff, Driving forces for oppositely charged polyion association in aqueous solutions: enthalpic, entropic, but not electrostatic, J. Am. Chem. Soc. 138(3) (2016) 980-990.

[19] Q. Wang, J.B. Schlenoff, The polyelectrolyte complex/coacervate continuum, Macromolecules 47(9) (2014) 3108-3116.

[20] A.B. Kayitmazer, Thermodynamics of complex coacervation, Adv. Colloid Interface Sci. 239 (2017) 169-177.

[21] C.G. De Kruif, F. Weinbreck, R. de Vries, Complex coacervation of proteins and anionic polysaccharides, Curr. Opin. Colloid Interface Sci. 9(5) (2004) 340-349.

[22] H. Shao, R.J. Stewart, Biomimetic underwater adhesives with environmentally triggered setting mechanisms, Adv. Mater. 22(6) (2010) 729-733.

[23] R.A. Ghostine, R.F. Shamoun, J.B. Schlenoff, Doping and diffusion in an extruded saloplastic polyelectrolyte complex, Macromolecules 46(10) (2013) 4089-4094.

[24] R. Porsche, Z.R. Brenner, Allergy to protamine sulfate, Heart Lung 28(6) (1999) 418-428.

[25] S.K. Gupta, F.J. Veith, E. Ascer, K.R. Wengerter, C. Franco, D. Amar, E.-S. El-Gaweet, A. Gupta, Anaphylactoid reactions to protamine: an often lethal complication in insulin-dependent diabetic patients undergoing vascular surgery, J. Vasc. Surg. 9(2) (1989) 342-350.

[26] K.W. Park, Protamine and protamine reactions, Int. Anesthesiol. Clin. 42(3) (2004) 135-145.

[27] Assessment Report for Protamine Containing Medicinal Products, Europen Medicines Agency, London, UK, 2012.

[28] P. Sautière, G. Briand, M. Gusse, P. Chevaillier, Primary structure of a protamine isolated from the sperm nuclei of the dog-fish Scylliorhinus caniculus, Eur. J. Biochem. 119(2) (1981) 251-255.

[29] C.A. Fitch, G. Platzer, M. Okon, E. Garcia-Moreno, L.P. McIntosh, Arginine: Its pKa value revisited, Protein Sci. 24(5) (2015) 752-761.

[30] N.J. Treat, D. Smith, C. Teng, J.D. Flores, B.A. Abel, A.W. York, F. Huang, C.L. McCormick, Guanidine-containing methacrylamide (co)polymers via a RAFT: Toward a cell-penetrating peptide mimic, ACS Macro Lett. 1(1) (2011) 100-104.

[31] S.E. Exley, L.C. Paslay, G.S. Sahukhal, B.A. Abel, T.D. Brown, C.L. McCormick, S. Heinhorst, V. Koul, V. Choudhary, M.O. Elasri, Antimicrobial peptide mimicking primary amine and guanidine containing methacrylamide copolymers prepared by RAFT polymerization, Biomacromolecules 16(12) (2015) 3845-3852.

[32] Y. Yonamine, K. Yoshimatsu, S.-H. Lee, Y. Hoshino, Y. Okahata, K.J. Shea, Polymer nanoparticle–protein interface. Evaluation of the contribution of positively charged functional groups to protein affinity, ACS Appl. Mater. Interfaces 5(2) (2013) 374-379.

[33] M.S. Bernatowicz, Y. Wu, G.R. Matsueda, 1H-pyrazole-1-carboxamidine hydrochloride an attractive reagent for guanylation of amines and its application to peptide synthesis, J. Org. Chem. 57(8) (1992) 2497-2502.

[34] J.R. Van Wazer, C.F. Callis, Metal complexing by phosphates, Chem. Rev. 58(6) (1958) 1011-1046.

[35] J.I. Watters, S. Kalliney, R.C. Machen, A study of basicity of tri- and tetrametaphosphate and the stability of their complexes with copper(II) by means of the glass pH and the dropping amalgam electrodes—I, J. Inorg. Nucl. Chem. 31(12) (1969) 3817-3821.

[36] N. Angelova, D. Hunkeler, Effect of preparation conditions on properties and permeability of chitosan–sodium hexametaphosphate capsules, J. Biomater. Sci. Polym. Ed. 12(12) (2001) 1317-1337.

[37] M. Kawabe, O. Ohashi, I. Yamaguchi, Phosphorus nuclear magnetic resonance in polyphosphates and determination of their hydrolysis rate constants, Bull. Chem. Soc. Jpn. 43(12) (1970) 3705-3710.

[38] J.R. Van Wazer, K.A. Holst, Structure and properties of the condensed phosphates: Some general considerations about phosphoric acids, J. Am. Chem. Soc. 72(2) (1950) 639-644.

[39] F. Rashchi, J.A. Finch, Polyphosphates: A review their chemistry and application with particular reference to mineral processing, Miner. Eng. 13(10) (2000) 1019-1035.

[40] A.S. Puri, R. Rahbar, J. Dearden, R.J. Graham, C. Lillehei, D.B. Orbach, Stretched and sheared microcatheter retained after onyx embolization of infantile myofibromatosis, Interv. Neuroradiol. 17(2) (2011) 261-266.

[41] J.G. Ren, H.F. Wang, G. Chen, W. Zhang, H.Z. Jia, J. Feng, Y.F. Zhao, *In vivo* synergetic effect of *in situ* sclerotherapy and transient embolotherapy designed for fast-flow vascular malformation treatments with the aid of injectable hydrogel, J. Mater. Chem. 1(20) (2013) 2601-2611.

[42] N.E. Larsen, E.A. Leshchiner, E.G. Parent, J. Hendrikson-Aho, E.A. Balazs, S.K. Hilal, Hylan gel composition for percutaneous embolization, J. Biomed. Mater. Res. 25(6) (1991) 699-710.

[43] J. Raymond, A. Metcalfe, P. Leblanc, I. Salazkin, K. Papineau, D. Roy, J.P. Soucy, J.A. Krom, A. Schwarz, Production of radioactive particles for endovascular therapeutic interventions, Biomaterials 27(8) (2006) 1566-1572.

[44] A. Schwarz, H. Zhang, A. Metcalfe, I. Salazkin, J. Raymond, Transcatheter embolization using degradable crosslinked hydrogels, Biomaterials 25(21) (2004) 5209-5215.

[45] E.R. Clark, E.L. Clark, Observations on living arterio-venous anastomoses as seen in transparent chambers introduced into the rabbit's ear, Am. J. Anat. 54(2) (1934) 229-286.

[46] J.L. Morris, R.D. Bevan, Development of the vascular bed in the rabbit ear: scanning electron microscopy of vascular corrosion casts, Am. J. Anat. 171(1) (1984) 75-89.

[47] H.H. Hariri, A.M. Lehaf, J.B. Schlenoff, Mechanical properties of osmotically stressed polyelectrolyte complexes and multilayers: Water as a plasticizer, Macromolecules 45(23) (2012) 9364-9372.

[48] R. Chollakup, J.B. Beck, K. Dirnberger, M. Tirrell, C.D. Eisenbach, Polyelectrolyte molecular weight and salt effects on the phase behavior and coacervation of aqueous solutions of poly(acrylic acid) sodium salt and poly(allylamine) hydrochloride, Macromolecules 46(6) (2013) 2376-2390.

[49] J.B. Schlenoff, A.H. Rmaile, C.B. Bucur, Hydration contributions to association in polyelectrolyte multilayers and complexes: Visualizing hydrophobicity, J. Am. Chem. Soc. 130(41) (2008) 13589-13597.

[50] R.K. Avery, H. Albadawi, M. Akbari, Y.S. Zhang, M.J. Duggan, D.V. Sahani, B.D. Olsen, A. Khademhosseini, R. Oklu, An injectable shear-thinning biomaterial for endovascular embolization, Sci. Transl. Med. 8(365) (2016) 156.

[51] F. Zhou, L. Chen, Q. An, L. Chen, Y. Wen, F. Fang, W. Zhu, T. Yi, Novel Hydrogel Material as a Potential Embolic Agent in Embolization Treatments, Sci. Rep. 6 (2016) 32145.

[52] X. Li, W. Liu, G. Ye, B. Zhang, D. Zhu, K. Yao, Z. Liu, X. Sheng, Thermosensitive *N*-isopropylacrylamide–*N*–propylacrylamide-vinyl pyrrolidone terpolymers: Synthesis, characterization and preliminary application as embolic agents, Biomaterials 26(34) (2005) 7002-7011.

[53] J.W. Weisel, The mechanical properties of fibrin for basic scientists and clinicians, Biophys. Chem. 112(2) (2004) 267-276.

[54] P. Riha, X. Wang, R. Liao, J.F. Stoltz, Elasticity and fracture strain of whole blood clots, Clin. Hemorheol. Microcirc. 21(1) (1999) 45-49.

[55] C. Storm, J.J. Pastore, F.C. MacKintosh, T.C. Lubensky, P.A. Janmey, Nonlinear elasticity in biological gels, Nature 435(7039) (2005) 191-194.

[56] R.F. Diegelmann, M.C. Evans, Wound healing: an overview of acute, fibrotic and delayed healing, Front. Biosci. 9 (2004) 283-289.

[57] S.K. Natarajan, D. Born, B. Ghodke, G.W. Britz, L.N. Sekhar, Histopathological changes in brain arteriovenous malformations after embolization using onyx or n-butyl cyanoacrylate: Laboratory investigation, J. Neurosurg. 111(1) (2009) 105-113.

[58] S. Stampfl, N. Bellemann, U. Stampfl, B. Radeleff, R. Lopez-Benitez, C.-M. Sommer, H. Thierjung, I. Berger, G.M. Richter, Inflammation and recanalization of four different spherical embolization agents in the porcine kidney model, J. Vasc. Interv. Radiol. 19(4) (2008) 577-586.

[59] A. Gruber, P.R. Mazal, G. Bavinzski, M. Killer, H. Budka, B. Richling, Repermeation of Partially Embolized Cerebral Arteriovenous Malformations: A Clinical, Radiologic, and Histologic Study, Am. J. Neuroradiol. 17(7) (1996) 1323-1331.

[60] I.M. Germano, R.L. Davis, C.B. Wilson, G.B. Hieshima, Histopathological follow-up study of 66 cerebral arteriovenous malformations after therapeutic embolization with polyvinyl alcohol, J. Neurosurg. 76(4) (1992) 607-614.

[61] M. Brothers, J. Kaufmann, A. Fox, J. Deveikis, *N*-Butyl 2-cyanoacrylate--Substitute for IBCA in interventional neuroradiology: Histopathologic and polymerization time studies, Am. J. Neuroradiol. 10(4) (1989) 777-786.

[62] J.A. Champion, A. Walker, S. Mitragotri, Role of particle size in phagocytosis of polymeric microspheres, Pharm. Res. 25(8) (2008) 1815-1821.

[63] D. Paul, S. Achouri, Y.-Z. Yoon, J. Herre, Clare E. Bryant, P. Cicuta, Phagocytosis dynamics depends on target shape, Biophys. J. 105(5) (2013) 1143-1150.

[64] J.A. Champion, S. Mitragotri, Role of target geometry in phagocytosis, Proc. Natl. Acad. Sci. U. S. A. 103(13) (2006) 4930-4934.

[65] Z. Zheng, M.A. Yenari, Post-ischemic inflammation: Molecular mechanisms and therapeutic implications, Neurol. Res. 26(8) (2004) 884-892.

[66] J.C. Chaloupka, F. Viñuela, H.V. Vinters, J. Robert, Technical feasibility and histopathologic studies of ethylene vinyl copolymer (EVAL) using a swine endovascular embolization model, Am. J. Neuroradiol. 15(6) (1994) 1107-1115.

[67] D.P. Link, J.D. Strandberg, R. Virmani, K. Blashka, F. Mourtada, M.A. Samphilipo, Histopathologic appearance of arterial occlusions with hydrogel and polyvinyl alcohol embolic material in domestic swine, J. Vasc. Interv. Radiol. 7(6) (1996) 897-906.

CHAPTER 6

RELEASE PROFILE OF ANTIANGIOGENIC EMBOLIC COACERVATES LOADED WITH SUNITINIB MALATE

6.1 Abstract

Transcatheter embolization procedures are used to obstruct blood flow in a blood vessel or vascular bed. Embolization results in localized hypoxia, which stimulates the release of a variety of pro-angiogenic factors, most notably vascular endothelial growth factor (VEGF). This can eventually lead to revascularization of the embolized area. Moreover, after transarterial embolization (TAE) of hypervascularized tumors, this hypoxia induced angiogenesis has been linked to various measures of poor prognosis, including increased tumor size and eventual metastases. Here, previously developed embolic coacervates are augmented to release sunitinib malate, an FDA approved antiangiogenic drug. Over the course of 14 days, 80% of the loaded drug was released in an *in vitro* release assay. Release of the drug was linear with time, consistent with zero-order release kinetics. This study represents a promising first step to developing an embolic agent that prevents ischemia induced angiogenesis.

6.2 Introduction

Hepatocellular carcinoma (HCC) is the second leading cause of cancer deaths worldwide, with 782,000 new cases occurring in 2012 [1]. HCC is a hypervascular tumor that most often develops in patients with chronic fibrosis and/or cirrhosis [2]. Surgical resection or orthotopic liver transplantation, depending on liver function, are considered the best option for patients with early stage HCC (<3cm) [3, 4]. Unfortunately, HCC is typically undiagnosed until it has reached an intermediate to advanced stage where resection or transplantation are no longer viable options [4]. Even when resection is done, 55% of patients exhibit tumor recurrence within 2 years, most of which are inoperable [3, 5]. In these advanced cases, transcatheter embolization has emerged as the primary mode therapy for extending survival [6, 7]. HCC is especially amenable to embolization because tumor blood supply is derived from the hepatic artery, while blood supply to healthy liver tissue is supplied through the portal vein [3].

While HCC is the most common target for embolotherapy, other hypervascular tumors such as renal cell carcinoma, head and neck tumors, and colorectal carcinoma can also be treated by embolization. Embolization for tumors can be divided into conventional transarterial embolization (TAE) and transarterial chemoembolization (TACE). In both procedures, a microcatheter is placed into a feeder artery and an embolic agent is delivered into the arterial branches that supply the tumor. In TAE, an embolic agent is delivered alone to cause ischemic tumor necrosis [8]. TACE differs in that an embolic agent is co-administered with a chemotherapeutic agent, often doxorubicin [3]. However, both embolization

methods result in tumor hypoxia which stimulates the release of VEGF, eventually leading to revascularization and rebound of the tumor through angiogenesis [6].

Angiogenesis is the sprouting of new blood vessels from pre-existing vessels, usually in response to hypoxia or nutrient deprivation [9]. Activated by a variety of proangiogenic signals, endothelial cells detach from perivascular smooth muscle cells, sprout along gradients of angiogenic growth factors, coalesce to form endothelial tubes, and recruit perivascular cells to form vessels. Finally, remodeling and pruning complete the process of maturation [10]. Of relevance in embolization therapy, hypoxia is known to stimulate angiogenesis, primarily through the transcription factor Hypoxia Inducible Factor 1 (HIF-1). HIF-1 directly upregulates transcription of target genes by binding hypoxic responsive elements (HREs) within their promoter region. Notably, these include Vascular Endothelial Growth Factor (VEGF) and its primary receptor, VEGFR-1 [11]. Through binding receptor tyrosine kinases [12], VEGF stimulates endothelial cell mitosis and promotes vascular permeability, allowing the extravasation of plasma proteins and the formation of a provisional extracellular matrix (ECM), which the endothelial cells migrate along. Thus, embolization and chemoembolization procedures, by causing hypoxia, can stimulate angiogenesis and revascularization of the embolized area. In addition, growing evidence correlates this process with poor clinical outcomes [6]. Following TACE, patients have demonstrated significantly increased VEGF expression and microvessel density compared to non-embolized control groups and pre-embolization baseline levels [13, 14]. Some studies have also found that overexpression of VEGF after TACE was associated with later

metastases [6, 15, 16]. Depressed VEGF levels following embolization was found to be predictive of longer patient survival in another study [17].

The potential benefits of antiangiogenic therapy in combination with TAE or TACE is well recognized. However, clinical studies regarding the efficacy of such combination therapies have exclusively focused on combinations of systemic antiangiogenic therapy with embolization and have demonstrated mixed results. Phase II clinical trials with the anti-VEGF humanized antibody bevacizumab [6] and the receptor tyrosine kinase inhibitors sorafenib [18] and sunitinib [19, 20] in combination with TACE and/or TAE have demonstrated decreases in tumor size along with increases in mean time to progression and overall survival. However, systemic antiangiogenic therapy can have serious side effects [21]. Consequently, other clinical trials with sorafenib [22], sunitinib [23], and bevacizumab [6] in conjunction with TACE have been stopped because of severe adverse events. Thus, localized delivery of an antiangiogenic agent with embolization could improve outcomes and diminish safety concerns associated with antiangiogenic therapies.

Previously, our lab has developed embolic agents based upon complex coacervates, which, upon injection, harden *in situ* in response to decreasing ionic strength [24]. In early iterations, the embolic coacervates (ECs) were comprised of protamine, a cationic polypeptide, and an oligophosphate, phytic acid or sodium hexametaphosphate. In Chapter 5, ECs made from a synthetic polyguanidinium and MP were produced. These ECs demonstrated superior rheological properties compared to the protamine versions, with a lower initial viscosity and much stiffer

final form. Furthermore, both protamine and synthetic polymer based ECs have generated stable occlusion out to 4 weeks in embolization of the central auricular artery of rabbit ears.

Previously, coacervate-based PECs have been widely used for encapsulation and delivery of small molecule drugs [25, 26]. Based upon these studies, we hypothesize that passively loading ECs with an antiangiogenic drug would allow for localized, sustained delivery into the tissue surrounding the embolization site. Here, we report the loading of synthetic ECs with an FDA-approved antiangiogenic drug, sunitinib malate (Sutent ®; SUN). As a type I receptor tyrosine kinase inhibitor (TKI), it inhibits all subgroups of VEGF and PDGF receptors [27]. The *in vitro* release profile of loaded ECs is characterized and compared with models of drug release. Based upon these findings, implications of future design of antiangiogenic embolic coacervates (AA-ECs) are discussed.

6.3 Results

6.3.1 Production of EC and SUN Loading

Guanylation of 3-aminopropyl methacrylamide (APMA) was used to produce the monomer 3-guanidinopropyl methacrylamide (GPMA). For this study, a copolymer containing 78 mol% GPMA and 22 mol% methacrylamide (MA) was produced by RAFT polymerization, which had a molecular weight of 18 kg/mol (M_w) and a polydispersity index (PDI) of 1.04. As in Chapter 5, embolic coacervates made using this synthetic guanidinium containing polymer (PG) and hexametaphosphate (MP) were produced in 800 mM NaCl to preserve yield

(Figure 6.1 A). Previously, a concentrated solution of NaCl was used to raise the concentration of monovalent ions within the EC producing an injectable formulation. This process is shown in Figure 6.1 B, where a cloudy, viscous polyelectrolyte complex made in 800 mM NaCl was converted to a clear, readily flowing coacervate with the addition of 4 M NaCl. Here, to simultaneously raise the NaCl concentration and load the EC with SUN, a solution of 4 M NaCl and 4 mg/mL SUN was added (Figure 6.1 C). The brightly colored SUN was soluble and well-dispersed in the liquid coacervate. Total loading of SUN was 750 µg/mL. When the AA-EC was injected into balanced salt solution (BSS) it qualitatively hardened as rapidly and to the same extent as unloaded coacervates, and the SUN remained entrapped in the coacervate. In other words, the high concentration of SUN did not drastically affect the material properties or setting reaction of the EC.

6.3.2 Release Profile of AA-ECs

In vitro, AA-ECs exhibited sustained release of SUN for 14 days (Figure 6.2). The release profile was determined by placing 50 µL of EC into a cuvette containing 1 mL balanced salt solution (BSS) at pH 6.9. These cuvettes allowed for controlling surface area of EC exposed to the solution (0.4 cm^2), and thus the amount released normalized to surface area was calculated. The BSS release solutions were replaced at 1, 3, 6, 9, and 13 days to maintain sink conditions. Overall, more SUN was released from ECs without Ta (83%) than from those containing Ta (75%) (Figure 6.2 A). However, this difference in release was not statistically significant. Because of their similar release profiles, release with Ta will

be discussed specifically, but general conclusions are applicable to ECs +/- Ta. Over the first 24 h, 4.2 μg of SUN was released (10.6 μg/cm^2), which was 11% of the total drug loaded (Figure 6.2 B). By day 2, daily release had declined to 1.75 μg/day, where it remained essentially constant (+/-0.4 μg/day) until 14 days. At 14-15 days, the system reached a state of depletion, after which no significant release occurred.

This release profile was unexpected. Drug release from nonswelling polymer matrices is typically governed by Fickian diffusion [28, 29]. In this scenario, cumulative release is proportional to time$^{1/2}$, and release is modeled by the Higuchi model [30, 31]. However, a zero-order release model was a much better fit for the experimental data than the Higuchi model (R^2=0.99 vs. 0.94). In zero-order kinetics, the cumulative release is linear with time and is represented by the equation [30]:

$$Q_t = Kt + Q_0$$

The cumulative drug released (Q_t) at time, t, can either be a nominal value or a fraction of total drug released (Q_t/Q_∞). Q_0 represents the initial amount of drug in solution (which in this case is none) and/or an initial bolus release. In this case, a bolus was observed in the first day. EC (+Ta) was fit to this model in Figure 6.3. The intercept (bolus) determined by the model is 1.68 μg (4.2 μg/cm^2). This closely matches the observed data (Figure 6.2 B), where release on day 1 was more than double that seen over the rest of the experiment. Overall, however, this bolus

release is small and the release profile can be generally considered zero-order to the point of depletion.

6.4 Discussion

Zero-order release is desirable in drug delivery, as a constant amount of drug is delivered regardless of the concentration within the carrier and provides predictability. The exact mechanism behind the observed zero-order release remains to be fully elucidated. The classical polymeric system for achieving zero-order release is a reservoir device. This system is comprised of a matrix, which contains a low solubility drug, and a rate controlling membrane [28]. This rate-limiting membrane decouples release from diffusion because diffusion inside the matrix is much faster than transport across the membrane. Through interactions between the drug and polymer, the phase boundary between the coacervate and solution could conceivably function as a rate limiting surface. The guanadinyl sidechains of PG, with their cationic charge and Y-aromaticity [32] , provide three possible mechanisms of interaction with SUN. First, the GPMA functional group could associate with the hydrophobic aromatic rings in SUN through π-π interactions. Second, the positive charge could allow guanidinium to interact with these same aromatic rings through cation-π bonds, which are among the strongest noncovalent bonds [33, 34]. Third, the weak hydration shell above and below the guanidinium plane could allow hydrophobic interactions with SUN [35]. Several examples of systems with release limited by drug-matrix interactions are found in the coacervate and hydrogel literature. However, these systems typically release

only a few percent the loaded drug [36-38]. In contrast, ECs released approximately 80% of their overall drug payload. This high overall release suggests that interactions between PG and SUN are relatively weak and that these polymer-drug interactions may not account for this release profile.

In Chapter 3, it was demonstrated that injecting PRT-MP ECs into physiological saline produced a closed porous structure (Figure 3.4). When injected into saline, PG-MP ECs exhibit a similar structure, but macroscopically the pores are smaller because of faster gelation. Heterogeneous structures, including those with pores, have been used to create drug-delivery systems with non-Fickian release profiles. In these systems, the release profile depends on the solubility and diffusivity of the drug in each of the domains [39]. Under certain circumstances, these systems can produce zero-order release [40, 41]. Berg et. al. developed a porous polyelectrolyte complex which displayed a linear release profile for two model drugs over 20 days [42]. This system utilized a tortuous path of mostly connected pore networks to deliver drugs via small surface openings of the pores. The pores in ECs could provide channels for diffusion of SUN that allow for faster diffusion than through the polymer matrix. However, these pores are mostly closed, so it is unlikely that this accounts for the observed zero-order release.

The most plausible explanation for the observed zero-order release involves the pores acting as a reservoir, with the continuous polymer matrix limiting diffusion. In a biphasic system, if a drug preferentially partitions into the discontinuous phase but is released through the continuous phase, the microdomains can serve as a reservoir that keeps drug concentration in the bulk

phase nearly constant and produces zero-order release [41]. In ECs, this could occur if the drug preferentially partitioned into the *in situ* formed pores upon setting. SUN has a pH and salt concentration dependent aqueous solubility. These closed pores are mostly water, but also contain unknown concentrations of salt and possibly small amounts of polymer. Conceivably, the solubility of SUN in these pores could be up to 25 mg/mL, much higher than the overall drug loading. Under this scenario SUN would be released into the media through the concentrated polymer phase, but would be mostly excluded from it. The pores would serve as a reservoir, keeping the overall concentration in the polymer phase at a pseudo-steady state and producing zero-order release. This mechanism is depicted in Figure 6.4. To generate zero-order release via this mechanism, the fluxes (pore to polymer phase and polymer phase to release media) must be similar. This is a reasonable assumption, given that the pores and release media are both aqueous phases. The reservoir explanation seems the most likely as it considers the entire structure of the material, and is consistent with the high fraction of drug payload released and the release profile. Future studies on AA-ECs will be designed to examine this hypothesis.

AA-ECs released 80% of their 750 µg/mL payload. While efficacy depends on clearance rates and diffusion of the drug, the amount released from 1 mL of AA-EC is large compared to the clinically effective plasma range for SUN (50 ng/mL) [43], suggesting that AA-ECs can likely release sufficient quantities of SUN to affect localized angiogenesis. Furthermore, based on the 14 day sustained release of SUN from ECs, this system is well suited to limiting ischemia-induced

angiogenesis from embolization. After an embolization procedure, hypoxia and activation of HIF-1 will occur on a time scale of minutes [44]. The resultant initiation of angiogenesis and recruitment of new blood vessels to the tumor occurs through the effector functions of RTKs, which are the therapeutic targets for SUN. This process normally occurs on the time scale of a few days [45-47]. If new blood vessels are not supplied after this period of time, the cells can become dormant or even apoptotic through ischemia [48], which suggests that SUN release could reduce ischemia induced angiogenesis and slow tumor progression in hypervascular tumors.

However, this *in vitro* experiment has limitations in predicting results *in vivo*. Given the zero-order release profile, overall drug release is likely to be determined by total surface area, with the duration of release being a function of surface to volume ratio. Diffusivity of the drug into tissue might also occur at a different rate than into saline. Changing the GPMA mol% or molecular weight of the polymer alters the properties of the EC and thus might be a tool for modifying and maintaining the desired release profile *in vivo*.

6.5 Conclusion

Release of SUN from AA-ECs is linear with time, closely following a zero-order release profile. The exact mechanism behind this release profile remains a topic of future study, but it likely results from closed pores within the set EC complex acting as a reservoir system with release occurring through the polymer matrix. In these *in vitro* release studies, AA-ECs delivered 80% of the loaded SUN

over the course of 2 weeks. While this release profile would be well suited to counteract ischemia induced angiogenesis after embolization procedures, it is only a small first step. Further evaluation is needed to gauge release of SUN after an *in vivo* embolization procedure.

6.6 Materials and Methods

6.6.1 Materials

N-(3-aminopropyl) methacrylamide hydrochloride (APMA) was obtained from Polysciences, Inc. (cat# 21200). ^{1}H-Pyrazole-1-Carboxamidine hydrochloride was purchased from Chem-Ipex International (cat# 21678). Methacrylamide (MA; L15013) and glacial acetic acid (cat# 36289) were obtained from Alfa Aesar. 4-methoxyphenol was purchased from TCI chemicals (cat #M0123). 4,4′-Azobis(4-cyanovaleric acid) (V501; cat# 11590) and azobisisobutyronitrile (AIBN; cat# 441090) were obtained from Sigma-Aldrich. 4-Cyano-4-(thiobenzoylthio)pentanoic acid was purchased from Strem Chemicals (cat# 16-0422). Sunitinib malate (SUN) was obtained from Selleckchem (cat#S1042). Sodium acetate was purchased from VWR (cat# 0602). USP grade sodium chloride was obtained from MP Biosciences (cat# 102892). All solvents were ACS grade or better. Solutions were made in ultrapure double deionized water.

6.6.2 Production of Polyguanidinium

Production of *N*-(3-methacrylamidopropyl) guanidinium chloride (GPMA) and p(GPMA-co-MA) was performed as thoroughly described in Chapter 5. Briefly,

GPMA monomer was synthesized by guanylation of *N*-(3-aminopropyl) methacrylamide hydrochloride (APMA) with *1H*-pyrazole-1-carboxamidine hydrochloride. The purified GPMA product was then copolymerized with methacrylamide (MA) in acetate buffer (pH=5.3), using V-501 as the initiator and 4-Cyano-4-(thiobenzoylthio)pentanoic acid as the chain transfer agent. An 18 kg/mol (M_w) polymer (PG) was produced with a PDI of 1.04 and 78 mol% GPMA. The final product was converted to the hydrochloride salt and purified using ultrafiltration.

6.6.3 Production of Anti-Angiogenic Embolic Coacervates

Coacervates of PG and MP were prepared with 1-5 micron Ta powder added as a radiocontrast agent (30 wt.% of final coacervate). Aqueous stock solutions of PG and MP were made at 100 mg/mL and 200 mg/mL, respectively. The pH of both solutions was adjusted to 7.2. Coacervation was achieved by sequential addition of DI water, 5M NaCl, MP solution, Ta, and PG solution. In this final mixture, PG concentration was fixed at 50 mg/mL; MP concentration was 42 mg/mL based upon calculated charge densities and a 1:2 charge ratio. Amounts of DI water and 5 M salt were adjusted to form an overall NaCl concentration of 800 mM. Phase separation occurred immediately upon addition of PG, and the coacervate was allowed to settle for 12 h before removing the supernatant.

A stock solution of 4 mg/mL SUN solution in 4 M NaCl was produced by dissolving SUN in 1 part DI water at 20 mg/mL and subsequently diluting it with 4

parts 5 M NaCl. After removal of the PG-MP supernatant, the SUN+NaCl stock was added to raise the salt to 1400 mM and load SUN at 750 μg/mL, forming the antiangiogenic embolic coacervate (AA-EC). This supersaturated high-salt solution of SUN was used immediately as it would precipitate within an hour. The brightly colored SUN appeared soluble and remained well-dispersed in the high-salt liquid coacervate.

6.6.4 SUN Release

SUN-containing AA-ECs were produced with and without tantalum. Release of SUN was measured by dispensing 50 μL of the AA-ECs (containing 37.5 μg SUN) into the bottom of disposable UV-Vis cuvettes and adding 1 mL of BSS (pH=6.9). The cuvettes were placed in a temperature controlled incubator at 37°C and were shaken at 60 rpm. SUN release was determined at 1, 2, 4, 6, 8, 10, and 24 h and daily thereafter out to 17 days. To maintain sink conditions, the BSS solution was replaced at 1, 3, 6, 9, and 13 days. To measure SUN in the release media, absorbance was measured at 431 nm and concentration was determined from a standard curve. Cumulative release at each timepoint is reported and is normalized by the surface area of the AA-EC exposed to BSS in the cuvette (0.4 cm^2). Student's t-test was used to statistically compare overall release.

6.6.5 Statistical Analysis

Differences in mean overall release (cumulative release at day 17) from ECs with and without tantalum was analyzed for statistical significance using one-way ANOVA with IBM SPSS Statistics 24 software.

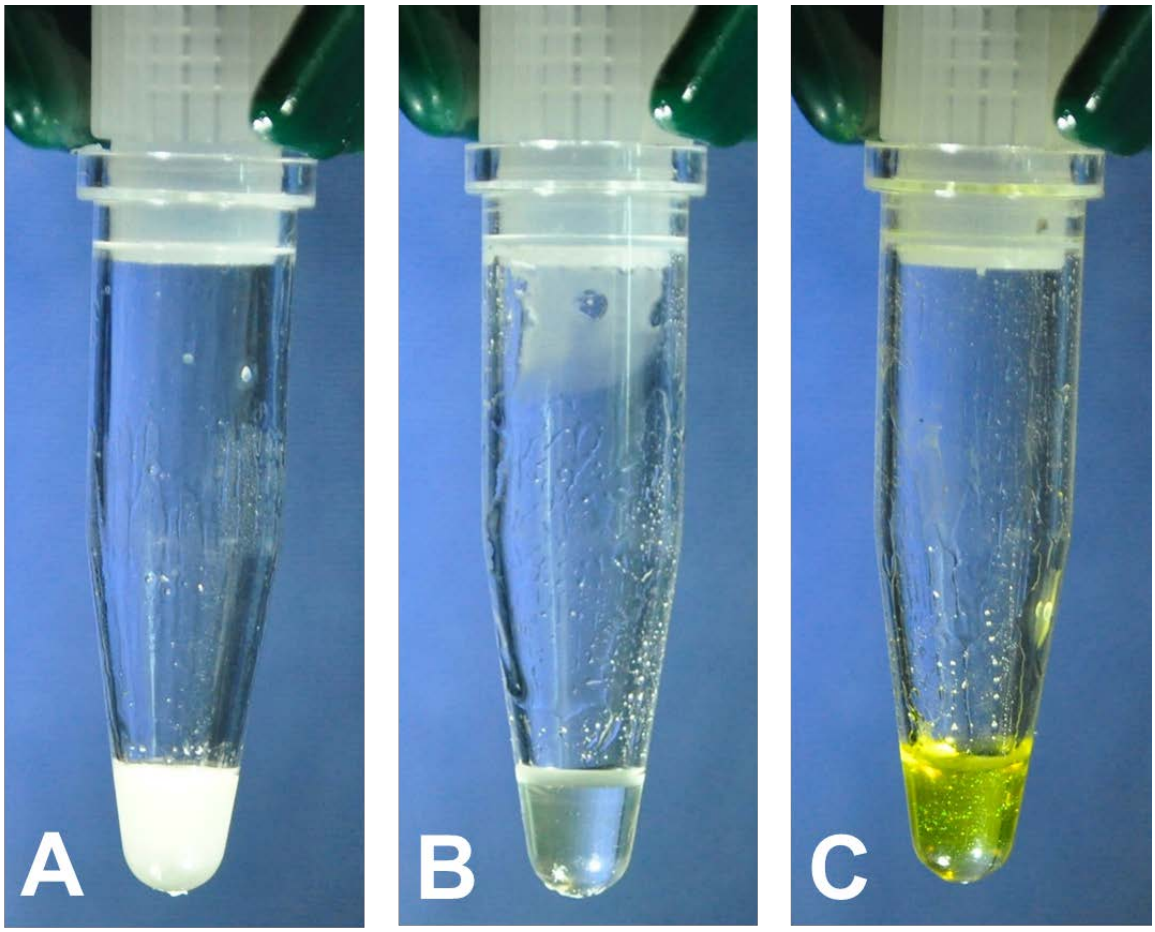

Figure 6.1. Loading of PG-MP ECs with sunitinib. (A) PG-MP formed in 800 mM NaCl. (B) PG-MP EC raised to 1400 mM NaCl. (C) PG-MP EC raised to 1400 mM NaCl and loaded with SUN.

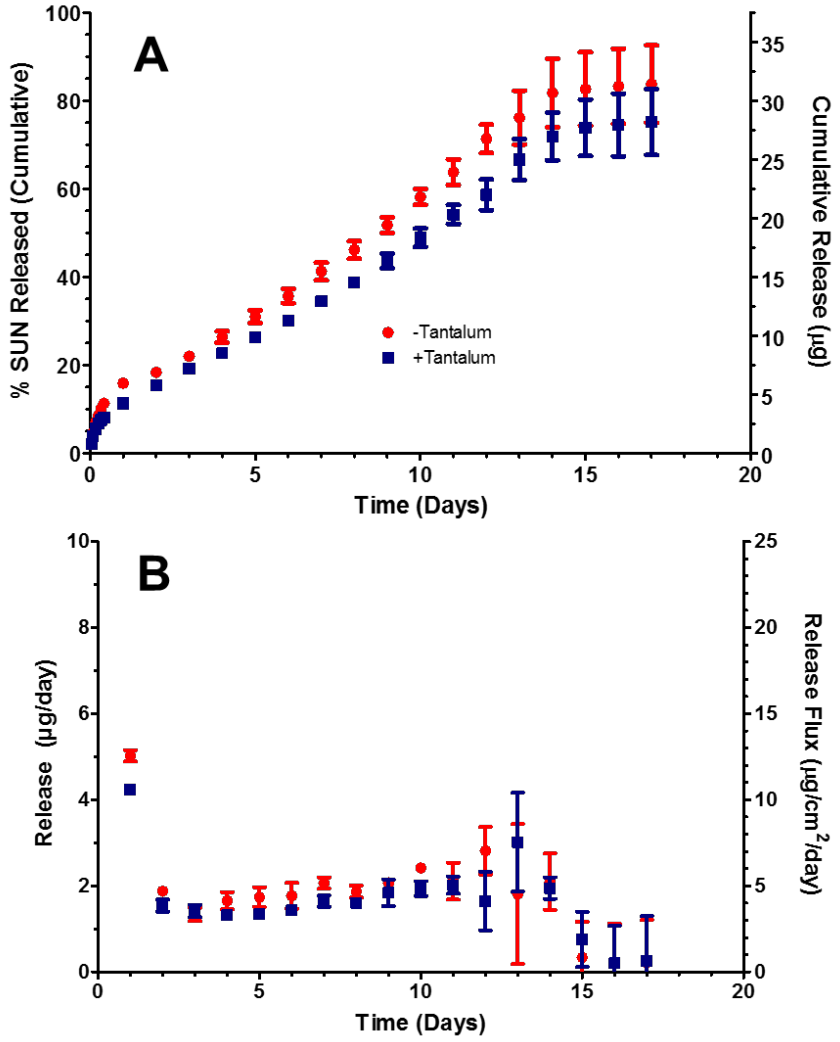

Figure 6.2. Release of sunitinib from PG-MP ECs in BSS. (A) Cumulative release profile of SUN. Percent released is out of total SUN loaded. (B) Daily SUN release. Data points represent an average of three runs, and error bars are +/- SD.

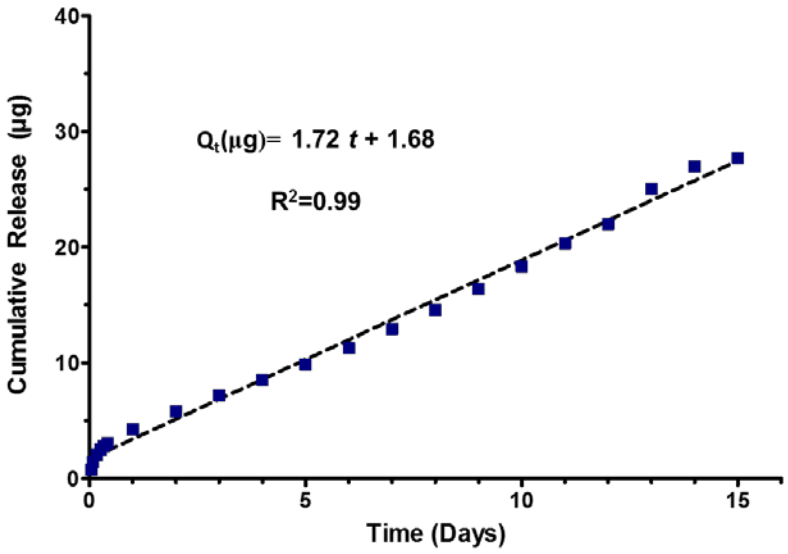

Figure 6.3. EC (+Ta) fit to zero-order release model out to depletion (15 days).

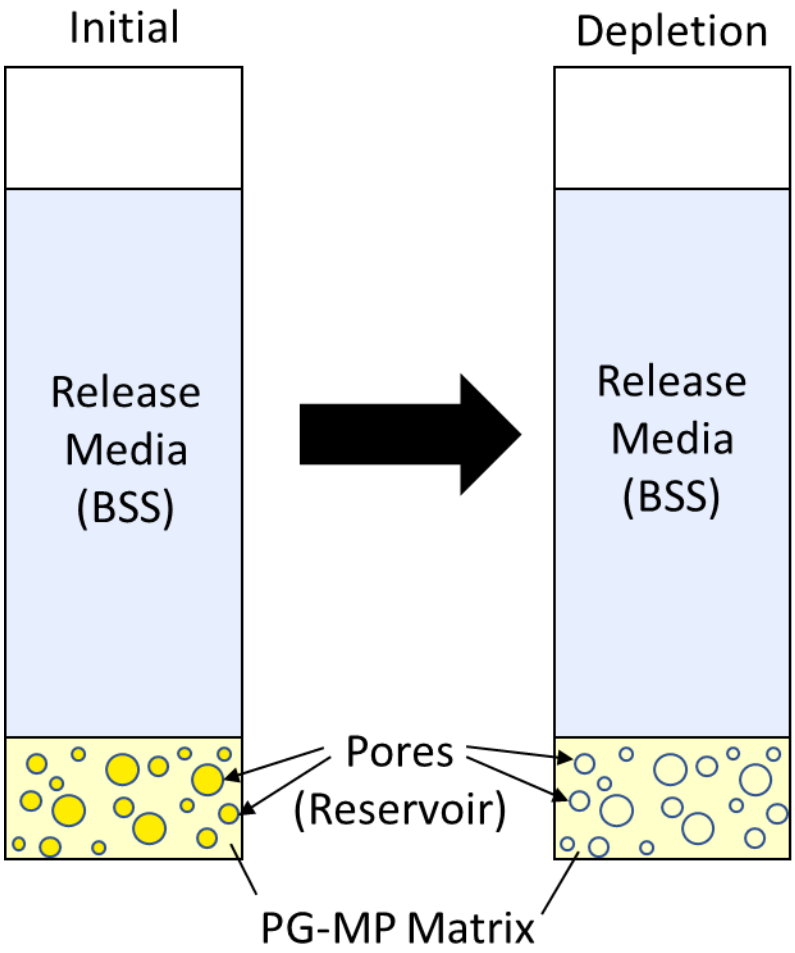

Figure 6.4. Proposed mechanism for first-order release of SUN from ECs.

6.7 References

[1] L.A. Torre, F. Bray, R.L. Siegel, J. Ferlay, J. Lortet-Tieulent, A. Jemal, Global cancer statistics, 2012, CA Cancer J. Clin. 65(2) (2015) 87-108.

[2] S.F. Altekruse, K.A. McGlynn, M.E. Reichman, Hepatocellular carcinoma incidence, mortality, and survival trends in the United States from 1975 to 2005, J. Clin. Oncol. 27(9) (2009) 1485-1491.

[3] Z.V. Fong, K.K. Tanabe, The clinical management of hepatocellular carcinoma in the United States, Europe, and Asia: A comprehensive and evidence-based comparison and review, Cancer 120(18) (2014) 2824-2838.

[4] A. Raza, G.K. Sood, Hepatocellular carcinoma review: current treatment, and evidence-based medicine, World J. Gastroenterol. 20(15) (2014) 4115-4127.

[5] C. Cha, Y. Fong, W.R. Jarnagin, L.H. Blumgart, R.P. DeMatteo, Predictors and patterns of recurrence after resection of hepatocellular carcinoma, J. Am. Coll. Surg. 197(5) (2003) 753-758.

[6] C.D. Gadaleta, G. Ranieri, Trans-arterial chemoembolization as a therapy for liver tumours: New clinical developments and suggestions for combination with angiogenesis inhibitors, Crit. Rev. Oncol./Hematol. 80(1) (2011) 40-53.

[7] L. Bester, B. Meteling, D. Boshell, T.C. Chua, D.L. Morris, Transarterial chemoembolisation and radioembolisation for the treatment of primary liver cancer and secondary liver cancer: A review of the literature, J. Med. Imaging Radiat. Oncol. 58(3) (2014) 341-352.

[8] A.D. Talenfeld, A.K. Sista, D.C. Madoff, Transarterial therapies for primary liver tumors, Surg. Oncol. Clin. N. Am. 23(2) (2014) 323-351.

[9] D. Hanahan, J. Folkman, Patterns and emerging mechanisms of the angiogenic switch during tumorigenesis, Cell 86(3) (1996) 353-364.

[10] S.M. Weis, D.A. Cheresh, Tumor angiogenesis: molecular pathways and therapeutic targets, Nat. Med. 17(11) (2011) 1359-1370.

[11] D. Liao, R.S. Johnson, Hypoxia: A key regulator of angiogenesis in cancer, Cancer Metastasis Rev. 26(2) (2007) 281-290.

[12] P. Carmeliet, R.K. Jain, Molecular mechanisms and clinical applications of angiogenesis, Nature 473(7347) (2011) 298-307.

[13] E.-H. Xiao, Effect of preoperative transcatheter arterial chemoembolization on angiogenesis of hepatocellular carcinoma cells, World J. Gastroenterol. 15(36) (2009) 4582.

[14] B. Wang, H. Xu, Z. Gao, H. Ning, Y. Sun, G. Cao, Increased expression of vascular endothelial growth factor in hepatocellular carcinoma after transcatheter arterial chemoembolization, Acta Radiol. 49(5) (2008) 523-529.

[15] J.H. Shim, J.W. Park, J.H. Kim, M. An, S.Y. Kong, B.H. Nam, J.I. Choi, H.B. Kim, W.J. Lee, C.M. Kim, Association between increment of serum VEGF level and prognosis after transcatheter arterial chemoembolization in hepatocellular carcinoma patients, Cancer Sci. 99(10) (2008) 2037-2044.

[16] Z.P. Xiong, S.R. Yang, Z.Y. Liang, E.H. Xiao, X.P. Yu, S.K. Zhou, Z.S. Zhang, Association between vascular endothelial growth factor and metastasis after transcatheter arterial chemoembolization in patients with hepatocellular carcinoma, Hepatobiliary Pancreat. Dis. Int. 3(3) (2004) 386-390.

[17] A. Sergio, C. Cristofori, R. Cardin, G. Pivetta, R. Ragazzi, A. Baldan, L. Girardi, U. Cillo, P. Burra, A. Giacomin, Transcatheter arterial chemoembolization (TACE) in hepatocellular carcinoma (HCC): The role of angiogenesis and invasiveness, Am. J. Gastroenterol. 103(4) (2008) 914-921.

[18] T.M. Pawlik, D.K. Reyes, D. Cosgrove, I.R. Kamel, N. Bhagat, J.F.H. Geschwind, Phase II trial of sorafenib combined with concurrent transarterial chemoembolization with drug-eluting beads for hepatocellular carcinoma, J. Clin. Oncol. 29(30) (2011) 3960-3967.

[19] W.C. Chen, B.G. Lee, D.W. Park, K. Kim, H. Chu, K. Kim, J. Huard, Y. Wang, Controlled dual delivery of Fibroblast Growth Factor-2 and Interleukin-10 by heparin-based coacervate synergistically enhances ischemic heart repair, Biomaterials 72 (2015) 138-151.

[20] V.K. Pokuri, G.M. Tomaszewski, S. Ait-Oudhia, A. Groman, N.I. Khushalani, A.A. Lugade, Y. Thanavala, E.A. Ashton, C. Grande, G.J. Fetterly, Efficacy, safety, and potential biomarkers of sunitinib and transarterial chemoembolization (TACE) combination in advanced hepatocellular carcinoma (HCC): Phase II trial, Am. J. Clin. Oncol. (2016).

[21] T. Kamba, D. McDonald, Mechanisms of adverse effects of anti-VEGF therapy for cancer, Br. J. Cancer 96(12) (2007) 1788-1795.

[22] M.-W. Welker, J. Trojan, Anti-angiogenesis in hepatocellular carcinoma treatment: Current evidence and future perspectives, World J. Gastroenterol. 17(26) (2011) 3075-3081.

[23] W. Sieghart, M. Pinter, M. Reisegger, C. Müller, A. Ba-Ssalamah, J. Lammer, M. Peck-Radosavljevic, Conventional transarterial chemoembolisation in combination with sorafenib for patients with hepatocellular carcinoma: A pilot study, Eur. Radiol. 22(6) (2012) 1214-1223.

[24] J.P. Jones, M. Sima, R.G. O'Hara, R.J. Stewart, Water-borne endovascular embolics inspired by the undersea adhesive of marine sandcastle worms, Adv. Healthc. Mater. 5(7) (2016) 795-801.

[25] S.L. Perry, W.C. Blocher, Complex coacervate-based materials for biomedicine, Wiley Interdiscip. Rev. Nanomed. Nanobiotechnol. 9(4) (2016) e1442.

[26] N.R. Johnson, Y. Wang, Coacervate delivery systems for proteins and small molecule drugs, Expert Opin. Drug Deliv. 11(12) (2014) 1829-1832.

[27] S. Faivre, G. Demetri, W. Sargent, E. Raymond, Molecular basis for sunitinib efficacy and future clinical development, Nat. Rev. Drug Discov. 6(9) (2007) 734-745.

[28] Y. Fu, W.J. Kao, Drug release kinetics and transport mechanisms of non-degradable and degradable polymeric delivery systems, Expert Opin. Drug Deliv. 7(4) (2010) 429-444.

[29] D.G. Kanjickal, S.T. Lopina, Modeling of drug release from polymeric delivery systems—A review, Crit. Rev. Ther. Drug Carrier Syst. 21(5) (2004).

[30] S. Dash, P.N. Murthy, L. Nath, P. Chowdhury, Kinetic modeling on drug release from controlled drug delivery systems, Acta Pol. Pharm. 67(3) (2010) 217-223.

[31] D. Paul, Elaborations on the Higuchi model for drug delivery, Int. J. Pharm. 418(1) (2011) 13-17.

[32] P. Gund, Guanidine, trimethylenemethane, and "Y-delocalization." Can acyclic compounds have "aromatic" stability?, J. Chem. Educ. 49(2) (1972) 100.

[33] J.C. Ma, D.A. Dougherty, The cation-π interaction, Chem. Rev. 97(5) (1997) 1303-1324.

[34] J.P. Gallivan, D.A. Dougherty, Cation-π interactions in structural biology, Proc. Natl. Acad. Sci. U. S. A. 96(17) (1999) 9459-9464.

[35] P.E. Mason, G.W. Neilson, J.E. Enderby, M.L. Saboungi, C.E. Dempsey, A.D. MacKerell, J.W. Brady, The structure of aqueous guanidinium chloride solutions, J. Am. Chem. Soc. 126(37) (2004) 11462-11470.

[36] D.D. Lane, A.K. Fessler, S. Goo, D.L. Williams, R.J. Stewart, Sustained tobramycin release from polyphosphate double network hydrogels, Acta Biomater. 50 (2017) 484-492.

[37] A. Tiwari, S. Bindal, H. Bohidar, Kinetics of protein−protein complex coacervation and biphasic release of salbutamol sulfate from coacervate matrix, Biomacromolecules 10(1) (2008) 184-189.

[38] P.G. Lawrence, P.S. Patil, N.D. Leipzig, Y. Lapitsky, Ionically cross-linked polymer networks for the multiple-month release of small molecules, ACS Appl. Mater. Interfaces 8(7) (2016) 4323-4335.

[39] R.A. Siegel, M.J. Rathbone, Overview of Controlled Release Mechanisms, in: J. Siepmann, R.A. Siegel, M.J. Rathbone (Eds.), Fundamentals and Applications of Controlled Release Drug Delivery, Springer US, Boston, MA, 2012, pp. 19-43.

[40] R.A. Siegel, Porous Systems, in: J. Siepmann, R.A. Siegel, M.J. Rathbone (Eds.), Fundamentals and Applications of Controlled Release Drug Delivery, Springer US, Boston, MA, 2012, pp. 229-251.

[41] C.G. Varelas, D.G. Dixon, C.A. Steiner, Zero-order release from biphasic polymer hydrogels, J. Controlled Release 34(3) (1995) 185-192.

[42] M.C. Berg, L. Zhai, R.E. Cohen, M.F. Rubner, Controlled drug release from porous polyelectrolyte multilayers, Biomacromolecules 7(1) (2006) 357-364.

[43] J. Christensen, A preclinical review of sunitinib, a multitargeted receptor tyrosine kinase inhibitor with anti-angiogenic and antitumour activities, Ann. Oncol. 18(suppl 10) (2007) x3-x10.

[44] U.R. Jewell, I. Kvietikova, A. Scheid, C. Bauer, R.H. Wenger, M. Gassmann, Induction of HIF-1α in response to hypoxia is instantaneous, FASEB J. 15(7) (2001) 1312-1314.

[45] J. Folkman, Angiogenesis: an organizing principle for drug discovery?, Nat. Rev. Drug Discov. 6(4) (2007) 273-286.

[46] S. Taylor, J. Folkman, Protamine is an inhibitor of angiogenesis, Nature 297(5864) (1982) 307-312.

[47] D.H. Ausprunk, J. Folkman, Migration and proliferation of endothelial cells in preformed and newly formed blood vessels during tumor angiogenesis, Microvasc. Res. 14(1) (1977) 53-65.

[48] L. Holmgren, M.S. O'Reilly, J. Folkman, Dormancy of micrometastases: Balanced proliferation and apoptosis in the presence of angiogenesis suppression, Nat. Med. 1(2) (1995) 149-153.

CHAPTER 7

CONCLUSIONS AND FUTURE DIRECTIONS

7.1 Conclusion

Embolic coacervates (ECs) represent a promising developmental liquid embolic agent. These agents, unlike liquid embolics in clinical use, are aqueous based systems that eliminate the intraarterial injection of vasotoxic organic solvents and exothermically polymerizing monomers. A novel ionic strength based setting mechanism is employed which causes a phase transition from liquid coacervate to ionic gel. This setting mechanism represents a paradigm shift from other approaches to creating aqueous based liquid embolics, approaches that are based upon temperature changes or two component mixtures. ECs offer a system that can be packaged as a single component preloaded into a syringe, avoiding the need for dual lumen catheters. In addition, the non-temperature based hardening mechanism ensures that the embolic will not begin to set until exiting the catheter and allows for small repeated injections of embolic agent under fluoroscopic guidance. Radiographic contrast, such as micronized tantalum metal, can be suspended in the ECs offering a low-viscosity, shear thinning formulation that can be injected through clinically available embolic microcatheters. When injected into the relatively low ionic strength environment of

the blood stream, sodium chloride diffuses out of the EC and the polyelectrolyte chains begin to interact more strongly, resulting in solidification of the EC. The hardening of the ECs upon exposure to low ionic strength environment produces a large change in mechanical properties. ECs made with synthetic polyguanidinium (PG) and the oligoanion hexametaphosphate (MP) exhibited an almost 4 order of magnitude increase in complex shear modulus compared with the high salt injectable form. In a percutaneous transcatheter embolization of a rabbit kidney, ECs demonstrated the ability to occlude vessels down to the capillary level without crossing into venous circulation. Moreover, after embolization of the central auricular artery of rabbit ears, the occlusions remained stable at 4 weeks. No signs of direct cytotoxicity were observed with the embolic agents. However, histological examination revealed neutrophilic inflammation which led to destruction of the vessel structure and partial resorption of the material. By 4 weeks, this response had begun to resolve and early signs of fibrous connective tissue deposition were seen.

In Chapter 6, ECs were augmented to encapsulate and release the antiangiogenic agent Sunitinib malate (SUN). *In vitro* release experiments revealed that ECs released 80% of their SUN payload over the course of 2 weeks. A zero-order release profile was observed, indicating that the release was not governed by diffusion. It is suspected that this release profile results from closed pores within the set EC complex acting as a drug reservoir which keeps concentration in the polymer matrix at a pseudo steady state. The high fraction of drug released from the EC and the desirable zero order release profile

demonstrate the potential of these agents for preventing angiogenic revascularization of embolized tissues.

7.2 Future Work

7.2.1 Long-Term Tissue Biocompatibility

The long-term tissue response to PG-MP ECs needs further investigation. In embolization of rabbit auricular arteries, PG-MP ECs generated occlusions that were stable out to 4 weeks. These ECs incited a severe neutrophilic inflammatory response that resulted in destruction of the vessel wall. At 4 weeks, this reaction had begun to subside, but some neutrophils were still present. Extensive resorption of the material had occurred, and the micronized tantalum was being phagocytosed. This phagocytosed tantalum would likely be transported to the regional lymph nodes. Another preliminary investigation could examine the use of larger tantalum to prevent this transport, although it might incite a more persistent inflammatory response. In either case, the tissue response data raises several questions that should be addressed in future animal experiments with larger sample sizes. First, the long-term fate of the embolus and the tissue surrounding the embolization site remains unclear. Early signs of fibrosis suggest that the eventual progression might result in the formation of a fibrous scar, but this remains speculative. This investigation would also serve to evaluate the permanence of the occlusion. Revascularization is seen with virtually all embolic agents, but considering the obliteration of vessel structure, it seems unlikely that revascularization will proceed by recanalization of the previous vessel lumen.

Arterial blood flow to the surrounding tissue would probably be restored via a combination of enhancement of extant collateral blood flow and neovascularization. A 6-12 month study should more accurately gauge the chronic tissue response and eventual fate of the occlusion.

7.2.2 Nonparticulate Contrast Agent

Like current liquid embolic agents, the ECs used in this study contain micronized tantalum metal powder as a contrast agent. However, these particles settle over time and require vigorous mixing before, and sometimes during, a procedure. Furthermore, questions remain about the long-term fate of the tantalum particles, especially if the embolus is not destined for later surgical resection. An ideal solution would be to covalently incorporate contrast directly into the embolic agent. The synthetic guanidinium monomer (GPMA) described in this dissertation (GPMA) can be copolymerized with a variety of different monomers. Wang et. al. has described the synthesis of a tri-iodinated methacrylate monomer [1]. While macro chain transfer agents were produced with this monomer, its low solubility would need to be overcome to produce random copolymers with GPMA for production of ECs. Additionally, the unknown effects of this dense, hydrophobic monomer on the properties of the ECs would likely necessitate reformulation. Another possible strategy would be to make the EC in a high ionic strength solution of sodium iodate (NaI) rather than NaCl. Work by Ghostine et. al. has shown that NaI is more effective than NaCl at disrupting interchain ion pairing in polyelectrolyte complexes due to hydration effects [2]. Thus, producing an injectable EC would

likely require a lower overall ionic strength. However, the replacement of NaCl with NaI might affect the safety profile of ECs. While doses >60 mg/kg of NaI are used in veterinary medicine (EC would contain <200 mg in a 1 mL injection), the effect of I^- on the local tissue environment remains a concern with this approach.

7.2.3 Effects of Polymer Characteristics

From the literature on ionic strength dependent phase transitions in polyelectrolyte complexes, it is well reported that higher molecular weight and charge density favor complexation; that is, they decrease the critical salt concentration for the solution-coacervate and coacervate-precipitate phase transitions [3-6]. From the work done on ECs thus far, this appears to hold true for low salt rheological properties. Particularly, the complexes in physiological saline become stronger with increasing molecular weight and charge density. This was illustrated by the >2 order of magnitude increase in complex modulus in switching from the polycation from PRT to PG. However, confounding factors cast uncertainty about the magnitude of these effects. In this case, the molecular weight was ostensibly modified. While the molar fraction of guanidinium containing sidechains was increased from 65% to 80%, the charge density per unit mass was the same in both cases. Hydrophobicity is another factor that can drastically affect the behavior of PEs [7], and the aliphatic backbone of PG is more hydrophobic than the peptide backbone of PG. Furthermore, while PG ECs had stronger mechanical properties in physiological saline, they had a lower viscosity at high salt. In other words, the shift from PRT to PG made the ECs more salt sensitive,

but the reason for this increased salt sensitivity is unclear.

The synthetic guanidinium copolymers described in this dissertation provide a tool for studying the effects of these characteristics on rheology both in high and low salt concentrations. The polymers can easily be made with varying monomer feed ratios, and RAFT polymerization provides precise control of the molecular weight. While changing the backbone to study hydrophobicity is more difficult, GPMA could easily be copolymerized with other monomers to examine this effect. Beyond fundamental knowledge about PEC behavior, these studies could guide design and optimization of ECs. For example, the degree of distal penetration is an important feature of embolic agents, but the amount of penetration desired varies with the procedure. An agent that causes more distal penetration will cause more ischemia, which is desired in certain situations such as AVMs, but undesired in other scenarios such as a small GI hemorrhage [8]. Carugo et. al. has developed a microfluidics device with bifurcations and progressively smaller vessels to gauge the distal penetration of PVA particles [9]. A similar device could be used to evaluate the distal penetration of ECs into smaller vessels. Correlating these observations with rheological properties of the embolics in both low and high salt could allow for the optimization of EC formulations for specific surgical outcomes.

7.2.4 Future Development of Antiangiogenic ECs

The experiments described in Chapter 6 demonstrate feasibility for using ECs as combination embolic and drug delivery agents, but these agents need to be more thoroughly characterized. Injection force measurements, followed by

rheological characterization of these ECs in high and low salt, would be the first steps in this process, as these experiments will identify any effects of SUN loading on material properties and guide any reformulation of the ECs to accommodate these changes. Angiogenesis is a difficult process to replicate using *in vitro* assays, and because SUN is already a clinically proven antiangiogenic agent, these assays would be of little value. After the release profile and material properties are fully characterized, evaluation in animal models should be pursued. For *in vivo* evaluation of the antiangiogenic ECs, two options exist. Testing the AA-ECs in a hypervascular tumor model would allow direct testing of the hypotheses for this treatment: AA-ECs will (1) reduce postembolization angiogenesis and (2) slow tumor progression in embolization of hypervascular tumors. The rabbit VX2 tumor model is virus-induced squamous cell carcinoma which can be rapidly grown in rabbit skeletal muscle and transplanted to the liver, where it is commonly used as a model of hepatocellular carcinoma. It can be accessed and embolized using interventional radiology techniques [10]. Finally, there are well-established techniques for semi-quantitatively evaluating angiogenesis in this model [11]. However, this model is technically demanding and large numbers of animals would be needed to derive statistical significance. For this reason, it may be useful to begin *in vivo* evaluation with a pilot study in simpler model like the corneal angiogenesis model, which would allow for more direct measurement of angiogenesis inhibition but would not address embolization or tumor related endpoints.

7.3 References

[1] Z. Wang, T. Chang, L. Hunter, A.M. Gregory, M. Tanudji, S. Jones, M.H. Stenzel, Radio-opaque micelles for X-ray imaging, Aust. J. Chem. 67(1) (2014) 78-84.

[2] R.A. Ghostine, R.F. Shamoun, J.B. Schlenoff, Doping and diffusion in an extruded saloplastic polyelectrolyte complex, Macromolecules 46(10) (2013) 4089-4094.

[3] R. Chollakup, J.B. Beck, K. Dirnberger, M. Tirrell, C.D. Eisenbach, Polyelectrolyte molecular weight and salt effects on the phase behavior and coacervation of aqueous solutions of poly(acrylic acid) sodium salt and poly(allylamine) hydrochloride, Macromolecules 46(6) (2013) 2376-2390.

[4] R. Chollakup, W. Smitthipong, C.D. Eisenbach, M. Tirrell, Phase behavior and coacervation of aqueous poly (acrylic acid)− poly (allylamine) solutions, Macromolecules 43(5) (2010) 2518-2528.

[5] Q. Wang, J.B. Schlenoff, The polyelectrolyte complex/coacervate continuum, Macromolecules 47(9) (2014) 3108-3116.

[6] A. Kayitmazer, A. Koksal, E.K. Iyilik, Complex coacervation of hyaluronic acid and chitosan: effects of pH, ionic strength, charge density, chain length and the charge ratio, Soft Matter 11(44) (2015) 8605-8612.

[7] J.B. Schlenoff, A.H. Rmaile, C.B. Bucur, Hydration contributions to association in polyelectrolyte multilayers and complexes: Visualizing hydrophobicity, J. Am. Chem. Soc. 130(41) (2008) 13589-13597.

[8] M. Lubarsky, C. Ray, B. Funaki, Embolization agents—Which one should be used when? Part 2: Small-vessel embolization, Semin. Intervent. Radiol. 27(1) (2010) 99-104.

[9] D. Carugo, L. Capretto, S. Willis, A.L. Lewis, D. Grey, M. Hill, X. Zhang, A microfluidic device for the characterisation of embolisation with polyvinyl alcohol beads through biomimetic bifurcations, Biomed. Microdevices 14(1) (2012) 153-163.

[10] A. Parvinian, L.C. Casadaban, R.C. Gaba, Development, growth, propagation, and angiographic utilization of the rabbit VX2 model of liver cancer: a pictorial primer and "how to" guide, Diagn. Interv. Radiol. 20(4) (2014) 335.

[11] F. Dai, X. Zhang, W. Shen, J. Chen, L. Liu, G. Gao, Liposomal curcumin inhibits hypoxia-induced angiogenesis after transcatheter arterial embolization in VX2 rabbit liver tumors, Onco Targets Ther. 8 (2015) 2601.